

# Atomic, molecular and optical physics applications of longitudinally coherent and narrow bandwidth Free-Electron Lasers

Carlo Callegari<sup>a,\*</sup>, Alexei N. Grum-Grzhimailo<sup>b</sup>, Kenichi L. Ishikawa<sup>c</sup>, Kevin C. Prince<sup>a,\*</sup>, Giuseppe Sansone<sup>c</sup>, Kiyoshi Ueda<sup>d</sup>

<sup>a</sup>*Elettra Sincrotrone Trieste, 34039 Basovizza, Italy*

<sup>b</sup>*Lomonosov Moscow State University, Moscow 119991, Russia*

<sup>c</sup>*University of Freiburg, Physikalisches Institut, Albert-Ludwigs-Universität Freiburg, 79106 Freiburg, Germany*

<sup>d</sup>*Institute of Multidisciplinary Research for Advanced Materials, Tohoku University, Sendai 980-8577, Japan*

<sup>e</sup>*Graduate School of Engineering, The University of Tokyo, 7-3-1 Hongo, and Bunkyo-ku, Tokyo 113-8656, and Research Institute for Photon Science and Laser Technology, The University of Tokyo, 7-3-1 Hongo, Bunkyo-ku, Tokyo 113-0033, Japan*

---

## Abstract

Short wavelength Free-Electron Lasers (FELs) are the newest light sources available to scientists to probe a wide range of phenomena, with chemical, physical and biological applications, using soft and hard X-rays. These sources include the currently most powerful light sources in the world (hard X-ray sources) and are characterised by extremely high powers and high transverse coherence, but the first FELs had reduced longitudinal coherence. Now it is possible to achieve good longitudinal coherence (narrow bandwidth in the frequency domain) and here we discuss and illustrate a range of experiments utilising this property, and their underlying physics. The primary applications are those which require high resolution (for example resonant experiments), or temporal coherence (for example coherent control experiments). The currently available light sources extend the vast range of laboratory laser techniques to short wavelengths.

*Keywords:* FELs, AMO, short-wavelength coherence.

*2010 MSC:* 78A60, 81V45

*PACS:* 41.60.Cr

---

## Contents

<b>1</b>	<b>Introduction</b>	<b>3</b>
1.1	Historical background of FEL sources . . . . .	3
1.2	Introduction to Atomic, Molecular and Optical science with FELs . . . . .	5
1.3	Role of transverse and longitudinal coherence. . . . .	7
<b>2</b>	<b>Methods</b>	<b>7</b>
2.1	Seeded soft X-ray and XUV FELs. . . . .	7
2.2	Self-seeded soft and hard X-ray FELs. . . . .	9
2.3	Alternative light sources. . . . .	10
<b>3</b>	<b>Optical experiments with FELs</b>	<b>10</b>
3.1	SASE FELs as pumps for fully coherent X-ray FELs . . . . .	10
3.2	Superfluorescence and related phenomena . . . . .	11

---

\*Corresponding author

*Email addresses:* carlo.callegari@elettra.eu (Carlo Callegari), grum@sinp.msu.ru (Alexei N. Grum-Grzhimailo), ishiken@n.t.u-tokyo.ac.jp (Kenichi L. Ishikawa), kevin.prince@elettra.eu (Kevin C. Prince), giuseppe.sansone@physik.uni-freiburg.de (Giuseppe Sansone), kiyoshi.ueda@tohoku.ac.jp (Kiyoshi Ueda)

<b>4</b>	<b>Few photon, single ionization</b>	<b>12</b>
4.1	Brief introduction to photoionization . . . . .	12
4.2	One-colour, two-photon ionization . . . . .	13
4.3	XUV/X-ray + Near Infrared ionization and Circular Dichroism . . . . .	14
4.4	Orbital Angular Momentum . . . . .	16
4.5	Towards two-dimensional XUV spectroscopy . . . . .	16
4.6	Coherent control of one-colour ionization via biharmonic ionization . . . . .	17
4.7	Experimental determination of optical phase . . . . .	19
4.8	Photoemission time delay . . . . .	19
4.9	Generation and characterization of attosecond pulse trains . . . . .	20
<b>5</b>	<b>Few-photon sequential multiple ionization</b>	<b>24</b>
5.1	Early studies . . . . .	24
5.2	Complete experiments on Ne . . . . .	24
5.3	The role of autoionizing resonances in double ionization . . . . .	25
5.4	Single-photon Laser Enabled Auger Decay . . . . .	26
5.5	Two-photon excitation leading to interatomic Coulombic decay . . . . .	27
5.6	Multiphoton XUV + Near Infrared ionization and Circular Dichroism . . . . .	29
5.7	Two-photon, double core ionization . . . . .	29
<b>6</b>	<b>Multi-photon and multiple resonant excitation</b>	<b>30</b>
6.1	Two-photon excitation of two electrons in atoms: Early studies . . . . .	30
6.2	Two-photon excitation of two electrons in atoms: Narrow-band studies . . . . .	31
6.3	Two-photon excitation of two electrons in dimers . . . . .	31
6.4	Multi-photon, site-specific, multiple excitation of clusters and droplets . . . . .	32
<b>7</b>	<b>Pump-probe studies</b>	<b>32</b>
7.1	The dynamics of photo-excited thymine . . . . .	33
7.2	Photo-excited acetylacetone . . . . .	33
7.3	Isomerization of thiophenone . . . . .	34
7.4	Dynamics of photo-excited He droplets . . . . .	35
<b>8</b>	<b>Theoretical approaches</b>	<b>35</b>
8.1	Amplitudes and description of physical quantities . . . . .	35
8.2	Time-dependent Schrödinger equation (TDSE) . . . . .	36
8.3	Solution of the TDSE on the space-time grid . . . . .	37
8.4	Expansion methods . . . . .	37
8.5	Perturbation theory . . . . .	39
8.6	Strong-field-type approximations . . . . .	40
8.7	Density matrix approach . . . . .	40
8.8	Real-time <i>ab initio</i> simulations: Time-dependent multiconfiguration self-consistent-field method . . . . .	41
8.9	Theoretical proposals for XFEL experiments . . . . .	43
<b>9</b>	<b>Perspectives</b>	<b>45</b>
<b>10</b>	<b>Appendix: List of symbols</b>	<b>47</b>
<b>11</b>	<b>Acknowledgements</b>	<b>48</b>

## 1. Introduction

Free-Electron Lasers are modern light sources which use high energy beams of electrons moving in vacuum to generate radiation. Although there are many such sources producing infrared light, in this paper we focus on those producing ionizing radiation, that is, wavelengths from the Extreme Ultraviolet (XUV; 124–10 nm) to soft and hard X-rays (<10 nm).

### 1.1. Historical background of FEL sources

The interaction of light with matter is governed by the Einstein coefficients, which describe the spontaneous emission, absorption and stimulated emission of light. Einstein's recognition of the importance of stimulated emission was the basis for the invention (much later) of the maser (Gordon et al., 1954, 1955) and laser (Schawlow and Townes, 1958; Maiman, 1960). In atoms, molecules, and solids the electrons involved in the lasing process are all bound in specific orbitals or bands, that is, they reside in a strong electromagnetic field. The wavelengths which such lasers can emit is limited by the quantum transitions which are possible, so that it is not possible to tune over wide ranges. Long ago it was recognised that stimulated emission may occur in free electrons, that is, electrons moving in vacuum. The word "free" is perhaps slightly misleading, as an electron moving in field-free space cannot be stimulated to emit radiation. Rather, the electron is free in the sense that it is not confined to an atom or molecule but moves in an external field. Microwave devices, such as klystrons, are mostly based on electric fields, whereas short-wavelength devices are generally based on relativistic particle accelerator technology, where high-energy electrons are deflected, focused, and guided by magnetic fields. Since the electron energy and magnetic fields can be tuned continuously, the idea of using light from free electrons travelling through a periodic magnetic structure (Ginzburg, 1947; Motz, 1951) offered the possibility of a light source with continuously tunable wavelength (Motz et al., 1953). Let us note that because of the methods used to produce and accelerate the electrons, the latter are not uniformly distributed, but rather are grouped in packets ("bunches"). A strong distinction must be made between microwave emission at one end (where the bunch size can be externally controlled, and be shorter than the radiation wavelength) and X-rays at the other end (where the bunch size is much longer than the radiation wavelength). In the latter case one generally ignores the finite length of the bunch, and analyzes the periodic grouping of the electrons *within* the bunch. This grouping, which grows as part of the amplification process, is termed "microbunching" (Yu, 1984), and the short form "bunching", is a confusing but accepted terminology. Motz (1951) recognized the importance of pre-bunching to make the radiation coherent, and even analyzed the case of an electron moving through an electromagnetic wave traveling in the opposite direction, but did not consider the process of stimulated emission and the associated bunching growth. This was later done by Madey (1971), who is generally credited as the father of the Free-Electron Laser; an analysis of the formal equivalence of the spontaneous and stimulated emission from electrons in atoms and that from quasifree electrons was later done by Friedman et al. (1988).

There exist several reviews of the history of Free-Electron Lasers: Colson and Sessler (1985) trace the evolution of free-electron sources back to the 1940s, from non-relativistic electron tubes, and list a number of schemes suitable for long-wavelength operation (down to  $\sim 5000 \text{ \AA}$ ). Madey (2014) gives a personal account of how short-wavelength free-electron lasers are the result of a cross fertilization between the fields of electron tubes, masers/lasers, and particle accelerators, and borrow fundamental concepts from all these fields. The considered electron energies varied over a broad range, hundreds of keV to hundreds of MeV; modern FELs all utilise electron beams of GeV energies, and are thus highly relativistic devices (we recall that the rest energy of the electron is 0.511 MeV); a non-relativistic precursor – the "ubitron" – was built by Phillips (1960, 1988).

Just as for optical lasers, long-wavelength FELs can be classified as oscillators or amplifiers, depending on the presence or absence of a resonant cavity (Colson and Sessler, 1985). Early FELs were conceived as low-gain amplifiers (Madey, 1971; Madey et al., 1973) and later as oscillators, for wavelengths where mirrors were available. The efficiency and tunability were seen as promising characteristics, and applied research on single-pass FELs was carried out, for example by the United States Office of Naval Research (Roberson and Sprangle, 1989a).

The coherence properties of FELs were immediately recognised as important, and at long wavelength longitudinal coherence was not difficult to attain. There was clearly great interest in FELs as sources for short wavelength ranges, where no convenient alternatives were available; high harmonic generation from FELs operating as single-pass amplifiers was recognized as a means of overcoming the limitations of mirrors in the UV region and beyond (Colson, 1981; Colson et al., 1985). Kondratenko and Saldin (1979, 1980) proposed a single-pass amplifier (in the infrared)

starting from noise, and Murphy and Pellegrini (1985) extended the concept to soft X-rays. The process is called Self-Amplified Spontaneous Emission (SASE), and implies exponential growth up to saturation; this was observed at 530 nm by Milton et al. (2000, 2001). The first successful demonstration of production of XUV radiation was the TESLA Test Facility (TTF) VUV-FEL (Ayvazyan et al., 2002), which later evolved into FLASH (Ayvazyan et al., 2006). Abandoning the use of a cavity and/or pre-bunching of the electrons, made the property of longitudinal coherence secondary: as remarked in the review work of Bonifacio et al. (1990a) the initial intensity is linearly proportional to the electron current, i.e., the radiation is incoherent. We will elaborate this aspect below; for now we note that for this reason, longitudinal coherence has not been a distinctive feature of short-wavelength (SASE) FELs, and of the experiments performed with them, until the advent of seeded sources, which are the subject of this review.

In this context, what we call “FEL spontaneous emission” is exactly the same as the synchrotron radiation produced by an undulator, with the difference that in the latter case the back-action of the radiation on the electrons is negligible, i.e., there is no amplification: the spectro-temporal properties of synchrotron radiation are determined by the incoherent sum of the emission of the single electrons in the bunch. In the rest frame of the electrons, one can see synchrotron radiation as the pseudo-radiation field of the moving magnetic structure (“undulator”) being reflected by the electron, through Compton back-scattering.

For a discussion of the most important formulas, it is useful to introduce some physical quantities:  $c$  is the speed of light,  $m_e$  the rest mass of the electron,  $\lambda_u$  and  $B_0$  the undulator period and the peak magnetic field on the undulator axis in the laboratory frame,  $\mathcal{E}$  the electron beam energy,  $\gamma = \mathcal{E}/(m_e c^2)$  the associated Lorentz factor,  $\gamma_{\parallel}$  the Lorentz factor in the forward direction. In the laboratory frame the radiation peaks at a wavelength  $\lambda_s = \lambda_u/(2\gamma_{\parallel}^2)$ ; the relation can be interpreted as the Lorentz-FitzGerald contraction of the undulator period in the rest frame of the electrons *and* of the radiation emitted in the forward direction in the laboratory frame.

Alternatively, one can observe that the electrons have a forward velocity  $v_{\parallel} < c$ , and see the resonance condition as that for which they lag the radiation by one unit of  $\lambda_s$  per undulator period, i.e.,  $\lambda_u(c - v_{\parallel})/v_{\parallel} = \lambda_s$ , noting that  $(c - v_{\parallel})/v_{\parallel} \approx (c - v_{\parallel})/c \approx 1/(2\gamma_{\parallel}^2)$ . This condition is technically known as “slippage”, and the total slippage length ( $N_u \lambda_s$ , with  $N_u$  the number of undulator periods) defines the maximum separation between two electrons such that their respective emission can still overlap in time (i.e., interfere); thus the slippage length is important in discussing the longitudinal coherence of the pulse. In the presence of gain, it is replaced by the shorter cooperation length.

The resonance condition can be tuned either by changing the electron beam energy, or by changing the amount of energy transferred into the transverse direction, via the strength of the undulator field. Both methods have their advantages and disadvantages. The former is more complicated in that the electron accelerating cavities and transport optics have to be tuned; the latter in that it requires variable-gap undulators, which are mechanically demanding. Nevertheless, the latter solution is generally more flexible, also in terms of controlling the polarization of the radiation (Sasaki, 1994). It is convenient to introduce an *undulator parameter*  $K = eB_0 \lambda_u / (2\pi m_e c)$ ; the resonance condition becomes  $\lambda_s = \lambda_u(1 + K^2/2)/(2\gamma^2)$  (see, e.g., Attwood and Sakdinawat, 2016). The fractional bandwidth of this radiation is of order  $1/N_u$ ; the rms angular divergence and source size are respectively of order  $\sqrt{\lambda_s/(2\lambda_u N_u)} \approx \frac{1}{2\gamma} \sqrt{\frac{1+K^2/2}{N_u}}$  and  $\sqrt{\lambda_s \lambda_u N_u/2}$ , i.e., their product is diffraction-limited ( $\sim \lambda_s$ ; Kim et al., 2017).

Let us now discuss the back-action of the radiation on the electrons, i.e., the amplification: Bonifacio et al. (1990a) explain that in the presence of a radiation field of wavelength  $\lambda \approx \lambda_s$ , electrons at the resonant energy remain in phase with the radiation, with which they interact undergoing either absorption or stimulated emission according to the value of their phase. This implies that for a monoenergetic electron beam, with uniformly distributed (random) phase, the net gain will be zero; this is however a condition of unstable equilibrium, and random fluctuations that fall within the gain bandwidth will be amplified. In the low-gain condition, the resulting FEL equations are the same as those describing a simple pendulum (Colson, 1977; Bonifacio et al., 1990a; Seddon et al., 2017; Kim et al., 2017). The exact treatment of FEL gain is instructive but lengthy and complex (Kim et al., 2017), and we will mention here some simplified results of interest for longitudinal coherence; in a 1-dimensional model one studies the evolution of the phase-space of an initially uniform (in space and in a narrow energy band) distribution of electrons; we note that the phase relative to the radiation field is customarily used as the spatial coordinate. In the low-gain initial phase, the first departure from uniformity is an energy modulation at the resonant wavelength, whereas the spatial density remains initially constant (to first perturbation order), but is then driven to grow by the energy modulation; seeded FELs are based on the concept that an initial energy modulation much stronger than that driven by spontaneous emission can be imprinted onto the electron bunch. It is important to remark that the emitted intensity contains a term that scales with

the square of the number of electrons in the bunch,  $N_e^2$ , times the absolute square of the “bunching factor”, defined as the Fourier coefficient of the electron density modulation at the resonant frequency of the amplifier.

The cooperation length (defined as the slippage length accrued over one gain length) versus the length of the electron bunch directly determines the coherence properties of the radiation. Note that (as for undulator radiation in synchrotrons) relativistic effects confine the emitted light to a forward cone of aperture  $1/\gamma_{||}$ , and that leading electrons that are spatially separated by more than the slippage length cannot be reached by the light emitted by trailing electrons, so they emit as independent sources. Thus, the shape in both time and wavelength of a SASE pulse from a long electron bunch is the incoherent sum of a set of spikes (Bonifacio et al., 1994; Yu et al., 2003; Penco et al., 2015); the coherence properties of SASE FELs have been discussed by Saldin et al. (2008), and references therein. In the hard X-ray region, short, intense pulses are obtained by passively restricting below the cooperation length the portion of the emitting electrons (Coffee et al., 2019).

External seeding is an alternative approach to manipulating the electron bunch, and we will discuss in Section 2.2 the concept of self-seeding, i.e., amplifying a monochromated (or cleaned-up) pulse from a SASE FEL in a second stage of undulators. Historically, the concept of seeding has been associated with that of High Gain Harmonic Generation (HGFG, Section 2.1) This scheme (Yu, 1991; Bonifacio et al., 1990b; Yu et al., 2000, 2003) is based on the concept of introducing, by interaction with a seed laser in a first, dedicated, undulator (the modulator) a small energy modulation of the electron beam, see Fig. 1. This is then converted into a spatial modulation, via a magnetic chicane (dispersive section), and the modulation contains the fundamental seed frequency and – with progressively smaller coefficients – its higher harmonics. A second undulator (the radiator) tuned to the desired harmonic causes emission and exponential amplification of that harmonic, with “a single phase determined by the seed laser, and [a] spectral bandwidth [which] is Fourier transform limited.” (Yu et al., 2000). Yu et al. explicitly mentioned the excellent temporal coherence of the resulting pulses, and the fact that “the output properties at the harmonic wavelength are a map of the characteristics of the high-quality fundamental seed laser. This results in a high degree of stability and control of the central wavelength, bandwidth, energy, and duration of the output pulse.” (Yu et al., 2000). The first demonstrations of the HGFG scheme were done at far- or near-IR seed wavelengths (Yu et al., 2000, 2003); Feldhaus et al. (2005) reviewed externally seeded and self-seeded FELs, concentrating on the machine physics aspects. When that paper was written, seeding had been demonstrated at optical and UV wavelengths, with few if any applications. Then, in 2012 the FERMI FEL1 (Allaria et al., 2012a) became the first short-wavelength, externally seeded facility open to users.

Several recent reviews have covered Free-Electron Lasers and their role as instruments for research: Seddon et al. (2017) have provided a wide-ranging overview of the physics of FELs, beamline and diagnostics design, and a very wide range of applications, including crystallography and high energy density matter. Bostedt et al. (2009) summarised experiments at the FLASH FEL in Hamburg, while Coffee et al. (2019) discussed ultrafast X-ray techniques at the Linac Coherent Light Source, concentrating on instrumental aspects.

In the present work, we concentrate on applications of longitudinally coherent and narrow bandwidth light, to atomic, molecular and cluster systems. The narrow resonances and line widths of atomic and molecular systems find many uses for narrow bandwidth light. We will not discuss results in the fields of coherent diffractive imaging, warm dense matter, and will say little about condensed matter studies with FELs.

## 1.2. Introduction to Atomic, Molecular and Optical science with FELs

Atomic, molecular and optical (AMO) physics is a branch of science in which it is possible to study phenomena at their most fundamental level and with very high precision. Einstein developed his interpretation of Planck’s constant and quantization by recognising the similarity of radiation in a box to a gas, and analysing the energy and entropy (Einstein, 1905). Quantum mechanics evolved further based on the study of atomic spectra; for example, the concept of the fine-structure constant, developed by Sommerfeld (1916a,b), arose from the interpretation of atomic spectra, which are still used today for high precision measurements.

It is therefore no surprise that AMO physics was a leading field of research in the early development of laboratory lasers, for example to study dynamical phenomena in molecules, for which Ahmed Zewail was awarded the Nobel Prize in Chemistry in 1999 (Zewail, 2000). Now AMO is a field of intense activity for the newest light sources, i.e., short-wavelength Free-Electron Lasers, as seen in a series of recent review articles (Berrah et al., 2010; Ullrich et al., 2012; Yabashi et al., 2013; Feldhaus et al., 2013; Bostedt et al., 2016; Seddon et al., 2017; Meister et al.,

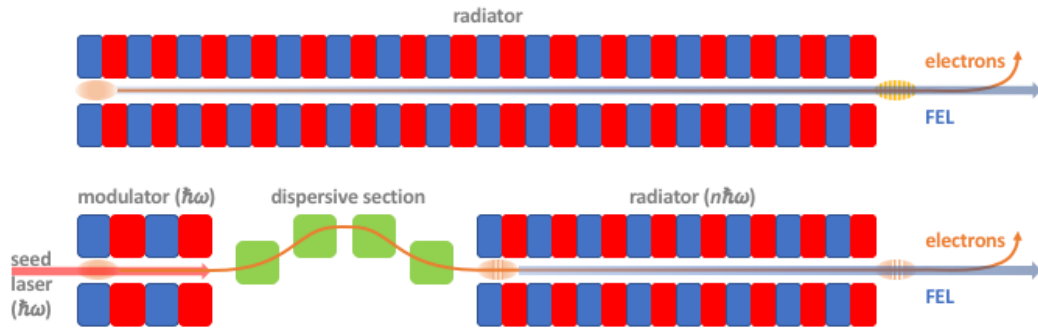


Figure 1: Schematic of a SASE FEL (top) and a seeded FEL (bottom). Although not to scale, the figure reflects the fact that a seeded FEL radiator is generally much shorter, and that only the central portion of the electron bunch, that has interacted with the seed laser, develops significant microbunching.

2020; Fukuzawa and Ueda, 2020). Some of the phenomena studied by optical lasers can now be studied at XUV and X-ray wavelengths, but it is also possible to observe new phenomena. One factor leading to new physics at short wavelengths is that when core levels are excited, they have an additional decay channel not available for low energy excitation, namely Auger decay. A second reason is that the ponderomotive shift for high fields and long wavelengths is very large and dominates the physics (see Section 8.6, Strong Field Approximations). At short wavelengths, the ponderomotive shift may become negligible and a different description is required.

The field of attosecond physics is growing rapidly, and many experiments are carried out on atoms and molecules, thereby avoiding various complications associated with condensed matter. The Fourier limit implies that an attosecond pulse of long wavelength radiation has a very broad frequency distribution on the scale of molecular excitations. However a Fourier transform limited attosecond X-ray pulse can have a bandwidth comparable, for example, to the (Auger decay) lifetimes of core holes, permitting high resolution spectroscopy.

Multiphoton processes are an important class of non-linear optical experiments, and only became possible with the invention of the laser. They have been explored for many years at long wavelengths, for example to ionize molecules by the absorption of many photons of the same colour, or of photons of different colour. The process may be non-resonant, occurring via virtual intermediate states, or resonant, with a much higher cross section due to the resonances; this is a standard technique in laboratory laser optics, known as REMPI [Resonance Enhanced Multi Photon Ionization; Zandee and Bernstein (1979) and references therein]. The process has been studied and widely used in FEL experiments, e.g., Young et al. (2010); Rudek et al. (2012), but there is an important experimental difference with respect to long wavelengths. At short wavelengths, it is often possible to ionize a target more than once by consecutive single photon processes, and when this situation occurs, the process is described as sequential multiphoton ionization, to distinguish it from processes requiring the absorption of two or more photons simultaneously. Generally, when the two processes are in competition, the sequential process dominates, as single-photon processes generally have higher cross sections than multi-photon processes.

The narrow bandwidth and high intensity of laboratory lasers has often been used to control the outcome of a photochemical or photophysical event, for example the momentum of the ejected products, or ratio between the products. Both light and matter are described by waves which have an amplitude and a phase, and the light properties can be imprinted on atoms, to manipulate the outcome of an interaction. Generally these methods require fully coherent light in both the transverse and temporal domains. While optical lasers have long demonstrated these characteristics, only recently has fully coherent FEL light become available, and in this review we describe some of the ongoing experiments. The techniques may use temporally overlapping, mutually coherent wavelengths; a single wavelength split into temporally separated pulses with controlled phase; or other optical arrangements.

Because of the short time structure of pulsed lasers, they have been instrumental in studying the dynamics of matter after absorption of a photon. The advantage of FELs with respect to laboratory sources for valence ionization studies is a very large increase in signal-to-noise, and a wider spectral range. FELs can also photoionize core levels for femtosecond dynamics studies, and have enough intensity to perform core level photoelectron spectroscopy, which has not been demonstrated with other sources. In this case, coherence is not the primary concern, but rather a sufficiently

narrow bandwidth to provide good resolution.

### 1.3. Role of transverse and longitudinal coherence.

Radiation is transverse coherent when the electric field at two points across a wavefront have a fixed and well-defined phase relationship. The concept arose from Young’s slit diffraction experiments and is now widely applied in other fields. Mathematically, the degree of coherence is described by the correlation function  $g^{(1)}$ , and measures amplitude-amplitude correlations. Most Free-Electron Lasers produce radiation with a high degree of transverse coherence, which is important for applications such as Coherent Diffractive Imaging (Miao et al., 2015).

Longitudinal or temporal coherence relates to the phase relation of a wave at a given point and at different times. If the phase is perfectly periodic at that point, then the wave is temporally coherent. Thus in the frequency domain, temporally coherent light has a single frequency (or narrow band of frequencies), i.e. it is monochromatic. Temporally incoherent light consists of a large range of frequencies, and so has a large bandwidth. The degree of coherence of a beam is not a constant, but can be varied, for example by spatial or frequency filtering. Free-Electron Lasers based on SASE have rather low degrees of temporal coherence, which hinders high resolution spectroscopy. In this review, we will concentrate on experiments and applications where the degree of longitudinal coherence (or monochromaticity) of the light played a significant role. In the following sections, we give a brief description of the types of applications where this property is important, and what other properties of FELs are important.

## 2. Methods

Most FELs operating in the world today are based on the Self Amplified Spontaneous Emission (SASE) process, Table 1, and all of the FELs in this Table are based on SASE except FERMI and DCLS. As described above, in the SASE process, radiation is initially generated incoherently as the electron pulse passes through an undulator. For seeded FELs (FERMI and DCLS), the accelerator functions as an amplifier and wavelength shifter, so that the light has a naturally narrow bandwidth, and inherits the properties of the seed laser.

Name	starting year	wavelength (nm)	pulse duration (fs)	rep rate	References
FLASH	2005	4.2–52	30–200	1 Hz–1 MHz	(Ayvazyan et al., 2006)
FLASH2	2016	4–90	<10–200	1 Hz–1MHz	(Faatz et al., 2017)
LCLS	2009	0.11–6.2	<10–250	120 Hz	(Emma et al., 2010)
LCLS-II	[late 2020]	[0.05–6.2]	[30]	[120 Hz–1 MHz]	(Raubenheimer, 2018)
SCSS*	2008	50–60	30–100	10–60 Hz	(Shintake et al., 2008)
SACLA (HX)	2012	0.062–0.31	2–10	30–60 Hz	(Ishikawa et al., 2012)
SACLA (SX)	2016	8.3–31	70	30–60 Hz	(Owada et al., 2018)
EuXFEL	2017	0.05–4.7	< 100	27 kHz	(Tschentscher et al., 2017)
SwissFEL	2017	0.1–5	1–20	100 Hz	(Decking et al., 2020)
PAL	2017	0.083–0.56; 1–6.2	25; 80	10, 30, 60 Hz	(Milne et al., 2017)
FERMI, FEL1	2012	20–120	35–80	50 Hz	(Kang et al., 2017)
FERMI, FEL2	2016	4–20	5–35	10; 50 Hz	(Allaria et al., 2012a)
DCLS	2018	50–150	100–1000	20 Hz	(Allaria et al., 2013b)
Shanghai SXFEL	[late 2020]	[2–24]	[50–200]	[10–50 Hz]	(Yong et al., 2019)
*Now upgraded and incorporated in SACLA (SX) as BL1 (Owada et al., 2018).					

Table 1: List of short wavelength FELs open to users. “Starting year” is the actual (or expected) year of opening to users. In the electronic version, click on the name of the FEL to follow the associated hyperlink.

### 2.1. Seeded soft X-ray and XUV FELs.

The FERMI FEL, or more accurately FELs (Allaria et al., 2012a, 2013b), are seeded and have shown remarkable flexibility and potential for development of novel operating modes (Giannessi et al., 2018; Gauthier et al., 2016b; Roussel et al., 2015). The first report of lasing was published in 2012 (Allaria et al., 2012a), and was followed

shortly after by the announcement of cascaded lasing, which produced soft X-ray emission at 10.8 nm (Allaria et al., 2013b). Later developments pushed the wavelength down to 4 nm and below, with significant pulse energies. The predictability of the seed pulses supported by established theory allows the reliable prediction of the temporal duration and saturation behaviour of the pulses (Finetti et al., 2017).

Due to the longitudinal coherence provided by the seed pulse, FEL pulses can be analysed shot-by-shot using the technique of SPIDER, which has been applied in the optical wavelength range (De Ninno et al., 2015). Note that the possibility of deducing from the optical seed pulse the phase of the FEL pulse is invaluable when characterizing the latter, and can be exploited to fine-tune its properties. Gauthier et al. (2015) compared the experimental measurements of the FEL spectrum as a function of the strength of the initial modulation with existing theory, and were able: to produce the first direct evidence of the full temporal coherence of the pulses; to retrieve the phase of the FEL pulse, showing the presence of a linear chirp introduced by the electron bunch; to use the linear frequency chirp of the seed laser to precisely cancel that from the electron bunch, thus attaining Fourier-transform-limited pulses (Fig. 2). The Figure is easily understood in the two limit-case scenarios of strongly-chirped pulse versus transform-limited (zero-chirp) pulse: the time behaviour of the pulse envelope only depends on the strength of the seed process (the instantaneous intensity of the seed laser scaled by the dispersive strength of the subsequent magnetic chicane) and develops into a set of maxima and minima corresponding to an instantaneous condition of optimal seeding or overseeding. For a dominating linear chirp, the time envelope is streaked onto the wavelength coordinate, and the pulse structure has the same appearance in wavelength as in time; for a Fourier-limited pulse, the spectrum corresponds to the interference of two or more pulses of the same carrier frequency, separated in time.

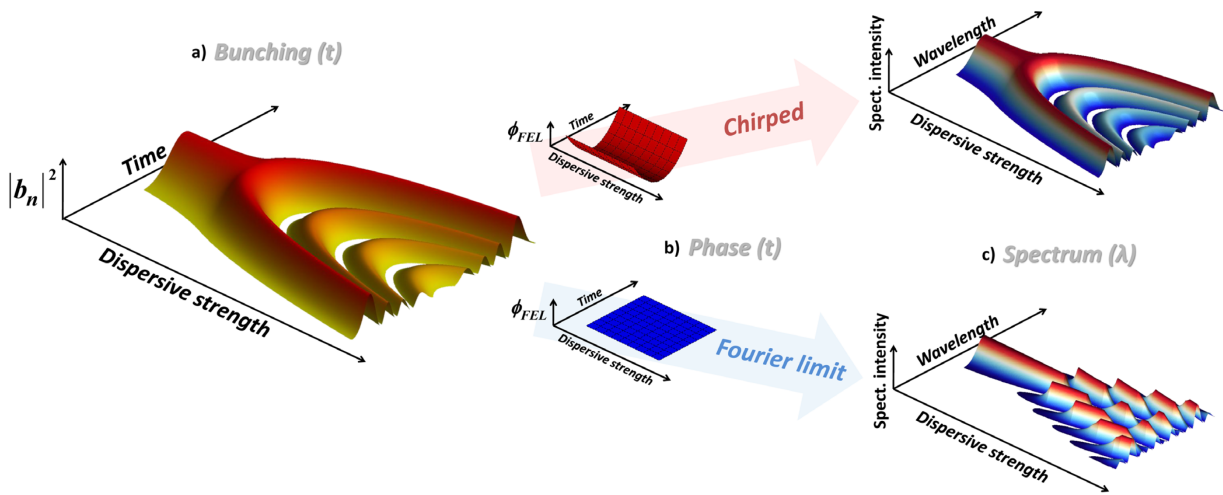


Figure 2: Simulated temporal FEL pulse shape (left) and FEL spectrum (right) as a function of the strength of the seeding process for strong linear chirp (middle, top) versus flat phase (middle, bottom). Figure reprinted from Gauthier et al. (2015), with permission. Copyright (2015) by the American Physical Society.

Importantly, since FERMI's inception, a number of developments of the sources, directly related to various seeding schemes, have permitted operation with: double pulses of the same wavelength (Gauthier et al., 2016a), or different wavelengths (Allaria et al., 2013a; Ferrari et al., 2016); single-seed multiple wavelengths (Roussel et al., 2015), and other variations. The machine physics results include the realisation of a proof-of-principle demonstration of chirped pulse amplification (Gauthier et al., 2016b), which is the state-of-the-art method for producing short intense pulses in optical and infrared lasers, as recognised by the award of the 2018 Nobel prize for physics (Mourou, 2019; Strickland, 2019). Novel ways of generating light have been demonstrated, in particular Echo Enabled Harmonic Generation (Rebernik Ribič et al., 2019) promises to provide shorter wavelengths with higher pulse energies and greater pulse-to-pulse stability. Another mode of operation is superradiance (Giannessi et al., 2013; Yang et al., 2020), which can provide pulses with durations below 10 fs, and higher peak power than normal operation.

Conceptually, the radiator section of a FEL consists of a single long undulator; in reality, the practical length of an undulator is typically much shorter than the gain length, and the radiator consists of a sequence of identical modules.



There are two technical reasons for using undulators shorter than the gain length. The electron beam is divergent, and has to be periodically refocused by magnets. Also there is a mechanical limitation due to the strong magnetic forces: it is difficult to attain sufficient rigidity over more than a few meters with forces of  $10^4$  Newton or more, corresponding to a few metres of magnets. For example, FEL-1 of FERMI consists of six identical 2.4 m modules separated by 1.3 m breaks (Allaria et al., 2012a; Diviacco et al., 2011). The need then arises to preserve the phase relationship between electron bunching and the emitted light between two modules. This is accomplished by the introduction within the gap of a short magnetic chicane (“phase shifter”; Diviacco et al., 2011) to slightly delay the electrons. This lengthens the path of the relativistic electrons with respect to the light by distances on the nm scale. The trimming of the delay is easily accomplished by setting the phase to maximise the FEL intensity, and it is reproducible, so that a lookup table can be created (Diviacco et al., 2011). Indeed, the fields produced in different modules need not be of the same polarization, and one can use the phase shifter to control the *vector sum* of the two fields, producing for example circularly polarized pulses from crossed linearly-polarized undulators, or vice versa (Ferrari et al., 2019). Note that this scheme remains valid for a coherence length shorter than the length of the pulse, and was first implemented at a synchrotron source (Bahrtdt et al., 1992); interestingly, it has also been applied for the production of polarized gamma rays (Yan et al., 2019). By further extension, one need not consider a single wavelength for all undulators: we will discuss in detail in sections 4.6 to 4.9 specific experiments which use a combination of two or more phase-locked harmonics generated in distinct undulators.

Feng and Deng (2018) provide a recent overview of the development of fully coherent FEL facilities in China. The Dalian light source is in operation at long wavelengths, and there are ambitious plans to build SXFEL, a seeded source in the soft x-ray region.

## 2.2. Self-seeded soft and hard X-ray FELs.

The considerable advantages of seeded FELs with respect to SASE suggest that this technique would be useful in the hard X-ray range as well as the soft X-ray range. However there is a lack of sufficiently intense and monochromatic X-ray sources to use as a seed, although FELs can be used indirectly, see Section 3.1. For now, external seeding cannot be applied, but an attractive alternative is to use self-seeding. The potential of self-seeding was recognised quite early (Feldhaus et al., 1997), but it took many years before it was implemented. The subject has been reviewed recently by Geloni (2016), and will be briefly summarised here. In self-seeding, SASE lasing is initiated, and then the electron and photon beams are separated: the electrons are deviated in a magnetic chicane while the photon beam is filtered. The photon beam is then recombined with the electron beam and acts as a seed.

This was first demonstrated in the hard X-ray region at the LCLS (Amann et al., 2012), based on a previously published scheme (Geloni et al., 2011). The resulting X-rays were near Fourier-transform limited, had a bandwidth of 0.5 eV at 9 keV, corresponding to a bandwidth reduction by a factor of 40–50 with respect to SASE. Soon after, self-seeding was demonstrated for soft X-rays (Ratner et al., 2015), using a monochromator.

The implementation of hard X-ray self-seeding is more complicated than this simple description suggests. If a conventional X-ray monochromator is used, the path length of the X-rays destined to act as seed is increased by centimetres, so the electron beam path must be increased by the same amount to ensure overlap on recombination. High energy electrons cannot be deflected easily, so the chicane needs to be tens of metres long, which is a severe technical limitation.

A solution to this problem is to substitute the monochromator, which is a bandpass filter, with a notch filter (Geloni et al., 2011). This counter-intuitive idea works because a broad pulse, from which a narrow band has been removed in the frequency domain, consists of a pulse with a monochromatic tail in the time domain. The wavelength of the tail or “wake” corresponds to the notch in the frequency domain. This structure arises primarily because of dynamical scattering in the diffraction process; the thickness of the crystal and the extinction length must be carefully optimised. In these calculations, the monochromatic wake appears at about 20 fs (or 6 microns in path length) after the main, multi-spike pulse. By using a very short electron pulse, with a duration of about 6 fs, it is possible to overlap this seed with the electron bunch, while the broad-band part of the seed pulse does not overlap, because it precedes the electron bunch.

Technically, this scheme is easy to implement. Thin diamond crystals (about 0.1 mm) diffract well and are resistant to the high thermal load of the FEL pulse. The crystal is set at the Bragg angle for the central energy of the SASE pulse, and reflects most of the X-rays in a narrow band out of the beam, but also creates the monochromatic tail.

The requirements on the chicane, which deviates the electrons so that they do not strike the diamond crystal, are much reduced, and it has three functions. It separates and recombines the electron and photon beams. It delays the electrons so that they now overlap the monochromatic wake of the photon beam; now the delay is of the order fs in the time domain or microns in path length. The third function of the chicane is to smooth out the micro-bunching in the electron beam, which was created by lasing during the creation of the seed pulse. If this is not done, the microbunched electrons continue to lase in SASE mode in the second stage.

In the soft X-ray region, this scheme is more difficult to implement, because of a lack of tunable notch filters. For this reason the first implementation of self-seeding used a conventional monochromator, and the beam was seeded with monochromatic light (Ratner et al., 2015). Soon after, an application was demonstrated in a near edge x-ray absorption fine structure experiment (Kroll et al., 2016), where the bandwidth of SASE pulses is generally too large to allow accurate measurements. This method of self-seeding has the drawback that a “pedestal” is created, that is, there is a broad background of other wavelengths. For experiments where only the monochromatic beam produces signal this is not problematic, but for experiments where the other wavelengths produce background signal, this is an issue (Marcus et al., 2019; Hemsing et al., 2019, 2020).

Since the development of self-seeding, the method has been applied at other light sources and there have been various other schemes reported to further improve self-seeding (Min et al., 2019; Emma et al., 2017; Inoue et al., 2019; Prat and Reiche, 2018; Halavanau et al., 2019). These rapid developments mean that X-ray beams of narrower bandwidth, shorter duration and higher peak power are becoming available at an increasing number of SASE FELs.

### 2.3. *Alternative light sources.*

Other light sources which could be used for some of the experiments described here are HHG and plasma sources. Comparisons have been made recently by Seddon et al. (2017) and Schoenlein et al. (2019) of X-ray FELs and other short wavelength sources. At long wavelength (ca. 100 nm, 12 eV), laboratory sources can provide good numbers of photons per pulse, but this declines rapidly for shorter wavelengths (ca. 10 nm, 120 eV; Fig. 3)

Optical lasers are based on the principle of creating a population inversion by pumping the lasing medium, and the upper state generally has a long lifetime. Thus the population can be built up over a period of time before lasing is initiated. It has long been a goal in photon science to create a coherent X-ray laser, but the technical difficulty is that all excited states at very short wavelength, which may potentially be used for lasing, have extremely short lifetimes, of the order of femtoseconds or less. Thus the population inversion cannot be built up over time by a weak source, but must be created in an extremely short time, i.e., a very intense source is required. This difficulty has now been overcome, adopting the approach of the old proverb “set a thief to catch a thief”, that is, use a laser to pump a laser.

At a wavelength of 20 nm (62 eV) Matthews et al. (1985) used a laser pulse to excite a thin film of selenium, and Wang et al. (2008) used similar methods at 13.9 (89 eV) and 18.9 nm (65.6 eV). At a wavelength of 18.2 nm (68 eV), a laser-induced plasma column was used to create the necessary population inversion to sustain stimulated emission (Suckewer et al., 1985). These papers and others demonstrated the principles of the techniques, and have been reviewed (Suckewer and Jaeglé, 2009). The light produced is significantly less bright than that of FELs, and being based on atomic resonances, it is not tunable. However these methods have the considerable advantages of being laboratory based and cheaper than large facilities. In some cases, for example when the signal is a linear function of the pulse energy, experiments are possible even with pJ pulse energies (Kleine et al., 2019; Bhattacharjee et al., 2017)

## 3. **Optical experiments with FELs**

### 3.1. *SASE FELs as pumps for fully coherent X-ray FELs*

The XUV laboratory lasers mentioned in the last section used optical lasers to pump a medium and create a population inversion, which then lased. It is also possible to use a SASE FEL to pump a medium which then lases in the soft or hard X-ray regions. Rohringer et al. (2012) used intense soft X-ray pulses from the Linac Coherent Light Source to produce X-ray lasing at the wavelength of 1.46 nm (849 eV). The FEL pulses ionized Ne 1s core levels, which have a lifetime of 2.4 fs and normally undergo Auger decay as the main de-excitation mechanism, with fluorescence a much weaker channel. However the FEL pulses had sufficiently high intensity and short duration to create a high enough population of core ionized states, providing the necessary population inversion and leading to

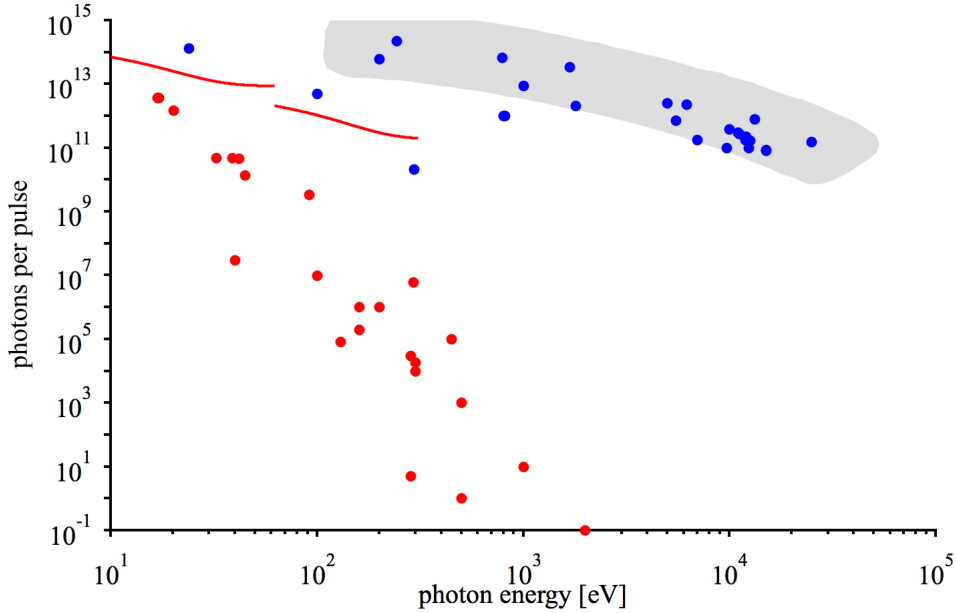


Figure 3: Typical numbers of photons per pulse for FERMI FELs 1 and 2 (red lines), soft and hard x-ray FELs (blue markers and laser driven HHG sources (red markers). The shaded area is derived from the data of Seddon et al. (2017). The FEL data are from FLASH, LCLS, PAL-FEL, SACLA, SwissFEL, EuXFEL: references in Table 1 or the respective webpages. Even for a fixed photon energy and machine, the actual pulse energies will vary over a range depending on machine parameters, pulse duration, and other factors. The HHG data are from Chen et al. (2010); Cousin et al. (2014); Ding et al. (2014); Feng et al. (2020); Hong et al. (2012, 2014); Nayak et al. (2018); Rudawski et al. (2013); Seres et al. (2006); Takahashi et al. (2002); Teichmann et al. (2016); Wang et al. (2018); Zhang et al. (2018), and aim to show the state-of-the-art for various ranges of wavelengths. Note that some of the vertical scatter in the data is due to the range of bandwidths used to report the data in the original work, and to the varying repetition rates. As a rule of thumb, for a given wavelength the energy per pulse scales inversely with the repetition rate: see for example Heyl et al. (2016).

lasing. The efficiency is far below 100% so the reader may ask why one would create a much weaker laser pulse than the FEL pump pulse. The point is that the FEL is very intense, but is created by the SASE process; it is a laser if one defines the term to mean a device with a very large number of photons per unit phase space and time. It has poor longitudinal coherence, and the statistical properties of a chaotic source (Gorobtsov et al., 2018), whereas a true laser pulse is fully coherent, according to the definition of Glauber (1963), and among other things, has different statistical properties. The pulse created in the experiment of Rohringer et al. (2012) has narrow bandwidth, and is a laser pulse according to this definition.

Lasing has also been achieved at 0.15 nm (8 keV), using the SACLA FEL as the pump (Yoneda et al., 2015). In this case, FEL radiation was focused to a 120 nm spot on a 20 micron thick copper target. The pump radiation was bichromatic, consisting of a pump wavelength of 0.14 nm which ionized the Cu 1s shell, and a seed pulse tuned to Cu  $K\alpha_1$  or Cu  $K\alpha_2$ . Thus the setup functioned as an amplifier rather than an oscillator. The radiation produced had a narrower line width, and higher density of photons in phase space than the FEL radiation used as pump.

### 3.2. Superfluorescence and related phenomena

There have been optical experiments at FELs which involve coherence and population inversion, but do not result in lasing. Nagasono et al. (2011) and Harries et al. (2018) investigated superfluorescence and other phenomena by performing experiments in which He was irradiated by strong SASE radiation. In the first experiment, ground state He was excited to the 1s3p Rydberg state. This can decay spontaneously by fluorescence to the ground state, or to the 1s2s state by emitting a photon of wavelength 501.6 nm. If however the number density of excited states (denoted  $\rho$ ) is sufficiently high, they interact and a new decay channel opens. This is termed superradiance, superfluorescence or collective spontaneous emission, and the condition for the process to occur is that the mean distance between atoms is less than the wavelength of the emitted radiation. Superfluorescence of an excited state population is manifested with

a characteristic delay between excitation and emission, is strongly directional, has an intensity proportional to  $\rho^2$ , and the emitted pulse has a temporal duration proportional to  $\rho^{-1}$ . All of these signatures were observed, confirming that the superfluorescence mechanism was operative.

Harries et al. (2018) irradiated He gas with light of central wavelength 24.3 nm (51.0 eV), again with SASE radiation. All photons ionize the gas, and those photons with a wavelength of exactly 24.302 nm excite the He<sup>+</sup> 1s ions to He<sup>+</sup> 4p states. These may decay, as above, by superfluorescence, but the authors observed other phenomena in addition. They assigned emission at 469 and 164 nm to cascade superfluorescence, at 30.4 nm to yoked superfluorescence, and at 25.6 nm to free induction decay.

These experiments were carried out using SASE light, which is of course not narrow bandwidth radiation. However the sample itself acted as a filter, as the resonances were very narrow; clearly narrow bandwidth radiation would make the experiments easier.

## 4. Few photon, single ionization

### 4.1. Brief introduction to photoionization

In the previous Section, optical experiments with FEL light were described. In this and the following Sections, we describe experiments based on photoionization, one of the most important methods used in soft X-ray experiments. Photoionization (the photoeffect) dominates photon interaction with matter in the XUV and soft X-ray domain, because the cross sections are much greater than those of elastic and inelastic photon scattering. The advantage of photoelectron spectroscopy, compared with other techniques, is that it is fast, and “photographs” the target on a time scale of a few attoseconds or femtoseconds. Other methods, such as ion spectroscopy or optical fluorescence, usually have time scales of picoseconds or nanoseconds, and so are much slower. The ultrafast nature of photoelectron spectroscopy is therefore very compatible with the femtosecond time structure of FELs.

In photoionization, one or more photons are absorbed by a target, and one or more electrons are ejected. The simplest case is of a single photon ejecting a single electron into the continuum, and Section 7 describes pump-probe experiments, in which an excited target is singly photoionized by one photon. In the present Section we will discuss several examples of experiments on targets in their ground state, with emission of a single electron by one or a few photons.

In other experiments, absorption of two or more photons can lead to the emission of two or more electrons. Short wavelength FELs produce radiation which is very often above the first ionization potential of the sample being studied, and is intense. This leads to the situation that sequential ionization dominates ionization by simultaneous absorption of two photons. Some cases of sequential ionization are examined in Section 5.

An important phenomenon in photoionization is resonant photoemission. If an electron or electrons are excited to states in the continuum, and there is no resonance, the outgoing electron waves are described simply by angular momentum selection rules, and the cross section varies smoothly. If there is a resonant, or quasi-bound, state embedded in the continuum, the cross section may vary rapidly with photon energy and the state may be subject to autoionization. Resonances have been studied for their own intrinsic interest, and also to gain access to other phenomena: we discuss some examples in Section 6. Here we give a brief introduction to autoionization, the emission of an electron following resonant excitation. For historical reasons, the term autoionization has been mostly used to describe phenomena at low energy, such as the decay of neutral, valence excited states. However autoionization includes Auger or Resonant Auger processes, in which an ion or neutral with a core hole decays; Interatomic Coulombic Decay, Sections 5.5 and 6, is also in this class.

Autoionization is among the most prominent manifestations of electronic correlation in atomic and molecular physics and indeed a seminal paper on autoionization by Fano (1961) has been cited more than eight thousand times. The interference between direct photoionization and time-delayed decay of a quasi-bound state in the continuum strongly affects the cross section and angular distributions of photoelectrons. These states have been widely investigated in the spectral domain (Beutler, 1935; Madden and Codling, 1963; Madden et al., 1969; Codling and Madden, 1971; Maeda et al., 1993; Sorensen et al., 1994; Domke et al., 1995, 1996) and temporal domain (Wang et al., 2010; Ott et al., 2013, 2014; Kotur et al., 2016; Gruson et al., 2016; Kaldun et al., 2016; Cirelli et al., 2018).

The excited state embedded in the continuum may have two electrons in excited orbitals, i.e., it is a doubly excited state. In the autoionization process, one of these electrons is emitted while the other is de-excited. In this case, initial

state correlation plays an important role in the excitation of the system from the ground state to the autoionizing state by single photon absorption. Employing two-photon absorption, however, one can access such doubly excited states rather straightforwardly. Autoionizing doubly excited states in atoms, dimers and clusters accessed by two-photon absorption will be further discussed in Section 5.

Autoionization may also take place when an electron is promoted from an inner orbital (i.e., not from the highest occupied orbital) to an unoccupied Rydberg orbital by one-photon absorption. If the energy of the state is high enough, this may decay leaving a residual ion with a single hole. Here the initial state correlation in the ground state does not play an important role in the process of excitation to the autoionizing state. Window resonances of the type  $ns \rightarrow mp$  in rare gas atoms are typical examples of this class of autoionization (Madden et al., 1969; Codling and Madden, 1971). For example, in Ar these authors reported the  $3s^2 3p^6 \rightarrow 3s 3p^6 mp$  resonances. In Section 4.5, we will describe a novel technique to study such autoionization resonances, or dephasing time in general, employing a unique feature of FERMI, i.e, temporal coherence of multiple light pulses.

#### 4.2. One-colour, two-photon ionization

Two-photon absorption leading to single ionization of hydrogen and helium atoms may be the simplest single-color multiphoton process, and such two photon processes have been extensively studied theoretically (Ishikawa et al., 2010; Ishikawa and Ueda, 2012, 2013). Ma et al. (2013) investigated two-photon single ionization of He in the photon energy range between 20 and 24 eV by velocity map imaging electron spectroscopy at SCSS, and discussed the coexistence of resonant versus direct two-photon ionization pathways, following theoretical predictions described by Ishikawa and Ueda (2012).

Using XUV radiation, two-photon above threshold ionization of the inner shell has been realized at FLASH in Xe for ionization of the 4d shell in the region of the giant  $4d \rightarrow \epsilon f$  resonance (Richardson et al., 2010). This process proceeds mainly along the path  $4d \rightarrow \epsilon f \rightarrow \epsilon g$ . Later this process was used to reveal a doublet structure of the giant resonance in Xe (Mazza et al., 2015b; Chen et al., 2015).

Holzmeier et al. (2018) employed resonant two-photon spectroscopy of  $H_2$  to investigate nuclear dynamics in the ionization process. Molecular ionization is much more complicated than the atomic case, even for a system as simple as hydrogen, because of the additional nuclear degrees of freedom, especially the vibrational degrees. For this experiment, resolution and wavelength stability sufficient to select single vibronic states were required, about 150 meV. When hydrogen is ionized by a single photon, for example at about  $\hbar\omega = 25.5$  eV, the main outcome is a stable molecular ion, and the probability of dissociative ionization (to  $H^+ + H$ ) is very low. Fig. 4 shows that at the ground state internuclear distance, only continuum ionic states can be reached, see grey shaded region. Absorption of two photons of energy  $\hbar\omega/2$  implies the molecule absorbs the same amount of energy, but there is an important difference. If the photon energy  $\hbar\omega/2$  excites a resonance, the two photons may be absorbed sequentially, rather than simultaneously. The vibrational wavefunction of the intermediate state is much more extended than that of the ground state, as seen in Fig. 4. The Franck-Condon region for transitions from the intermediate state to the final state is also at larger internuclear distance, so that different potential energy curves are probed.

This was what was predicted in the calculations and observed in the experiment by Holzmeier et al. (2018). Resonant excitation to the bound  $B^1\Sigma_u^+$  state causes an expansion of the vibrational wavefunction, and the expectation value of the internuclear distance is larger, Fig. 4. The full and dotted red curves on the left indicate the situation for simultaneous absorption of two photons; the  $2p\pi_u$  final state is not accessible. For sequential absorption, the transitions lying between the two dotted red arrows are possible. The ionized  $2p\pi_u$  final state then becomes accessible, Fig. 4: this is a strongly repulsive state, and so the molecular ion can dissociate into a proton and a hydrogen atom. Between the ground and the excited state, the internuclear distance changes, but this is not to be seen as classical vibrational motion. Rather, the wavefunction evolves to yield a larger expectation value of the bond length.

The photoelectrons and kinetic-energy resolved ions were detected and were interpreted with detailed calculations. By accessing this state, the ratio between dissociative and non-dissociative ionization was increased to values above 1, i.e., the two channels have comparable probability.

The time scale of this experiment was determined by the pulse duration, about 100 fs. The dynamics observed were thus intermediate between what is expected from attosecond/few femtosecond pulses (Palacios et al., 2006), where the absorption of two photons is almost simultaneous, and high resolution experiments, where the coherence time is nearly infinite.

Detailed theoretical calculations by Holzmeier et al. (2018) revealed that it is important to take account of the doubly excited autoionizing states in order for theory to reproduce the experimental results quantitatively. In the experiment, the bound  $B^1\Sigma_u^+$  state was resonantly excited by a first photon. The second photon accesses not only the  $2p\pi_u$  final state, but also the doubly excited states  $Q_1$  and  $Q_2$  in Fig. 4, at certain internuclear distances. The doubly excited states thus populated dissociate along the repulsive potential curves and in parallel, autoionize mainly to a continuum state associated with the  $1s\sigma_g$  ionic ground state above the dissociation limit, contributing to dissociative ionization. As a result of competition between dissociation and autoionization, which varies the partition between kinetic energy of the electron and the kinetic energy release of the ion, the kinetic energy of the electron is spread over a wide band of energy, see Fig. 4 of Holzmeier et al. (2018). It is worth noting that the autoionization is the main contribution to dissociative ionization when the pulse duration is short ( $\lesssim 10$  fs) and the range of nuclear distances is limited close to the Frank-Condon region of the neutral ground state (Palacios et al., 2006).

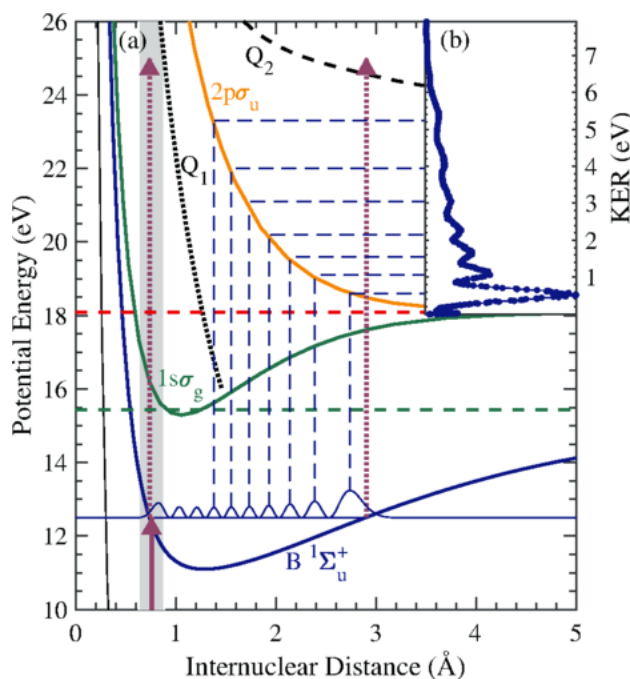


Figure 4: Potential energy curves of the singly and doubly excited states of the hydrogen molecule. The first photon excites the molecule to the  $B^1\Sigma_u^+(v = 9)$  intermediate state. Grey shaded area: Franck-Condon region for the ground state geometry. The  $Q_1$  and  $Q_2$  states are the lowest doubly excited states of  $^1\Sigma_g^+$  symmetry. Inset (b) shows the measured Kinetic Energy Release spectrum for dissociative ionization via the  $B(v = 9)$  state. Figure reprinted from Holzmeier et al. (2018), with permission. Copyright (2018) by the American Physical Society.

#### 4.3. XUV/X-ray + Near Infrared ionization and Circular Dichroism

The photoionization of atomic and molecular systems in a field consisting of a (usually weak) XUV or X-ray pulse and a (usually stronger) infrared (IR)/visible pulse, is a widely studied topic. One of the simplest examples is the use of an XUV pulse to promote an electron from an occupied orbital to an unoccupied Rydberg orbital and then use a near IR (800 nm) pulse to ionize it. The XUV pulse can be a laboratory laser based HHG source (Haber et al., 2009, 2010) synchrotron radiation (O’Keeffe et al., 2013), or FEL (Mondal et al., 2013, 2014). Interestingly, significant pulse delay effects in the photoelectron angular distribution of near threshold XUV + NIR two-photon ionization were found for Ne (Mondal et al., 2014) while there were no significant effects in He (Haber et al., 2009, 2010). Later, these observations were reproduced by theoretical simulations (Ishikawa et al., 2014).

Another example is the study of sidebands. Here an XUV pulse promotes a bound electron to the continuum, and simultaneous absorption or emission of an IR or visible photon by the outgoing photoelectron gives rise to sidebands in the electron spectrum. Two-colour photoionization of He in XUV free-electron and visible laser fields was studied immediately after FLASH started two-colour experiments, and the absolute amplitude ratio of the s and d partial

waves was extracted (Meyer et al., 2006, 2010). Sidebands can also be observed in the Auger spectrum for the case of overlapping IR/visible and X-ray pulses, known as laser-assisted Auger decay (Schins et al., 1994). Meyer et al. (2012) investigated the fine details of laser-assisted KLL Auger decay following 1s photoionization of atomic Ne with few-femtosecond X-ray pulses from the LCLS.

Optical pulses can be combined with FEL pulses to provide a useful diagnostic to characterise the time structure of the FEL pulses. The sideband intensity as a function of delay between the pulses is the cross-correlation curve, and its width is equal to the convolution of the temporal widths of the two pulses. If the duration of the optical laser pulse is known, the FEL pulse duration can be extracted. This method is usually applied to FEL pulses of tens of femtoseconds or longer.

For shorter FEL pulses, the methods of attosecond science can be applied (Krausz and Ivanov, 2009), which also involve the use of temporally overlapping optical and short wavelength pulses; see also Sections 4.8 and 4.9. The usual experimental approach is to overlap an IR pulse with an XUV attosecond pulse or an attosecond pulse train, in order to characterize the XUV pulse (Paul et al., 2001; Goulielmakis, 2004) or to perform time-resolved investigations of electron dynamics, such as photoionization delay (Dahlström et al., 2012; Pazourek et al., 2015). In this case, attosecond synchronisation of the pulses is required, that is, phase-sensitive control. Frequently employed approaches are photoelectron streaking (Paul et al., 2001; Pazourek et al., 2015) for an isolated attosecond pulse and RABBITT (Reconstruction of Attosecond Beating By Interference of Two-photon Transitions) (Muller, 2002) for attosecond pulse trains, see also the review of Dahlström et al. (2012), and Section 4.9. Streaking has been employed for characterizing XFEL pulses (Helml et al., 2014). See also Helml et al. (2017) for characterization of XFEL pulses by various methods, and Sections 4.8 and 4.9 for a more detailed description of these methods.

Circular dichroism (CD), i.e. the different response of a system to left and right circularly polarized radiation, has been widely investigated in the visible and infrared range (Barron, 2004; Starke, 2000) and also in the XUV and X-ray spectral region, exploiting the availability of circularly polarized pulses by synchrotron sources (Grum-Grzhimailo and Meyer, 2009). The recent availability of FELs delivering femtosecond pulses with variable polarization offers the opportunity to extend these investigations to time-resolved studies. In photoionization CD, the measurement of the photoelectron spectra and the photoelectron angular distributions gives access to additional information on the photoionization pathways with the possibility to reconstruct the amplitude and (relative) phases of the single photoionization channels.

Circular dichroism may arise because the target is chiral (natural circular dichroism), or because the conditions of the experiment break the reflection symmetry of the target. Thus a system containing a totally symmetric atom in a monochromatic, circularly polarized light field is not dichroic, because reflection symmetry is preserved. However if a second circularly polarized field at a different wavelength is applied, the symmetry is broken, and dichroism may be detected. These are the often-used conditions for two-colour photoionization.

Mazza et al. (2014) exploited the effect to measure the degree of circular polarization of light from FERMI. Although the FEL produces light with a high degree of helicity, the transport optics may depolarize it to a certain extent, and it is challenging to measure the degree of polarization at the end-station. In this experiment, helium was irradiated simultaneously with circularly polarized light of photon energy 48.4 eV (25.6 nm) and IR light of energy 1.58 eV (784 nm), and two-photon emission was observed as sidebands. The helicity of the IR was reversed, and the spectra re-measured; the dichroism was defined as the difference in intensity divided by the sum of intensities of the two situations. The dichroism was found to be  $0.04 \pm 0.004$ , corresponding to a degree of polarization of  $0.95 \pm 0.05$ , in agreement with the estimated value, 0.92, calculated from the optical constants of the transport mirrors. The importance of this work is not so much the physics, but the metrological application, providing a determination of the polarization at short wavelength.

Later, a detailed analysis of the photoelectron angular distribution and CD in the two-colour XUV+IR above-threshold ionization of helium, both experimental and theoretical, was presented by Mazza et al. (2016). In particular, the first “complete experiment” of two-colour, two-photon above-threshold ionization was realised, providing the partial s- and d-amplitudes, together with their relative phase, of transitions between the continuum states. See also Section 5.2 for a detailed discussion of a single-colour, two-photon complete experiment. The analysis covered also the second and third sidebands for higher intensities of the IR light. A short overview of early studies of the dichroism of the sidebands, generated by two-color XUV FEL + IR ionization is given in Mazza et al. (2015a).

#### 4.4. Orbital Angular Momentum

Photons have spin angular momentum of  $\pm\hbar$  depending on the polarization of the light. They may also possess orbital angular momentum, which depends on the spatial distribution of the phase of the wavefront. For example, “twisted light” can be created by passing a plane wave through a phase mask which transforms the wavefront into a vortex, where the phase varies in a spiral manner around the axis. While absorption of twisted light by a trapped atom had been previously observed (Schmiegelow et al., 2016; Afanasev et al., 2018), an effect in the photoelectron angular distribution of an extended sample was not observed, and it was argued that both a well defined phase singularity *and* the localization of sample atoms near the singularity are required to selectively observe nondipole transitions (Kaneyasu et al., 2017). In a recent experiment (De Ninno et al., 2020) the interaction of twisted light with atoms was investigated. The atoms were two-photon ionized by a Near Infrared photon and an XUV photon to generate sidebands (see Section 4.3). The IR field was circularly polarized and carried orbital angular momentum, while the XUV photon was circularly polarized. Dichroic effects were observed on changing the sign of the orbital angular momentum, confirming that effects are in fact observable. Theoretical analysis showed that the effect can be traced back to non-dipole transitions that would be optically forbidden for a gaussian beam and become allowed when the orbital angular momentum is taken into account.

#### 4.5. Towards two-dimensional XUV spectroscopy

A large number of experiments have been performed with optical lasers using phase-coherent, single-colour pulses, where the phase between two pulses separated in time is varied and the signal measured. It is a form of coherent control, with various names such as pump-dump spectroscopy or “wave packet dancing” (Kosloff et al., 1997). The name pump-dump arises from the simple interpretation that the first pulse pumps the target to an excited state, and if the second pulse is in antiphase, it pumps the target back down to the ground state. If it is in phase, it pumps the system further, that is, it increases the excited state population. The method is however much more sophisticated than this simple view suggests, and was used initially to control photochemical processes and yield a desired end-product (Rice, 1992; Gordon and Rice, 1997). Furthermore, adding one more pulse as a probe or read-out, one can read off the phase of the wavepacket created by a sequence of the two pulses that are phase-controlled (Ohmori et al., 2006). This branch of optical laser spectroscopy has evolved into multi-dimensional spectroscopy, with sequences of pulses, and control of parameters such as wavelength, time delay, chirp, etc. (Jonas, 2003; Goswami, 2003; Tan, 2008). The methods were originally developed in nuclear magnetic resonance (Aue et al., 1976; Ernst et al., 1990), and adapted to lasers.

As a first step towards multi-dimensional spectroscopy with FELs, phase-coherent double pulses have been generated at FERMI (Gauthier et al., 2016b). The method is in principle simple: FERMI is a seeded FEL, so it is sufficient to duplicate the optical seed pulse, and seed with two identical pulses separated in time. In reality, it is not easy to maintain the required attosecond-scale phase stability between the two pulses. Gauthier et al. (2016b) used a birefringent crystal to split the seed pulse. The thickness of the crystal determined the coarse delay, and the phase was tuned by rotating the crystal, producing small path length differences between the two pulses on the nm scale. Phase-coherent double-pulse generation has also been demonstrated at the XUV FEL facility FLASH (Usenko et al., 2017; Ding et al., 2019) using a split-and-delay unit based on diffractive optics. In contrast to the above scheme, single pulses are generated, and then split and delayed, rather than generating two phase-coherent pulses in the accelerator. Hikosaka et al. (2019) and Kaneyasu et al. (2019) claim to have demonstrated double pulse, coherent control using the synchrotron radiation facility UV-SOR. They used two undulators with a phase shifter between them.

At FERMI, Wituschek et al. (2020) built on the approach of Gauthier et al. (2016b), by introducing a monolithic Mach-Zehnder beam splitter. This showed improved temporal resolution and much improved flexibility, as the phase could be scanned over a range of 1 ps (limited only by the length and uniformity of the electron bunch), which was not possible using the birefringent crystals described above. Most importantly, phase-locked detection was implemented, with modulation provided by acousto-optic modulators, acting on the seed pulses. Since FERMI acts as a wavelength shifter and amplifier, the phase information was imprinted on all harmonics of the seed.

When two coherent and collinear pulses of the same wavelength are separated in time, they interfere and this is visible in their spectrum (Figure 5). If they are in phase, there is a maximum at the central wavelength, and the fringe spacing is inversely proportional to the delay between the pulses. If they are in anti-phase, the spacing is the same, but there is a minimum at the central wavelength. This is another way of looking at the pump-dump interpretation:



in-phase pulses have a maximum at the central wavelength, and so may excite a resonance at that wavelength. In antiphase, there is no net intensity, so the resonance is not excited.

The frequency domain picture gives an immediate and intuitive view of why at the end of a double pulse sequence, there is no excited state population (pump-dump): the excitation frequency was not present in the Fourier transform of the two light pulses. However it does not explain intuitively the effect of dynamics, or transient population of states, in which case the time domain picture may give a more intuitive description. For a closed quantum system (a few quantum states without a bath), such as the above example, the ‘‘pump-dump’’ time domain description or the ‘‘no absorption’’ frequency domain description are both correct and their relation is just a Fourier transform.

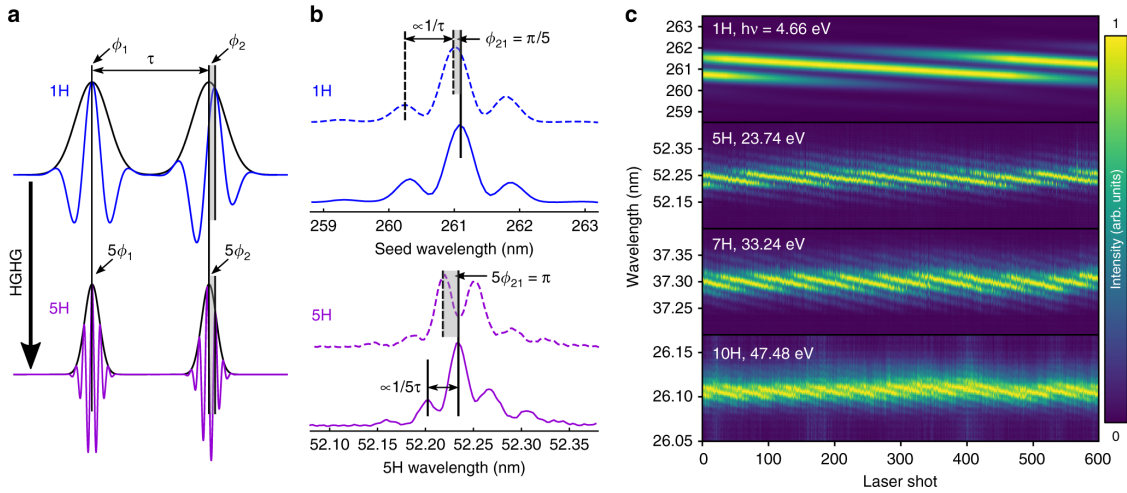


Figure 5: (a) Scheme of the timing and phase control of the XUV pulse pair (violet) by manipulation of the seed pulse (blue). Control of the pulse delay  $\tau$  and the phase difference  $\phi_{21} = \phi_2 - \phi_1$  are decoupled. (b) Example of interference fringes in the first harmonic and fifth harmonic spectra for fixed delay  $\tau = 250$  fs, and two values of phase  $\phi_{21}$ . The fringe spacing is inversely proportional to the delay  $\tau$  and the fringe phase is proportional to  $\phi_{21}$ . (c) Ramsey fringes for the first, fifth, seventh and tenth harmonics.  $\phi_{21}$  was incremented by 15 mrad steps between each laser shot. The data are intensity-normalised single-shot spectra with no additional processing. Reproduced from Wituschek et al. (2020); copyright 2020 by the Authors. The original figure has been published under a Creative Commons Attribution 4.0 license (CC BY) <http://creativecommons.org/licenses/by/4.0/>

Wituschek et al. (2020) demonstrated the method for the case of the argon  $3s \rightarrow 6p$  resonance, which is embedded in the continuum and decays by autoionization on a femtosecond time scale. The lifetime was already known from high resolution absorption spectra (Sorensen et al., 1994). However the new detection scheme measures both the real and imaginary parts of the susceptibility, whereas absorption provides only the imaginary part. This proof of principle experiment paves the way for full development of multi-dimensional spectroscopy, where a sequence of pulses is used (Jonas, 2003). . It promises to reveal phenomena, such as correlation between different states (peaks in the absorption spectrum), which cannot be observed in conventional one-dimensional spectroscopy (absorption spectroscopy).

#### 4.6. Coherent control of one-colour ionization via biharmonic ionization

Historically the first experiment which demonstrated coherent control in the XUV domain was performed in 2016 (Prince et al., 2016) at the seeded FEL FERMI exploiting the longitudinal coherence of the radiation, which is not present in radiation from SASE FELs. The theoretically predicted phase correlation between two different XUV beams was demonstrated for the fundamental frequency and its second harmonic. By varying the relative phase of the two fields, the angular distribution of photoelectrons ejected from the neon atomic target was controlled. The relative phase was, in turn, controlled using an accelerator physics method, so that the femtosecond pulse of one of the harmonics relative to the other was delayed with attosecond precision. For pulses of  $\sim 100$  fs duration, the time shift of the envelopes on the scale of a few attoseconds is not important, while the relative phase of the two XUV fields was controlled with a resolution of 3 as time delay. As mentioned at the end of Section 2.1, the delay was provided by an electron delay line, which shifts in time the electron bunch generating the second colour. It is very problematic

to control phase at short wavelengths, especially that of different harmonics, using laboratory optics methods, due to a lack of the required optical elements and strong absorption of the XUV radiation in matter. The need for optical elements to control the light is avoided by controlling the electron beam, and therefore the light. This is in contrast to physically equivalent experiments in the optical domain where variable pressure gas cells (Baranova et al., 1992; Yin et al., 1992; Wang and Elliott, 2001) or a rotating transparent plate (Yamazaki and Elliott, 2007) were used as phase shifters.

The fundamental frequency in the FERMI experiment corresponded to the  $2p^6 \rightarrow 2p^5(2P_{3/2}^o)4s$  resonance of Ne at 62.97 nm, selected to enhance the two-photon ionization branch and thus to provide stronger interference between one- and two-photon ionization, Fig. 6. The collinear beams of both harmonics were linearly polarized along the same direction. The photoelectron angular distributions were measured by a VMI (velocity map imaging) spectrometer.

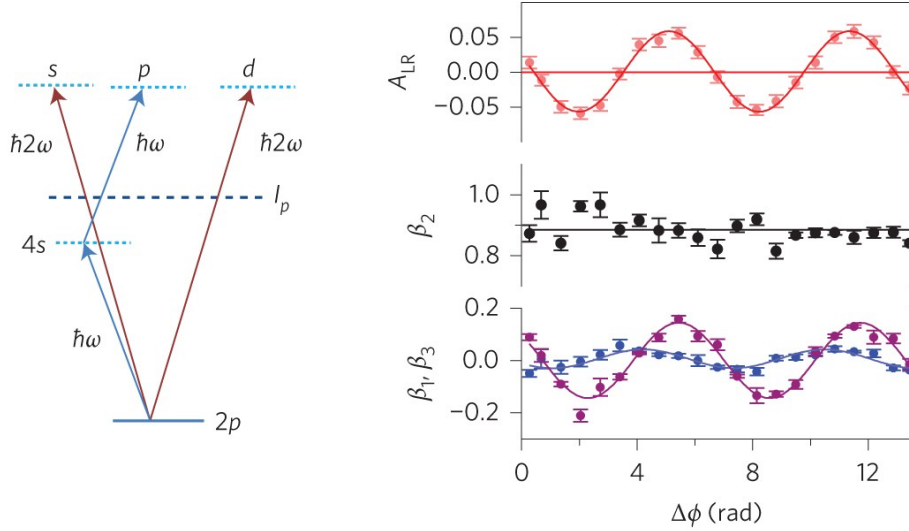


Figure 6: Left: Level diagram for coherent control of neon with short wavelength radiation. Single-photon (second harmonic) ionization leads to emission of s and d partial waves. Two-photon (fundamental) ionization via the 4s resonance leads to emission of p partial waves. The amplitude of f partial waves is negligible compared with the resonant path. Right: Asymmetry parameter  $A_{LR}$  and asymmetry parameters  $\beta_1$  (blue),  $\beta_3$  (magenta) and  $\beta_2$  (black) as a function of phase. Figure reprinted from Prince et al. (2016), with permission. Copyright (2016) by the Authors.

To describe theoretically the effect of varying the relative phase of the harmonics (Douguet et al., 2017; Gryzlova et al., 2018), the electric field may be written in the form

$$E(t) = F(t) [\cos \omega t + \eta \cos(2\omega t + \phi)] \quad (1)$$

where  $F(t)$  is the pulse envelope,  $\eta$  is the amplitude ratio of the fundamental and second harmonic. In the lowest non-vanishing order of the perturbation theory (see Section 8.5), the differential ionization probability for an initial atom with zero angular momentum ( $J_i = 0$ ) can be expressed as

$$\frac{dW}{d\Omega} \equiv W(\vartheta, \varphi) = \sum_{M_f} \left| \eta \langle f | T | i \rangle_1 + \langle f | T | i \rangle_2 \right|^2 \quad (2)$$

where the first and the second order amplitudes are given (in the dipole approximation) by Eqs. (27, 28), Section 8.5,  $M_f$  is the magnetic quantum number of the residual ion (with total electronic angular momentum  $J_f$ ). Eq. (2) can be written as a sum of three terms,

$$W(\vartheta, \varphi) = W^{(1)}(\vartheta, \varphi) + W^{(2)}(\vartheta, \varphi) + W^{(12)}(\vartheta, \varphi), \quad (3)$$

with the axial symmetric angular dependence described by the sum of Legendre polynomials  $P_k(\cos \vartheta)$ :

$$W(\vartheta, \varphi) = \frac{W_0}{4\pi} \left( 1 + \sum_{k=1}^4 \beta_k P_k(\cos \vartheta) \right) \quad (4)$$

Here the first and the second terms in Eq. (3) are the ionization rates due to the (two-photon) first and (single-photon) second harmonics, respectively, while the third term is due to the interference between the two paths; the angle  $\vartheta$  is measured from the direction of polarization. The interference term in Eq. (3) gives rise to odd Legendre polynomials ( $k = 1, 3$ ) in Eq. (4), due to the opposite parities of the final states in one- and two-photon ionization. As a result, a “forward-backward” asymmetry of the angular distribution Eq. (4) along the direction of the polarization vector appears, Fig. 6.

This asymmetry has an oscillatory dependence on the relative phase of the harmonics  $\phi$  and is quantified by the value

$$A_{\text{LR}} = \frac{W(\vartheta = 0) - W(\vartheta = \pi)}{W(\vartheta = 0) + W(\vartheta = \pi)} = \frac{\sum_{k=1,3} \beta_k}{1 + \sum_{k=2,4} \beta_k} = A_m \cos(\phi - \phi_m) \quad (5)$$

where  $A_m$  = the amplitude of the oscillations and  $\phi_m$  = the phase at which the asymmetry reaches its maximum value. The anisotropy parameters  $\beta_1$  and  $\beta_3$  are described by similar oscillations with their own amplitudes and phases analogous respectively to  $A_m$  and  $\phi_m$ . Such oscillations were indeed observed in the experiment (Prince et al., 2016) and were confirmation of the mutual coherence of the two XUV harmonics and coherent control of the angular distribution. Theoretical calculations (Gryzlova et al., 2018) were performed in the lowest non-vanishing order perturbation theory, taking into account the neighbouring excited states  $2p^5 4s$ ,  $3d$  of Ne, including their fine structure, and by solving the TDSE on the space-time grid (see Section 8.3) with a local potential and the perturbation theory, in the limit of infinite pulse duration. The resonance behaviour of the  $\beta_k$  parameters and the parameters  $A_m$  and  $\phi_m$  of the asymmetry, Eq. (5), as a function of the XUV photon frequency was revealed. A similar theoretical study of the coherent control for the region of the Ne( $2p^5 3s \ ^1P$ ) state (Douguet et al., 2017) and before that, for the H( $2p$ ) state (Grum-Grzhimailo et al., 2015b), were performed.

Some theoretical predictions for the same experiment on neon with two circularly polarized harmonics are available (Gryzlova et al., 2019b). In this case, the coherent control of the photoelectron angular distribution manifests itself through a change from a one-lobe to a three-lobe shape, for co- and counter-rotating harmonics respectively, a variation of the polar asymmetry with the light frequency, and a rotation of the distributions around the direction of the beam depending on the relative phase between the harmonics. The controlled parameters change sharply when the fundamental frequency passes through an intermediate resonance. These effects were first predicted for the hydrogen atom (Douguet et al., 2016).

#### 4.7. Experimental determination of optical phase

The experiment described in Section 4.6 was carried out at a single fundamental wavelength and its second harmonic, and while their *relative* phase was controlled, the *absolute* optical phase difference was unknown. Contrary to optical experiments, the characterization of this phase is not straightforward, because of the lack of suitable optical materials. To extend bichromatic coherent control to other applications, it would be useful to know the absolute optical phase at any chosen wavelength. This challenge was met by Di Fraia et al. (2019) who used He atoms as a nonlinear mixer, and measured the absolute phase relationships of fundamental wavelengths of FERMI FEL-1 and their second harmonics. They used bichromatic light, and measured the interference for single ionization of He in the photon energy range 14.3 to 19.1 eV (i.e., below the first  $1s$  to  $2p$  excitation) as a function of relative optical phase. The measurement exploits the asymmetry induced in the angle-resolved photoelectron distribution, and results in a system of equations that becomes solvable if the value of one of the scattering phase shifts is known. For He, scattering phase shifts over a wide range of photoelectron energies are available in the literature. The absolute phase value was measured at three photon energies (14.3, 15.9, 19.1 eV) with an error of 0.01 – 0.04 rad. An advantage of the method is that it also provides the effective relative photon intensities relevant for a bichromatic process, which is useful for the case of imperfect experimental conditions. The method is also of interest because it can potentially be extended to other  $s$  shell electrons (e.g.,  $C_{1s}$ ) at much shorter wavelengths.

#### 4.8. Photoemission time delay

In Section 8.1 below, we give an expression for the Eisenbud-Wigner-Smith (EWS) time delay (Eisenbud, 1948; Wigner, 1955; Smith, 1960), Eq. (17). This is the delay (with respect to a freely propagating electron) that a photoelectron experiences when exiting the potential of an atom or molecule, and it may depend on both the kinetic energy and emission direction of the electron. It can be shown that under appropriate circumstances, the derivative with

respect to energy of the phase of the photoionization amplitude,  $\partial\eta(\epsilon)/\partial\epsilon$ , is equal to the EWS time delay. Currently, the main methods applied to measure these time delays are based on laboratory ultrafast lasers, and the application of two techniques, attosecond streaking and RABBITT (Reconstruction of Attosecond Beating By Interference of Two-photon Transitions; see also Section 4.9). Usually two photoelectron signals are measured simultaneously, for example from two different atoms, or from two different levels of the same atom, so that the difference in time delay  $\Delta\tau$ , or the corresponding difference in phase  $\Delta\eta$ , is determined. Thus in attosecond streaking and RABBITT,  $\partial\Delta\eta(\epsilon)/\partial\epsilon$  is measured. Both of these methods depend on the presence of an infrared pulse which is synchronised to an attosecond XUV pulse (streaking) or to an attosecond pulse train (RABBITT) with attosecond precision, and require correction due to effects of the infrared pulse.

In Section 4.6, we discussed the application of fully coherent FEL light to control the emission of photoelectrons. Extremely high phase resolution corresponding to a few attoseconds was demonstrated, and the question immediately arises as to whether this exquisite control can be used to measure phenomena on this time scale. The first experiment aiming to do so has been carried out recently (You et al., 2020b) on a Ne target.

The method is based on the technique described above, namely the control of the phase difference between a fundamental and its second harmonic, and measurement of the PADs (photoelectron angular distributions) as a function of the phase difference between the two wavelengths at two or more kinetic energies of the photoelectron. From these measurements, intensities as a function of phase for a series of angles were derived; the relative phase between the two-photon and the single-photon ionization channels was extracted; and  $\partial\Delta\eta(\epsilon)/\partial\epsilon$  was calculated in the finite-difference approximation. For the ionization of an  $ns$  state, such as He 1s, this quantity is identified with the group delay of the photoelectron wave packet, as in the case of the EWS delay. Ionization of an  $ns$  state by linearly-polarized bichromatic light is a relatively simple case, as there are only three outgoing partial waves, a p wave due to single-photon ionization, and s + d waves, due to two-photon ionization; these interfering partial waves all have magnetic quantum number  $m = 0$ .

The situation is more complicated for the ionization of an  $np$  orbital, as in the experiment on Ne 2p (You et al., 2020b). There are four outgoing partial waves: s + d from single-photon ionization, and p + f from two-photon ionization. As well, the outgoing waves may have magnetic quantum number  $m = -1, 0, 1$ . Waves with the same value of  $m$  interfere, and the oscillations as a function of the relative phase between the fundamental and second harmonic then add incoherently, i.e., in terms of intensity rather than amplitude, for the three values of  $m$ . Nevertheless, clear oscillations were observed, but the interpretation is more complicated than for the case of s initial states. What is clear is that an average phase of photoionization amplitudes can be measured, and this is an important quantum mechanical quantity.

The derivative of the phase with respect to energy was taken, but the interpretation in terms of a photoemission time delay is more subtle than the case of He. A *generalized delay* for multiple wave packets was proposed, defined as

$$\Delta\tilde{\tau} = \frac{\partial\Delta\tilde{\eta}(\tilde{\epsilon})}{\partial\tilde{\epsilon}}, \quad (6)$$

where the phase difference of photoionization amplitudes was averaged (in the sense of sum of phasors) over  $m$  and then the resulting  $\Delta\tilde{\eta}$  was differentiated with respect to the average photoelectron energy,  $\tilde{\epsilon}$  (where  $\tilde{\epsilon}$  rather than  $\epsilon$  takes account of the finite bandwidth of the electron wave packet.) This is in contrast to the definition of Smith (1960), where the scattering phase of each wave packet is first

#### 4.9. Generation and characterization of attosecond pulse trains

The demonstration of coherence between two different harmonics of the FEL described in the previous Sections and also in Prince et al. (2016), naturally raises the question whether multiple harmonics of the seed wavelength are expected to be coherent. For the typical configuration of FERMI with an ultraviolet seed laser of angular frequency  $\omega_{UV}$ , the coherent superposition of two harmonics ( $q_1$  and  $q_2$ ) would lead to beating in the temporal domain, and to an intensity profile  $I(t)$  characterized by an attosecond time structure, which repeats itself periodically with the period between zeroes  $T = 1/[(q_2 - q_1)\omega_{UV}]$ . For consecutive (even and odd) harmonics of the seed laser this period is  $\simeq 880$  as.

Attosecond pulse trains generated by high-order harmonic generation usually consist of the odd harmonics of the fundamental near-infrared driving field with angular frequency  $\omega_{NIR}$ . The characterization of the relative phase between the harmonics of the fundamental radiation is accomplished through a cross-correlation between the pulse

train and a synchronized infrared pulse. The signal is the photoelectron spectrum generated by the two-colour fields, which, besides the photoelectrons corresponding to the absorption of a single XUV photon, contains additional peaks due to the absorption (emission) of one IR photon, indicated as  $S_{q-2,q}$  and  $S_{q,q+2}$  in Fig. 7a. These additional peaks are usually named sidebands and their intensity depends on the relative phase between the harmonics and on the relative delay  $\tau$  between the XUV and IR fields according to the relation:

$$S_{q,q+2}(\tau) \propto \cos(\varphi_{q+2} - \varphi_q + \Delta\varphi_{at} + 2\omega_{NIR}\tau), \quad (7)$$

where  $\varphi_q$  and  $\varphi_{q+2}$  indicate the phases of the two consecutive, odd harmonics  $q$  and  $q + 2$ , respectively, and  $\Delta\varphi_{at}$  indicates the difference of the additional phases accumulated along the two ionization pathways by the photoelectron wave packet due to the bound-continuum and continuum-continuum transitions. By measuring the variation of the sideband intensities as a function of the relative delay (which can be controlled with sub-fs accuracy in HHG-based experimental setups), the phase difference between consecutive odd harmonics can be extracted and the attosecond waveform can be reconstructed (Paul et al., 2001; Muller, 2002). The unknown phase term  $\Delta\varphi_{at}$  is derived from theoretical calculations. This reconstruction method is usually known as Reconstruction of Attosecond Bursts By Interference of Two-photon Transitions or RABBITT (Muller, 2002), see also Section 4.8.

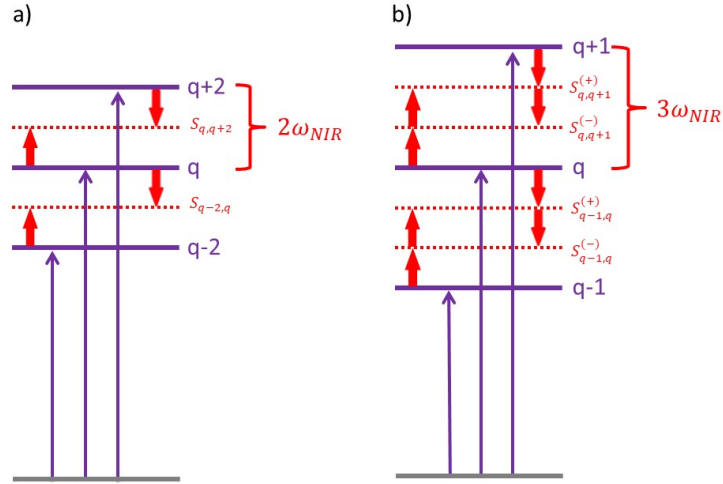


Figure 7: a) RABBITT method implemented for the temporal characterization of the relative phase between the consecutive odd harmonics  $q - 2$ ,  $q$ , and  $q + 2$ . The energy difference between consecutive main photoelectron peaks is  $2\omega_{NIR}$ . One-NIR-photon transitions give rise to sidebands of the main peaks  $S_{q-2,q}$  and  $S_{q,q+2}$ , whose intensity depends on the interference between two different pathways. b) Two-colour photoionization scheme for the characterization of the phase difference between consecutive harmonics ( $q - 1$ ,  $q$ , and  $q + 1$ ) of the seeded FEL FERMI. The energy difference between consecutive main photoelectron peaks is  $3\omega_{NIR}$ . One- and two-NIR-photon transitions give rise to the sidebands of the main peaks  $S_{q-1,q}^{(\pm)}$  and  $S_{q,q+1}^{(\pm)}$ , whose intensity depends on the interference between two different pathways.

The harmonics of the seeded FEL FERMI are the even and odd harmonics of the seed laser pulse, obtained by frequency tripling of the output of either a Ti:Sa system or of an optical parametric amplifier (OPA) (Danailov et al., 2011; Allaria et al., 2012b). In contrast to the HHG-based case, one-NIR-photon transitions are not sufficient to create two interfering pathways contributing to the same sideband. The interference between two different pathways encoding the relative phase between the harmonics needs (at least) two-NIR-photon transitions, as can be seen in Fig. 7b. For example, the sideband  $S_{q,q+1}^{(-)}$  is populated either by the absorption of a photon of the harmonic  $q$  and subsequent absorption of one NIR photon, or by the absorption of a photon of the harmonic  $q + 1$  and emission of two NIR photons.

Multiple sidebands of the fundamental photoelectron peaks were observed in the interaction of a single harmonic and a NIR field (Mazza et al., 2014), thus indicating the possibility to use the fundamental laser ( $\omega_{NIR}$ ) for cross-correlation measurements. Simulations based on the strong-field-approximation and solution of the TDSE in the

single-active electron approximation indicate that, also in the case of multiple NIR photon transitions, the sideband intensity oscillates depending on the relative phase between the harmonics ( $\varphi_{q+1} - \varphi_q$ ) and the temporal delay  $\tau$  between the fields according to the relation:

$$S_{q,q+1}^{(\pm)} = a_{q,q+1}^{(\pm)} \pm b_{q,q+1}^{(\pm)} \cos(\varphi_{q+1} - \varphi_q + \Delta\varphi_{at} + 3\omega_{\text{NIR}}\tau), \quad (8)$$

where the coefficient  $a_{q,q+1}^{(\pm)}$  and  $b_{q,q+1}^{(\pm)}$  on the photoelectron energy and on the intensity of the NIR pulse. Also in this case, the relative phase between the harmonics can be extracted by the oscillations of the sidebands as a function of the relative delay.

This approach, however, cannot be directly applied to the measurement of the relative phase between consecutive harmonics of FERMI, due to the lack of sub-femtosecond synchronization between the XUV waveform and the NIR lasers. For SASE FELs, the timing jitter can be as large as ten to a hundred femtoseconds (Coffee et al., 2019). For FERMI the timing jitter is of the order of a few femtoseconds (Finetti et al., 2017) and is, therefore, still too large for observing the sub-cycle intensity dependence of the sidebands.

Information about the relative synchronization between the harmonics can still be retrieved by correlating the intensities of different sidebands measured shot-by-shot. Indeed, using Eq. (8) we observe that the curve representing the variation of the intensity of the sideband  $S_{q-1,q}^{(+)}$  ( $S_{q-1,q}^{(-)}$ ) with respect to  $S_{q,q+1}^{(+)}$  ( $S_{q,q+1}^{(-)}$ ) is an ellipse, whose shape depends on the phase difference:

$$\Delta\varphi_{q-1,q,q+1} = \varphi_{q+1} + \varphi_{q-1} - 2\varphi_q \quad (9)$$

which can be regarded as the difference between the differences of the phases  $\varphi_{q-1}, \varphi_q, \varphi_{q+1}$  of three consecutive harmonics  $q-1, q, q+1$ . The phase difference  $\Delta\varphi_{q-1,q,q+1}$  is proportional to the group-delay dispersion of the phase  $\varphi(\omega)$  of the harmonic spectrum:

$$GDD(\omega) = \frac{d^2\varphi}{d\omega^2} \simeq \frac{\Delta\varphi_{q-1,q,q+1}}{\omega_{\text{UV}}^2}, \quad (10)$$

where  $\omega_{\text{UV}}$  indicates the angular frequency of the ultraviolet seed laser. In particular, if the three harmonics are in phase (i.e.  $\varphi_{q+1} - \varphi_q = \varphi_q - \varphi_{q-1}$ ), the phase difference  $\Delta\varphi_{q-1,q,q+1}$  is zero and the ellipse reduces to a line. Therefore, the shape of the correlation plots reveals the relative phase between the group of three harmonics. By using this approach, the total electric field, which depends only on these phase differences (apart from an overall time shift), can then be reconstructed.

This approach was recently demonstrated at FERMI for the temporal characterization of attosecond pulse trains composed of three and four harmonics (Maraju et al., 2020). In the three-harmonics scheme, each harmonic was generated by two undulators. The relative phase between the harmonics was changed by delaying the electron bunch using the phase shifters between each pair of undulators. The characterization of the phases between the harmonics was based on the single-shot correlation analysis of the sideband variations. In order to minimize the effect of intensity fluctuations of the single harmonics, the oscillating component of the sideband was isolated by considering the quantity:

$$P_{q,q+1} = \frac{S_{q,q+1}^{(+)} - S_{q,q+1}^{(-)}}{S_{q,q+1}^{(+)} + S_{q,q+1}^{(-)}} \quad (11)$$

It can be easily observed from Eq. 8, that, under the approximation  $a_{q,q+1}^{(+)} \simeq a_{q,q+1}^{(-)}$  and  $b_{q,q+1}^{(+)} \simeq b_{q,q+1}^{(-)}$  also the correlation plots ( $P_{q-1,q}, P_{q,q+1}$ ) are described by ellipses, whose shape depends on  $\Delta\varphi_{q-1,q,q+1}$ .

Figure 8a-j reports the correlation plots of the oscillating components of the sidebands  $P_{7,8}$  and  $P_{8,9}$  for different delays  $\tau_{s2}$  introduced by phase shifter PS2, which controls the phase of the ninth harmonic relative to the eighth and seventh harmonics. The plot evolves from a linear, to an elliptical, to a circular, to a linear plot with negative slope, then back to a linear plot with positive slope. For each delay  $\tau_{s2}$  the relative group delay dispersion between the three harmonics can be retrieved by estimating the correlation parameter  $\rho_{789}$  of the corresponding correlation plot. The values of the correlation parameter as a function of the delay are shown in Fig. 8k and clearly show a periodic evolution, which is well approximated by a sinusoidal. By assigning phase difference  $\Delta\varphi_{789} = 2m\pi$  (with m integer) to the maxima of the sinusoidal fit, a correspondence between phase difference and delay is determined, giving access

to the group delay dispersion of the harmonics for each position of the delay shifter. Using this information the pulse, the temporal structure of the attosecond train can be determined.

The experiment was also performed with four harmonics and, in principle, extension up to six harmonics is technically feasible, since six undulators are available at FERMI. Thus FERMI offers great flexibility, giving access to attosecond pulse trains in which the electric field is reproduced in each pulse (by using odd and even harmonics) or with a  $\pi$ -phase jump between consecutive pulses (only odd harmonics) and with a variable time-spacing (around 1 fs).

Attosecond pulse trains produced at a seeded FEL offer major advantages compared to HHG-based attosecond sources. Indeed, due to selective control of the relative phases and amplitudes of the different harmonic components, complete pulse-shaping control of the attosecond waveform was demonstrated. This capability goes beyond the shaping demonstrated so far for HHG-based sources (López-Martens et al., 2005; Hofstetter et al., 2011; Bartels et al., 2000). Moreover the very high energies per pulse (in the  $\mu\text{J}$  range) allow investigation of nonlinear optical processes induced by the absorption of multiple XUV photons.

The coherence between the different harmonics of the FEL is a fundamental prerequisite for the application of this approach. For SASE FELs, which can generate sub-femtosecond pulses, a single-shot technique (Li et al., 2018) is mandatory for the characterisation of the temporal structure of the attosecond waveform (Duris et al., 2020). For future experiments, the angular information contained in the photoelectron spectra could provide additional information about the different phases accumulated by the wave packets during the two-colour photoionization process (Dahlström et al., 2012). Velocity Map Imaging (VMI) spectrometers can provide this data (O’Keeffe et al., 2012).

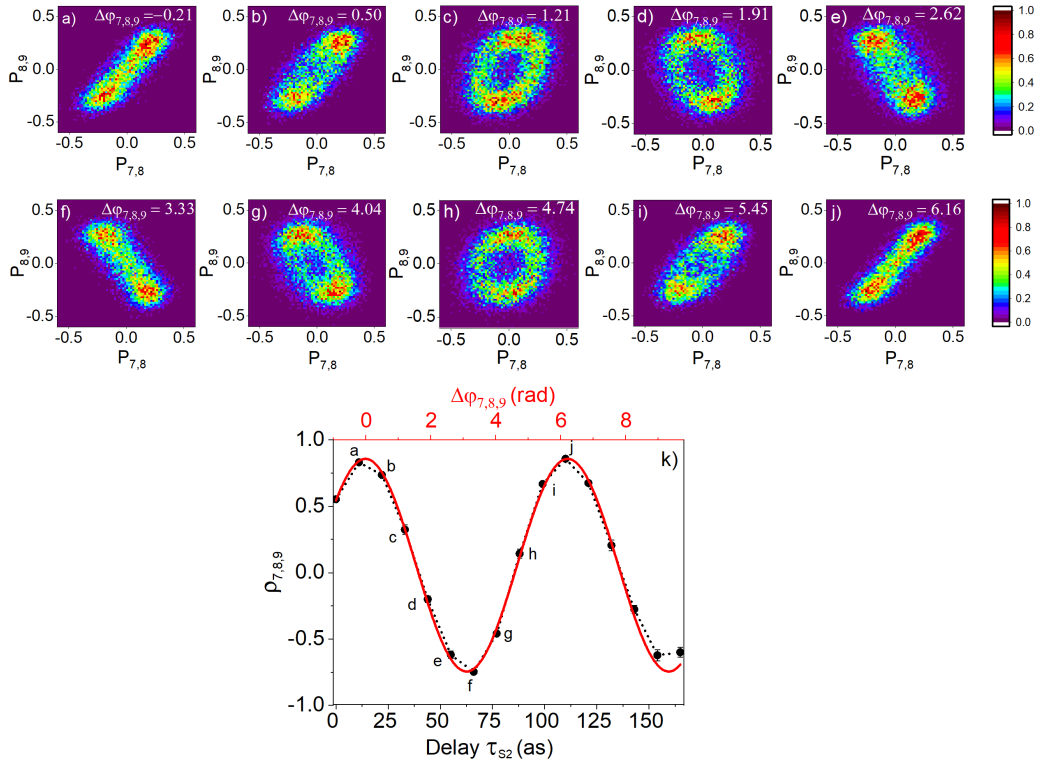


Figure 8: a-j) Correlation plots  $P_{8,9}$  vs  $P_{7,8}$  for different delays  $\tau_{s2}$  introduced by the phase shifter PS2. The corresponding phase difference  $\Delta\phi_{7,8,9}$  is shown in the right-upper corner of each panel. k) Evolution of the correlation parameter  $\rho_{7,8,9}$  as a function of the delay  $\tau_{s2}$  (black points and dashed line). The letters a-k indicate the experimental points corresponding to the correlation plots shown in panels a-j. The red curve is a sinusoidal fit of the experimental points. The error bars are the standard deviation of the average correlation coefficients evaluated over ten sets of experimental data, with 1200 single shots per set. The red upper axis of panel k) was obtained by fixing the maxima of the fit equal to  $\delta\phi_{7,8,9} = 2m\pi$ , where  $m$  is an integer. Figure reprinted from Maroju et al. (2020), with permission. Copyright (2020) by the Authors.

The development of attosecond pulses from a fully coherent FEL echoes the development of attosecond pulses from laboratory lasers, which first produced short pulses, then attosecond pulse trains, and now isolated attosecond pulses. Apart from the technical differences of FELs, the wavelengths are shorter, and the pulse energies much higher. More importantly, the method can be applied to even shorter wavelengths, in principle reaching core level energies.

## 5. Few-photon sequential multiple ionization

### 5.1. Early studies

In this Section, we mainly focus on few-photon sequential multiple ionization of atoms, as Seddon et al. (2017) have recently reviewed FEL studies of multiphoton multiple ionization of molecules. Early studies of multiphoton ionization using intense XUV laser sources were performed at FLASH by measuring the different ionic charge states of Ne and He. These preliminary investigations indicated that sequential ionization through ionic and resonance states dominates the direct multiphoton ionization through virtual states (Sorokin et al., 2007).

At SCSS, with a photon energy of 24 eV and a FEL power density  $\sim 10^{14}$  W/cm<sup>2</sup>, formation of Ar<sup>7+</sup> and Kr<sup>8+</sup> was found (Berrah et al., 2010). The total energies required to remove seven electrons from the Ar atom and eight electrons from the Kr atom are  $\sim 434$  eV and  $\sim 508$  eV, respectively, i.e., more than 18 and 21 times the photon energy of 24 eV. Such multiple ionization is likely to be due to sequential stripping of the outermost electrons (Motomura et al., 2009). With this assumption, the total numbers of photons absorbed by single Ar and Kr atoms should be 22 and 26, respectively. Details of these multi-photon multiple-ionization pathways, however, have not been fully analysed. Later, such ion charge distribution measurements have been extended to X-ray ranges (Young et al., 2010; Rudek et al., 2012; Fukuzawa et al., 2013). Modern *ab initio* theoretical calculations can reproduce these charge distributions accurately (Ho et al., 2014; Rudek et al., 2018). See also Section 4.1 for the role of resonant excitation in these studies.

Information about the momentum of the ejected electron or recoil ion provides additional insight into multiple ionization processes. Rudenko et al. (2008) investigated the recoil ion momentum distribution of singly and doubly ionized helium and neon after irradiation with intense XUV pulses. In the photon energy range 20–24 eV available at SCSS, single photon ionization of Ar first takes place followed by two-photon ionization of Ar<sup>+</sup> (Fukuzawa et al., 2010; Hikosaka et al., 2010; Miyauchi et al., 2011). In particular, Hikosaka et al. (2010) elucidated the role of an intermediate resonance in the two-photon ionization of Ar<sup>+</sup>, using a magnetic bottle electron spectrometer. At the higher photon energy of 93 eV at FLASH, three-photon triple ionization of Ne was investigated using a velocity-map imaging electron spectrometer (Rouzée et al., 2011).

In more refined experiments, both the photoion and the photoelectron momenta were measured to retrieve additional information on the photoionization process. At FLASH, with a photon energy of 44 eV, Kurka et al. (2009) performed a kinematically complete experiment for sequential two-photon double ionization of neon atoms, by measuring the momenta of both electrons in coincidence with Ne<sup>2+</sup> ions. A reaction microscope was used and the process fully characterized.

Another type of refined experiment is to measure energy correlations of two ejected electrons. At LCLS, Frasinski et al. (2013) investigated competition between hollow atom formation and sequential ionization by intense X-ray pulses using covariance mapping (Frasinski et al., 1989; Frasinski, 2016).

It is worth noting that several theoretical works have investigated electronic correlation effects exploiting the correlated momentum measurement of two-photon double ionization of helium (Ishikawa and Midorikawa, 2005; Feist et al., 2009). Extensive theoretical studies of angular distributions of the electron emission in the sequential two-photon double ionization of the valence shell of the noble gases started simultaneously with the corresponding experiments at FLASH (see references in Section 8.5).

### 5.2. Complete experiments on Ne

Upon ionization by absorption of an XUV photon, an electronic wave packet is released into the continuum. Depending on the initial electronic state and on the light polarization, several outgoing partial waves characterized by different angular momenta can be emitted. Their coherent superposition results in the three-dimensional photoelectron angular distribution (PAD) observed in experiments. For a complete characterization of the photoionization process, the complex amplitudes (that is, the modulus of the amplitudes and relative phases) of these partial waves must be measured. Such information cannot be obtained, in general, by measuring only the photoelectron angular distribution



and the total cross-section, but additional information is required. The high intensity available with FELs offers the opportunity to investigate the characteristics of the sequential multiple photoionization of atomic and molecular targets. In particular, it is known that photoionization leaves the ion in a polarized state, in which the angular momentum is preferentially aligned along a certain direction (Greene and Zare, 1982). This characteristic of the ionic electronic distribution influences the angular distribution of the photoelectron emitted by the absorption of a second XUV photon. By measuring the PADs of the two photoelectrons for different polarization states of the incident XUV light, and with suitable assumptions, information about the polarization state of the ion and the complete characterization of the two photoionization processes is possible. Such a scheme imposes significant constraints on the XUV source, which need to have high intensities and a controllable polarization state. These two conditions can be achieved by the seeded FEL FERMI. According to perturbation theory, for the absorption of two photons the PADs are described by the relation:

$$I^\nu(\vartheta) = \frac{I_0^\nu}{4\pi} \left[ 1 + \beta_2^\nu P_2(\cos \vartheta) + \beta_4^\nu P_4(\cos \vartheta) \right], \quad (12)$$

where  $P_k(x)$  is the  $k^{\text{th}}$  Legendre polynomial,  $\vartheta$  is the angle between the axis of symmetry  $z$  and the emission direction of the photoelectron,  $I_0^\nu$  is the angle-integrated intensity, the superscript  $\nu$  denotes linearly or circularly polarized pulses. In the cases of linearly and of circularly polarized pulses, the axis of symmetry  $z$  corresponds to the polarization direction and to the propagation direction of the XUV pulses, respectively. The polarization of the ion is linked to the coefficient  $\beta_4^\nu$  and it can be derived by measuring the three-dimensional PADs.

In the experiment performed at FERMI by Carpeggiani et al. (2019), Fig. 9, the PADs were measured using a velocity map imaging spectrometer, which gives access to the three-dimensional PADs, provided that the interaction is characterized by an axis of symmetry. As stated, this is the polarization direction (linear polarization) or propagation direction (circular polarization). The experimental results were compared with predictions based on the perturbation theory, within the single-configuration non-relativistic approximation, and a fitting procedure was implemented to determine the values of the ratio between the amplitude of the s and d-partial waves and their relative phase for the two photoionization steps. The photoelectron angular distribution of the residual ion and those of the scattering states of the corresponding photoelectron(s) were retrieved, providing a complete characterization of the two-photon double ionization of neon (Carpeggiani et al., 2019).

### 5.3. The role of autoionizing resonances in double ionization

As mentioned in Section 4.1, autoionization is an important phenomenon giving access to a number of physical quantities. Studies of this effect with synchrotron (Madden and Codling, 1963; Maeda et al., 1993; Sorensen et al., 1994; Domke et al., 1995, 1996) and attosecond XUV pulses (Ott et al., 2013, 2014; Kotur et al., 2016; Gruson et al., 2016; Cirelli et al., 2018) have been limited to the autoionizing states of neutral systems, which are embedded in the continuum state associated with the cation in the ground state and thus fragment into a cation and a free electron. With the intense pulses provided by FELs, one can ionize the sample first and then excite autoionizing resonances of cations, which are embedded in the continuum of the ground state dication, and therefore fragment into the dication and a free electron. Thus the pulse has two functions and the experiment elucidates the role of the autoionizing resonances in double ionization. The importance of autoionization resonances in both steps of sequential double ionization was confirmed by experiments on Ar at FLASH in the region of the Rydberg autoionizing states of  $\text{Ar}^+$  (Augustin et al., 2018). A clearly measurable value of  $\beta_4$  in the PAD [Eq. (12)] of the first electron in the double ionization process confirmed a theoretically predicted correlation between both electrons, resulting from the polarization of the intermediate state, the  $\text{Ar}^+$  ion.

It is worth noting that similar electronic decay pathways that enhance the degree of ionization can also be seen using X-rays. Rudek et al. (2012) reported an unprecedentedly high degree of ionization of xenon atoms by 1.5 keV free-electron laser pulses to charge states with ionization energies far exceeding the photon energy. Comparing ion charge-state distributions and fluorescence spectra with ab initio calculations, they speculated that these surprisingly high charge states are created via resonant excitation in highly charged ions, which are subject to autoionization, or resonant Auger decay. Later, this resonance-enabled X-ray multiple ionization (REXMI) pathway was fully confirmed experimentally and theoretically, at higher photon energies and with higher X-ray fluxes (Rudek et al., 2018).

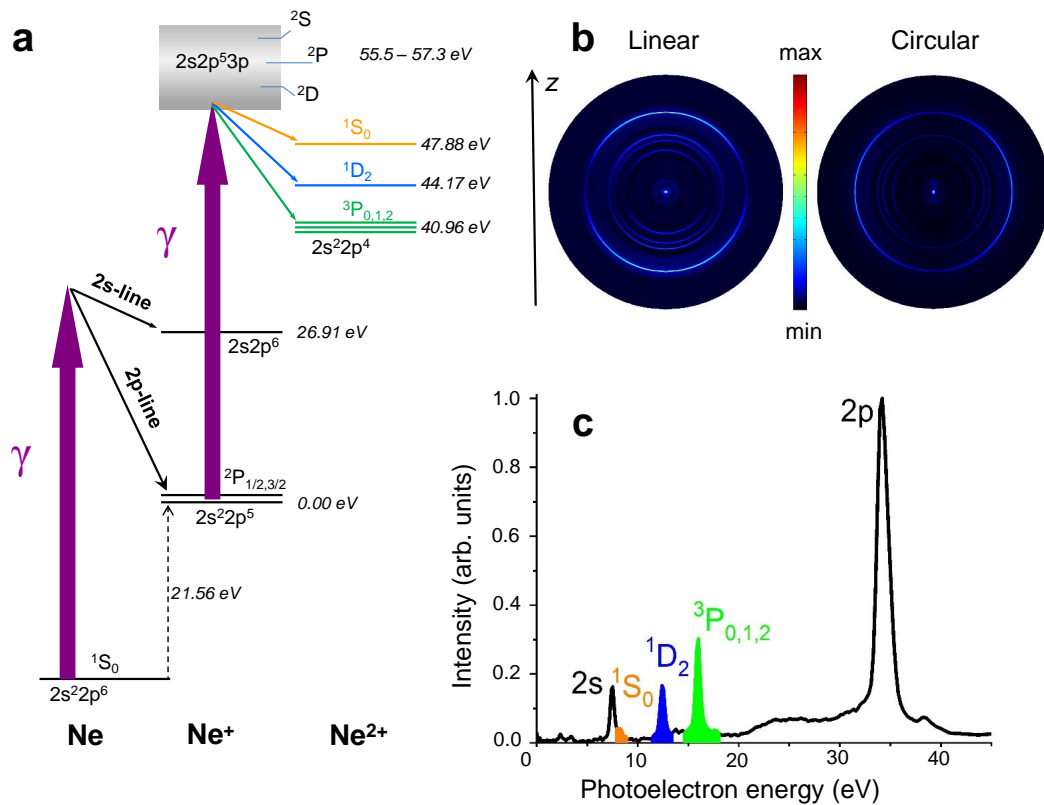


Figure 9: a) Scheme of the energy levels of Ne, Ne<sup>+</sup> and Ne<sup>2+</sup>. The three final ionic states of Ne<sup>2+</sup>, <sup>1</sup>S<sub>0</sub>, <sup>1</sup>D<sub>2</sub>, <sup>3</sup>P<sub>0,1,2</sub> are indicated by yellow, blue, and green lines, respectively. b) Inverted images of the photoelectron angular distributions obtained for linearly and circularly polarized XUV pulses using a velocity map imaging spectrometer. c) Photoelectron spectra obtained from Neon using linearly polarized intense XUV pulses. The three final ionic states of Ne<sup>2+</sup> (<sup>1</sup>S<sub>0</sub>, <sup>1</sup>D<sub>2</sub>, <sup>3</sup>P<sub>0,1,2</sub>) as well as the photoelectrons corresponding to ionization from the 2s and 2p levels of Neon are indicated. Figure reprinted from Carpeggiani et al. (2019), with permission. Copyright (2019) by the Authors.

#### 5.4. Single-photon Laser Enabled Auger Decay

The phenomenon of Auger decay is well-known as a relaxation mechanism after core ionization. In this process, a singly charged core hole state undergoes a valence-core or core-core transition, and simultaneously a second electron (the Auger electron) is emitted to form a doubly charged final state; the excess energy is carried away from the atom by the kinetic energy of the Auger electron. The field of Auger spectroscopy includes a number of other cases with their own terminology, for example, core-excited neutral states decay by resonant Auger Raman processes; when the process involves one electron from the same shell as the core hole, and one electron from another shell, it is said to be a Coster-Kronig transition. When both electrons are in the same shell as the hole, it is a super Coster-Kronig transition, and is usually a very fast processes. Auger electrons from a doubly core ionized atom are known as Auger hypersatellites.

The usual Auger process is equivalent to autoionization of the atomic ion discussed in the previous subsection. Historically, autoionization refers to inner valence and low energy excited states, whereas Auger processes refer to core ionized or core excited states. For shallow holes, the energy of the doubly charged state may be higher than the energy of the singly charged state, in which case Auger decay is energetically forbidden. However, if additional energy is available, the Auger decay becomes allowed. When the energy is provided by a laser, the process is known as Laser Enabled Auger Decay, and this has been observed in experiments where multiple laser photons provided the “enabling” energy (Ranitovic et al., 2011; Tong et al., 2011; Hogle et al., 2015). Thus, while normal Auger can be a single-photon, double ionization process, Laser Enabled Auger Decay is a few-photon, double ionization process.

If however the missing energy is provided by a single photon, then selection rules apply (Cooper and Averbukh, 2013). For a pure electronic state consisting of a single configuration, single-photon Laser Enabled Auger Decay (spLEAD) is forbidden. Due to the phenomenon of correlation, many electronic states are not pure, but are mixed with other configurations, so that spLEAD then becomes allowed. Thus this process represents a probe of the extent of correlation in a given ionic state.

Iablonskyi et al. (2017) reported the first observation of spLEAD, using the Free-Electron Laser FERMI. The sample was neon and the method employed was rather sophisticated, and took advantage of the fact that FERMI is longitudinally coherent. The sample was irradiated with phase-locked fundamental and second harmonic radiation and then the phase was tuned. The fundamental wavelength was chosen to be at the ionic resonance

$$2s^22p^5 + \omega \rightleftharpoons 2s2p^6 \quad (13)$$

This arrangement ensured that the final, doubly ionized Auger state could be reached by two different paths, one of which involved the spLEAD process. Interference occurred as the optical phase was scanned, and was manifested as an oscillation of the yield of photoelectrons corresponding to the final states. In the absence of the spLEAD process, the phase would have no effect on the yield. The final states are represented by the terms  $^1S$ ,  $^1D$  and  $^3P$ , and of these,  $^1S$  was not resolved from another spectral feature, so the work concentrated on  $^1D$  and  $^3P$ .

In the paper of Iablonskyi et al. (2017), it appeared that the triplet  $^3P$  term did not oscillate and this was interpreted as an indication that  $L-S$  coupling was a good approximation. However later calculations, and more accurate analysis, indicated that also this peak oscillated (You et al., 2019).

To understand the process, consider the main configurations which mix into the state which undergoes spLEAD, in this case  $2s$  ionized Ne. The main configuration is clearly  $2s2p^5$  (80%), but there are admixtures of  $2s^22p^4(^1S)ns$ ,  $2s^22p^4(^1D)nd$  and  $2s2p^5(^3P)np$ , as well as  $2s2p^5(^1P)np$ . For  $2s^22p^4nl$  configurations, the spLEAD process can be visualised as the ionization of the outer electron of these configurations by the “extra” energy supplied by the laser, leaving the ionic core of these states as the final doubly ionized state. The first three configurations lead to doubly charged ions with both holes in the  $2p$  shell. The calculations show that the  $2s2p^5(^3P)np$  configuration also has a significant electron yield, and this is due to a two-electron process, where one electron fills the  $2s$  hole and another is ejected. You et al. (2019) pointed out that Iablonskyi et al. (2017) had considered only configurations built on  $2s^22p^4(^3P)$  cores for the spLEAD process, but it is the configurations with  $2s2p^5(^3P)$  cores that make a significant contribution to final triplet states.

The newer theoretical analysis predicted all phenomena observed, and reproduced qualitatively or quantitatively the branching ratios of  $^3P$  to  $^1D$  final states, the ratios of oscillation amplitudes and the phase lags between the oscillations of different ionic states. An important aspect of this work is that it represents the observation and study of a new de-excitation process, and it is rare to discover such new processes. To perform this work, a key experimental requirement was the narrow bandwidth of the photons, which was tuned to the resonance described by Eq. (13).

### 5.5. Two-photon excitation leading to interatomic Coulombic decay

Interatomic Coulombic Decay (ICD) is a decay process which occurs in weakly bound systems, and was predicted more than 20 years ago (Cederbaum et al., 1997). Since then it has been observed in many different systems in various forms; see Jahnke (2015) for a review. If an inner valence level of an atom or molecule is ionized, and the energy is below the double ionization threshold, then it cannot decay by emission of an electron to form a doubly charged state. However, if the excited atom is weakly bound to another atom, and the internal energy is greater than the sum of the ionization potentials of the two, then it may decay to two singly ionized atoms, with the emission of an electron. A neutral atom weakly bound to a doubly charged ion clearly has a higher energy than two weakly bound singly charged ions, because the Coulomb repulsion is reduced. The ICD process may be viewed as autoionization occurring in a weakly bound system, and is generally a very fast process. It often competes with fluorescence decay, which is usually much slower.

In neon atoms, an inner-valence  $2s$  hole cannot decay via an Auger process, because the energy of an ion with two  $2p$  holes is greater than the energy of a  $2s$  hole. In a neon dimer, however, the final double positive charge can be shared between the two atoms, thus lowering the energy required for the second ionization step and the ICD decay channel may open up. ICD has been widely investigated using single-photon absorption of photons from synchrotron and FEL sources (Jahnke, 2015; Schnorr et al., 2013; Nagaya et al., 2016). In particular, taking advantage

of the development of tunable, femtosecond, intense XUV sources, Demekhin et al. (2011b) investigated theoretically the nonlinear excitation of the ICD mechanism through the absorption of two XUV photons. The energy scheme corresponding to the nonlinear excitation of the ICD process is illustrated in Fig. 10 (a): the dimer is first ionized, with the ejection of a 2p electron and then excited by the absorption of a second photon to a state characterized by a 2s hole in one atom (assuming a description of separated electronic levels for the atoms composing the dimer). The 2s hole is filled by a 2p electron and the excess energy is transferred to the second atom, inducing the ejection of a low energy electron (ICD electron). This work indicated that the preparation of the 2s hole in a dimer by sequential two-photon excitation should be more efficient than the single-photon ionization.

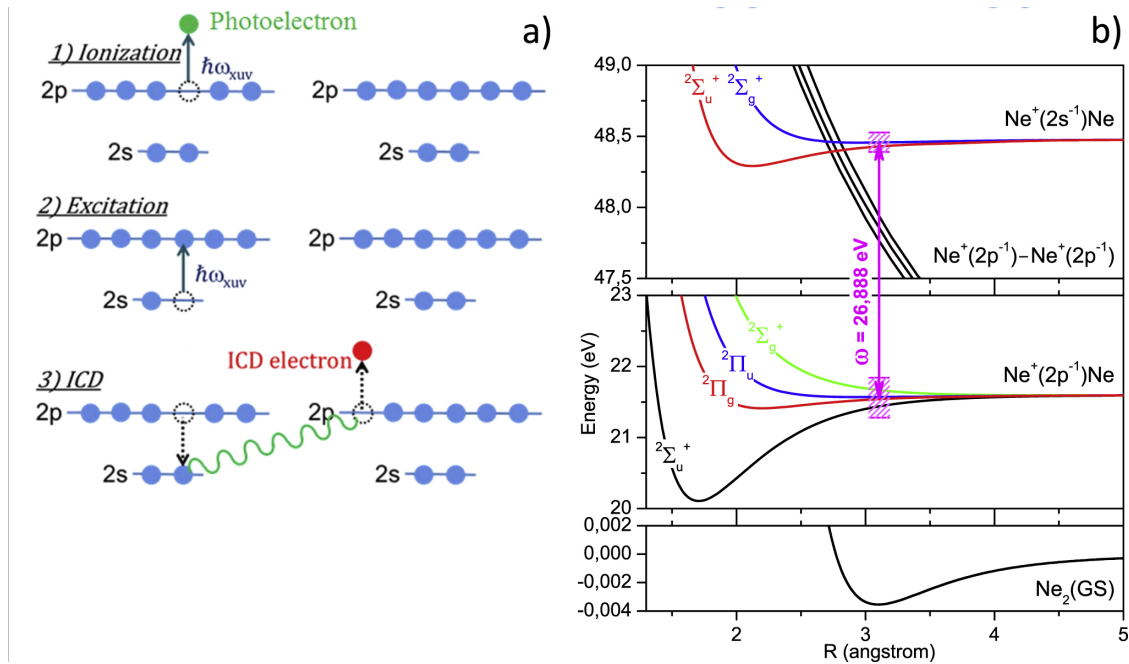


Figure 10: (a) Schematic representation of the two-photon excitation of ICD. In the Ionization step, the 2p electron is ionized by a photon from the XUV pulse with the emission of a photoelectron and population of the  $\text{Ne}_2(2p^{-1})$  states of the dimer. In the Excitation step, a second photon is resonantly absorbed leading to the population of the inner valence ionized  $\text{Ne}_2(2s^{-1})$  states. In the ICD step, the 2s hole of the initially ionized atom is filled by a 2p electron, and the excess energy is transferred to the neighboring atom, leading to the emission of the ICD electron. As a result, the two-site outer valence doubly-ionized dimer  $\text{Ne}_2(2p^{-1}2p^{-1})$  is populated, and undergoes Coulomb explosion. (b) Potential energy curves of the relevant neutral ground state, the outer and inner valence singly ionized states, as well as outer valence doubly ionized states of the neon dimer. Panel (a) is reprinted from Dubrouil et al. (2015), © IOP Publishing. Reproduced with permission. All rights reserved. Panel (b) is reprinted from Demekhin et al. (2011b), with permission. Copyright (2011) by the American Physical Society.

This excitation mechanism requires a resonant step corresponding to the excitation of a 2s electron to the 2p at 26.9 eV. At different energies, the resonant excitation step cannot take place, and also the ICD process cannot occur.

Figure 10 (b) presents the molecular potential energy curves for the neutral neon dimer  $\text{Ne}_2$  (lower panel), for the lowest energy states of the singly ionized dimer (corresponding to the configuration  $\text{Ne}^+(2p^{-1})\text{Ne}$ , central panel), and for the excited states of the ionized dimer corresponding to the configuration  $\text{Ne}^+(2s^{-1})\text{Ne}$ , upper panel). The Coulomb-repulsive energy curves of the double ionized neon dimer are also reported [ $\text{Ne}^+(2p^{-1})-\text{Ne}^+(2p^{-1})$ ]. An experiment on neon dimers was performed by (Dubrouil et al., 2015) to test this theoretical prediction, and it faced a number of challenges. Neon dimers were produced by a cold supersonic expansion of neon gas, resulting in a concentration of a few percent of dimers in atomic neon. The photons ionize both the dimer and the monomer, resulting in a very strong monomer 2p photoelectron signal, with the risk of saturating the atomic signal so that the weak dimer signal (with only a slightly different kinetic energy) could not be detected. This risk was avoided by measuring the dimer and monomer ion signals, which have a large dynamic range, and are well separated in the spectrum.

The photon energy was scanned across the predicted resonance energy (Demekhin et al., 2011b), and the ratio of

dimer ions to monomer ions showed a minimum at the resonant energy. The potential energy curves of the dimer are shown in Fig. 10 (b), where it can be seen that the Franck-Condon regions of the 2p and 2s ionized ions correspond to weakly bound ionic states. However the doubly ionized states, with one hole on each atom, are very strongly repulsive.

In the resonance region, the ionization probability of both dimers and monomers is constant, so the observation of a reduction of dimer ion intensity indicated that they were decaying faster at the resonant energy. This occurs because the 2p ionized dimer resonantly absorbs a second photon to become a 2s ionized dimer, which then decays via ICD, depleting the dimer ion signal.

### 5.6. Multiphoton XUV + Near Infrared ionization and Circular Dichroism

In Section 4.3, we discussed two-photon ionization by a single XUV and a single NIR photon. The availability of intense XUV pulses opens new frontiers for the investigation of the dynamical response of electronic systems to intense XUV and visible/near-infrared pulses. In this context, it is interesting to investigate the interplay between the dynamics induced by both fields.

Ilchen et al. (2017) investigated the photoelectron spectra of an ionic Rydberg state in a two-colour field for different relative helicities of the fields. The atom investigated was helium, which was first ionized to the ground state  $\text{He}^+(1s)$  by single photon absorption and then further excited to  $\text{He}^+(3p)$  by absorption of a second XUV photon. This situation is related to that discussed in Section 5.3, where ionization followed by resonant excitation was used to access autoionizing states; here the final state is long-lived, because it can decay only by fluorescence. The intense near-infrared pulse was co- or counter-rotating with respect to the circular polarization direction of the XUV pulse (as above), and photoionized the ion, thereby ejecting a second electron. Depending on the relative helicity between the two fields, different angular momentum states dominate the photoelectron angular distribution of the second electron. For low photoelectron energies (around 150 meV), in the co-rotating case, only the final continuum state characterized by quantum numbers  $l = 5$  and  $m = 5$  contribute to the photoelectron angular distribution. On the other hand, in the case of counter-rotating fields, two states with  $l = 3, m = -3$  and  $l = 5, m = -5$  contributed to the photoionization at low kinetic energies, and the photoelectron angular distribution depends, therefore, on the relative phase between these two contributions.

The CD is defined as:

$$CD = \frac{P_+ - P_-}{P_+ + P_-} \quad (14)$$

where  $P_+$  and  $P_-$  indicate the probability of ionization for fields with the same or opposite helicity, respectively. In the experiment a strong dependence of the CD as a function of intensity of the IR field was observed. In particular, at the intensity of  $I = 6 \times 10^{11} \text{ W/cm}^2$ , the CD reached almost the maximum value of unity, indicating the photoionization for the co-rotating case is more favoured with respect to the counter-rotating case. This difference can be interpreted by observing that four dipole transitions are required to reach the state  $l = 5, m = 5$  from the initial ionic state  $\text{He}^+(n = 3, l = 1, m = 1)$ . These transitions require in each step a change of one unit of the angular and magnetic quantum number:  $l \rightarrow l + 1$  and  $m \rightarrow m + 1$ , which are the most favourable dipole-allowed transitions for increasing  $l$ . For the counter-rotating case, the probability to reach the two final states  $l = 5, m = -5$  and  $l = 3, m = -3$  is much smaller (a factor 50) due to angular-momentum factors. This conclusion was confirmed also by TDSE simulation, which predicted an ionization probability two orders of magnitude smaller.

At higher IR intensities, the CD reduces and TDSE even predicts a change of sign for intensities exceeding  $1.5 \times 10^{12} \text{ W/cm}^2$ , see Fig. 11. This variation can be interpreted by investigating the role of the intense IR field on the population of the oriented ionic state  $\text{He}^+(3p)$ . In the case of co-rotating pulses, the IR induces a shift of the energy of the  $(3p, m = +1)$  level, which strongly reduces the population of this level. This shift is almost absent in the counter-rotating case. Therefore, the initial population of the ionic states compensates for the much less favourable photoionization pathway of the counter-rotating case. The results of Ilchen et al. (2017) were analysed in greater detail in a follow-up paper by Grum-Grzhimailo et al. (2019).

### 5.7. Two-photon, double core ionization

For a sufficiently intense X-ray pulse, it is possible to ionize two core levels with the same pulse. Core level photoelectron spectra are sensitive to the chemical surrounding of the ionized atom, observed as binding energy

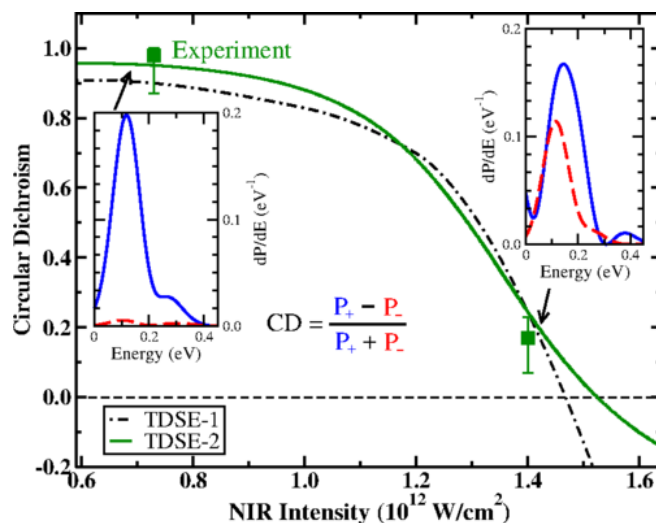


Figure 11: Experimental (green squares) and theoretical (green full line and black dashed line) circular dichroism CD for the electron peak at 200 meV as a function of the NIR intensity. The two theoretical curves were obtained using two TDSE models: black dash-dotted curve (Kazansky and Kabachnik, 2007); and green curve (Douguet et al., 2016). The insets present the electron energy spectra obtained from the TDSE calculations in correspondence to the two experimental points. Figure reprinted from Ilchen et al. (2017), with permission. Copyright (2017) by the American Physical Society.

differences in molecules and solids (Siegbahn, 1971). Santra et al. (2009) demonstrated theoretically that the advent of XFELs enabled a novel core spectroscopy: X-ray Two-Photon Photoelectron Spectroscopy (XTPPS). In this method, two core levels are ionized within the core hole lifetime, usually a few fs. Twenty four years earlier, Cederbaum et al. (1986) had demonstrated theoretically that the creation of double core vacancies in molecular systems probes the chemical environment more sensitively than the creation of single core vacancies, and that double ionization potentials (DIP) of two-site double-core-hole (tsDCH) states are particularly sensitive to the chemical environment. These tsDCH states, however, were not observed until 2011 (Lablanquie et al., 2011) because of extremely small cross sections for single-photon, double core ionization. Intense and short XFEL pulses made it possible to observe these tsDCH states via XTPPS where the two photons are absorbed sequentially by two atoms at different sites. Following the proposal of XTPPS (Santra et al., 2009), a series of calculations were performed to predict DIPs of tsDCH states for a number of molecules as a guide for experiments, for example (Tashiro et al., 2010a,b; Takahashi et al., 2011). Experiments at LCLS (Berrah et al., 2011; Salén et al., 2012) demonstrated the feasibility of XTPPS and at the same time its limitation; the photon bandwidth of the SASE beam was broad, hampering precise measurements. Use of narrow band and short (less than 5 fs) soft X-ray pulses, e.g., generated by seeded FELs (see Sections 2.1 and 2.2), is expected to improve significantly the performance of this method.

## 6. Multi-photon and multiple resonant excitation

### 6.1. Two-photon excitation of two electrons in atoms: Early studies

The simultaneous excitation of both electrons in the helium atom by a single photon was first observed by Madden and Codling (1963) using synchrotron radiation. The theoretical basis for describing this experiment had already been laid by Fano (1961), who had developed his earlier theory (Fano, 1935) to describe the electron scattering data of Lassette and Silverman. The double excitation of He has since been extensively studied, see Domke et al. (1995, 1996), and references to these papers. The importance of this system is that double excitation does not occur in an independent electron model, and becomes allowed by initial state correlation. Although these doubly excited states are subject to autoionization, they are qualitatively different from the autoionizing states discussed in Section 5.3, where one-photon excitation to the autoionizing states does not rely on the initial state correlation. For most of the cases discussed in that Section, two electrons were excited in two separate and sequential steps, for example ionization

followed by resonant excitation, and this led to double ionization. In this Section we discuss cases where the excitation occurs by simultaneous absorption of more than one photon.

The helium atom is the simplest three-body system for investigating correlation, and the narrow resonances can be measured and calculated with high precision. Double excitation is therefore a benchmark phenomenon for testing theoretical approaches and approximations. Indeed, for this reason, intensive state-of-the-art attosecond time-resolved studies have been carried out on helium doubly excited states (Ott et al., 2013, 2014; Gruson et al., 2016; Kaldun et al., 2016).

With intense FEL pulses, one can promote both electrons to these excited states with two or three photon absorption, without relying on initial state correlation: each photon can interact with each electron separately. At SCSS, Hishikawa et al. (2011) investigated three-photon single ionization of He employing a magnetic bottle electron spectrometer. The photon energy was  $\approx 24$  eV and the FEL power density was  $10^{13}$  W/cm<sup>2</sup>. Under these conditions one electron was promoted to the Rydberg manifold by single photon absorption and at the same time another electron was promoted to the Rydberg manifold by two-photon absorption. As a result, three-photon single ionization via autoionization of the doubly excited states was anomalously enhanced.

The role of doubly excited autoionizing states in Ar<sup>+</sup> populated via two-photon absorption of the ionic ground state of Ar<sup>+</sup> was studied by Gryzlova et al. (2011) using a velocity map imaging electron spectrometer and ab initio theory calculations.

### 6.2. Two-photon excitation of two electrons in atoms: Narrow-band studies

Single-photon excitation of He can access only <sup>1</sup>P<sub>o</sub> final states, but the helium atom has many other resonances of different angular momenta. In particular, states with term values <sup>1</sup>S<sub>e</sub> and <sup>1</sup>D<sub>e</sub> can be excited by two photons. At FERMI, Žitnik et al. (2014) investigated two-photon excitation of these even-parity, doubly excited, autoionizing states, taking advantage of the very narrow photon bandwidth of fully coherent FEL pulses.

The experiment is challenging because the ion or electron signal has a very large background due to non-resonant ionization. To overcome this difficulty, Žitnik et al. (2014) used an alternative detection scheme: instead of charged particles, they detected neutral metastable atoms. The resonantly excited atoms decay by autoionization to ionic states, and by fluorescence to neutral states. Some of these neutral states undergo cascades by fluorescent decay to the ground state, but some reach metastable states, which are long lived, as they cannot decay by fluorescence. The detector was very simple and consisted of a microchannel plate placed in front of the atomic He beam, with suitable meshes to repel charged particles. The yield of metastable atoms was low, but crucially it was background-free: the metastable atoms were created only at the resonance energies. This example shows how important narrow bandwidth is for the study of resonant phenomena, as well as the fundamental importance of good design of experiments.

### 6.3. Two-photon excitation of two electrons in dimers

In the previous subsection section we discussed the case where two-photon absorption of an atom promotes two electrons to two unoccupied Rydberg orbitals. In this section we discuss the case where a dimer absorbs two photons and both atoms are excited. Takanashi et al. (2017) investigated such a doubly excited state in Ne dimers. In the separated-atom picture, each atom in the dimer is resonantly excited to the 2p<sup>-1</sup>3s state: overall the order of the process is two-photon, the resulting molecular state is a neutral doubly-excited autoionizing one, and its energy is close to, but lower than, that needed for the double ionization of the system. The system decays by ICD to a singly-ionized dimer Ne<sub>2</sub><sup>+</sup> and a photoelectron e<sub>ICD</sub> as the final products.

The goal of this experiment was to measure the lifetime (inverse rate) of the ICD process. This approach, which depends critically on the rapid tunability and on the spectral purity of the exciting pulse, has two advantages: first, the single-photon energy is insufficient to ionize bare Ne atoms (the majority component of the gas jet) which then do not contribute a background signal; second, the resonant condition (at a photon energy of 16.39 eV, established by monitoring the Ne<sub>2</sub><sup>+</sup> ion yield while scanning the FEL wavelength, Fig. 12) allows a precise selection of the target excited state. If, before the system decays, one of the excited electrons is ionized by an external laser pulse (in this case: a UV laser; photon energy 4.75 eV), then the remaining Ne<sub>2</sub><sup>+</sup> ion is left in a repulsive state and dissociates into two atoms; the Ne<sub>2</sub><sup>+</sup> yield decreases, and a measurement of this as a function of the separation between the two pulses (XUV-UV delay, Fig 12) lets one extract the lifetime of the ICD process. The extracted lifetimes of the long-lived

doubly excited states,  $390_{-130}^{+450}$  fs, and of the short-lived ones,  $< 150$  fs, are in good agreement with *ab initio* quantum mechanical calculations (Demekhin et al., 2013).

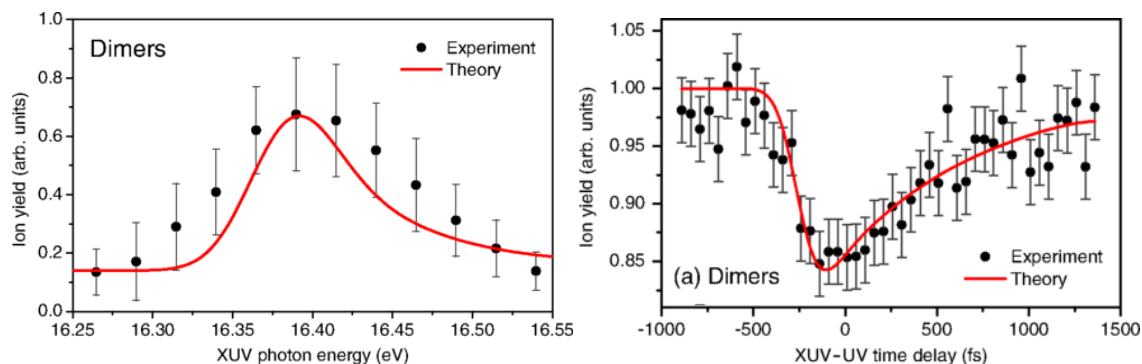


Figure 12: Left:  $\text{Ne}_2^+$  ion yield as a function of FEL wavelength. Right: normalized  $\text{Ne}_2^+$  ion yield as a function of pump-probe delay. Figures reprinted from Takanashi et al. (2017), with permission. Copyright (2017) by the American Physical Society.

#### 6.4. Multi-photon, site-specific, multiple excitation of clusters and droplets

Multiple excitation ICD, in which more than one atom in a loosely bound system is excited (Kuleff et al., 2010), may occur in more extended systems than dimers. Indeed much work has been done on large aggregates of atoms, namely clusters, using FEL light (Ovcharenko et al., 2014; LaForge et al., 2014; Nagaya et al., 2016) as well as intense NIR laser pulses (Schütte et al., 2015). Here we discuss experiments on neon clusters and helium droplets for the case of multiple atoms excited by single photons.

Iablonskyi et al. (2016) studied clusters of about 5000 Ne atoms, with resonant excitation of the 2p electrons to 3s states. The resonance energy of surface atoms, 17.12 eV, is slightly shifted with respect to the bulk, 17.65 eV. Thus by tuning the photon energy precisely, it was possible to excite surface or bulk atoms, and study them independently. In this case, ICD occurs as a de-excitation of adjacent excited atoms, neither of which has sufficient energy to emit an electron. They observed the evolution of the resulting electron spectrum as a function of the FEL intensity; the latter determines the number of excited atoms per cluster, which can easily exceed 2. The presence of many excited atoms within a cluster sets an upper limit to their abundance, by shifting the energy of the transition out of resonance (Coulomb blockade). Iablonskyi et al. (2016) found that the relaxation of excited surface atoms proceeded via a sequence of ICD processes, and as well, inelastic electron scattering in the surrounding cluster affected ICD of bulk atoms. Comparison with the  $\text{Ne}_2$  data described above (Takanashi et al., 2017) provided an estimate of the maximum excitation limit, found to be 8%. Although the experiment does not include pump-probe measurements, a lower limit of  $\sim 1$  ps was deduced for the ICD lifetime in a cluster, based on the  $\text{Ne}_2$  data and on the known inverse-sixth-power dependence of the ICD rate on interatomic distance. As a consequence of this long lifetime, cluster relaxation processes can occur before ICD takes place.

More recently, Ovcharenko et al. (2020) have investigated the dynamics of resonant, multiple excitation of He droplets for a wide range of droplet sizes and pulse intensity. Depending on conditions, a range of processes occurred: multi-step ionization, electronic relaxation, ICD, secondary inelastic collisions, desorption of electronically excited atoms, collective autoionization, and nanoplasma formation. The spectra were successfully described by numerical calculations based on rate equations.

## 7. Pump-probe studies

Ultrafast, short wavelength FEL pulses are a very useful tool for studying dynamics in molecules. The nuclei typically move on the fs time scale, while electrons move on the attosecond or few femtosecond scale, so that experiments are challenging with sources that range in duration from tens of femtoseconds to longer times. In pump-probe experiments, a sample is typically pumped by a laser pulse at one wavelength, and probed by a pulse at another wavelength. Most commonly the pump pulse is provided by an optical laser, and the FEL provides the probe pulse (Erk et al.,



2014; Gorkhover et al., 2016; Wolf et al., 2017a,b; Leitner et al., 2018; Nishiyama et al., 2019) but other arrangements are possible, e.g., FEL-pump, laser-probe (Takanashi et al., 2017; Kumagai et al., 2018; Fukuzawa et al., 2019), or FEL-pump, FEL-probe (Jiang et al., 2010; Liekhus-Schmaltz et al., 2015; Ferguson et al., 2016; Berrah et al., 2019). If the signal measured is, for example, total ion yield or Auger spectra (Wolf et al., 2017a), then high resolution of the probe may not be required. In this section, we give some examples of pump-probe studies which required narrow bandwidth in order to achieve sufficient spectroscopic resolution.

### 7.1. The dynamics of photo-excited thymine

Wolf et al. (2017b) have used transient core level absorption to investigate the dynamics of photo-excited thymine. Thymine, see Fig. 13, is one of the nucleobases of DNA, and like the others, is more resistant to damage by UV radiation than many other organic molecules. This suggests that its inclusion in DNA conferred an important characteristic for survival in a world before the ozone layer existed. The electronic energy deposited by UV absorption is converted to thermal energy in a very short time, but the exact mechanism of this process is still debated.

In their experiment, Wolf et al. (2017b) used 267 nm pulses to excite free thymine molecules to the  $\pi\pi^*$  state, that is, a state with a hole in a bonding  $\pi$  orbital, and an electron in a previously unoccupied  $\pi^*$  orbital. They probed the ensuing dynamics using Near Edge X-ray Absorption Fine Structure (NEXAFS) spectroscopy at the oxygen K edge, which requires a reasonably small bandwidth for the radiation. They obtained this from the LCLS SASE source by using a monochromator, which provided a bandwidth of 0.1%; for a SASE source this has the effect of increasing the intensity fluctuations, which can be as large as 0 to 100%. This was managed by post-sorting the data into bins of similar pulse energy.

The selection rules for NEXAFS permit transitions from the O 1s core level to unoccupied states of  $\pi$  symmetry. The UV excitation creates a hole in a valence orbital, thus allowing a new transition from the core to this hole; this occurs at lower photon energy than transitions to the unoccupied states of the neutral molecule. Such a feature was observed in the experiment, but theoretical calculations showed that it was not due to the initially excited  $\pi\pi^*$  state, but rather to an  $n\pi^*$  state, in which the hole is located in a non-bonding valence orbital. From this it was concluded that the excited state converts within 60 fs to the  $n\pi^*$  state, via a conical intersection. This state then undergoes further conversion with bi-exponential decay to a lower state, and with time constants of 1.9 and 10.5 ps.

We note in passing that this method, also known as transient absorption, has been used in experiments with laboratory sources (Attar et al., 2017). The details are different – a super-continuum soft X-ray light source was used with a spectrograph detector – but similar information was obtained. Both laboratory lasers and FELs are making rapid advances, and for now the techniques are complementary.

### 7.2. Photo-excited acetylacetone

XUV FEL light can also be used to probe the valence band, and here we discuss the example of photodynamics of acetylacetone, see Fig. 13. This representation portrays the position of the hydrogen between the two carbon atoms as asymmetric, but note that it can also be considered as effectively symmetric (Feyer et al., 2018). Squibb et al. (2018) pumped this molecule with 261 nm radiation to the  $S_2$  state, which has  $\pi\pi^*$  character, and probed the valence band spectrum using XUV radiation (24.0 eV, 51.57 nm) as a function of time after the pump. In core level spectroscopy, the identity of the emitting atom is evident (carbon, oxygen, etc) and its chemical state can be determined. For valence spectroscopy, theoretical calculations are necessary to determine the identity of a given feature in a spectrum.

After excitation, a number of peaks appear in the spectrum at lower binding energy than the ground state, so they are background free. Extra features may appear and overlap the ground state spectrum, however the excited state population is usually only a few % and the spectral features may be masked by the noise of the ground state. In Fig. 14, the valence spectrum shows three clear features at lower binding energy than the ground state (purple features), and these are plotted in colours light blue (peak 1), orange (peak 2) and green (peak 3). Their integrated intensities are plotted on the right as a function of time. Peak 1 appears immediately on excitation, then vanishes; it is identified from calculations as the  $S_2$   $\pi\pi^*$  state, which converts rapidly to an  $S_1$  state, peak 2. This has  $n\pi^*$  character, and then decays more slowly to a triplet  $T_1$ , peak 3, from which further decay occurs over long time scales, for example by fragmentation to yield methyl and hydroxyl radicals.

The theoretical description of this process is obviously complicated, and requires the calculation of the electronic structure of the ground and excited states, their ionization spectra, and the potential energy surfaces. These were

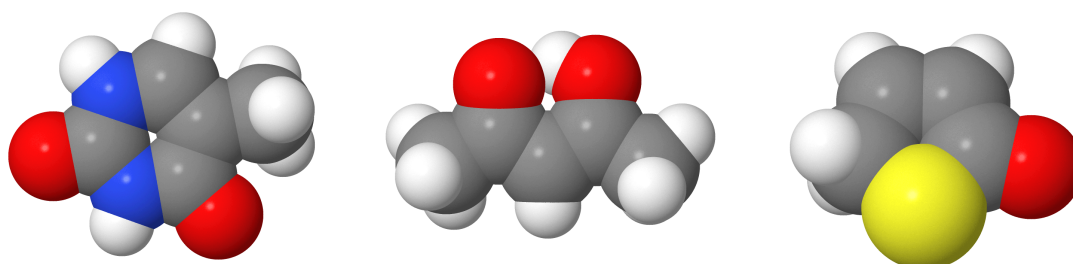


Figure 13: Schematic structure of thymine (left), acetylacetone (middle), 2(5H)-Thiophenone (right). Colours represent atoms of: grey, carbon; blue, nitrogen; red, oxygen; yellow, sulfur; white, hydrogen. Generated with Jmol: an open-source Java viewer for chemical structures in 3D. <http://www.jmol.org>

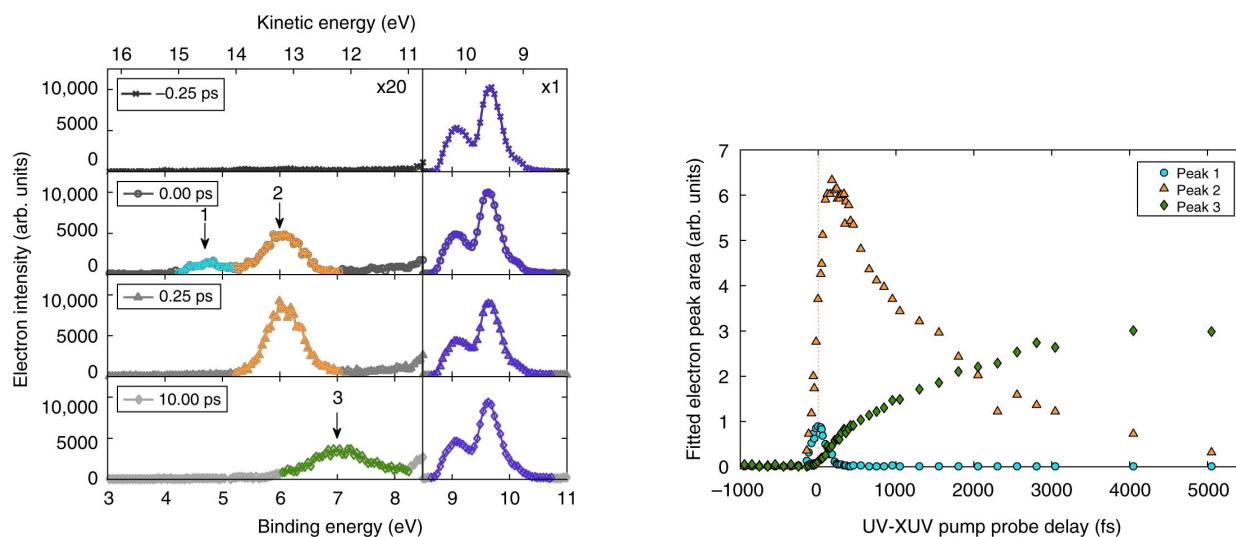


Figure 14: Photoelectron spectra and intensity versus time. Reproduced from Squibb et al. (2018); copyright 2018 by the Authors. The original figures have been published under a Creative Commons Attribution 4.0 license (CC BY) <http://creativecommons.org/licenses/by/4.0/>

compared with the experimental values of electron binding energies, time constants and ion yields to produce a detailed picture of the dynamics. A feature of this work was the high signal levels and high signal-to-noise ratio achieved, compared to laboratory HHG studies. However as laboratory sources continuously improve, we may expect that they will become competitive.

### 7.3. Isomerization of thiophenone

Besides fragmentation, there are many other important photo-induced chemical reactions, such as isomerization, and one of these is ring-opening, in which one of the bonds in a cyclic compound is broken. A well-known example is the synthesis of vitamin D in humans, one step of which involves exposure of the skin to sunlight, which in turn induces a ring-opening reaction. Many model systems of ring-opening reactions have been studied by a wide variety of techniques, and here we discuss a valence band photoemission study of the dynamics of thiophenone, Fig. 13, using FEL light (Pathak et al., 2020b).

The methods and apparatus used were similar to those described in the previous section, namely a magnetic bottle spectrometer at the Low Density Matter beamline of FERMI. High level calculations of electronic structure and molecular dynamics were carried out to understand the numerous possible pathways to final photoproducts, via a

complex multi-dimensional potential energy landscape. The ring opening occurs via the decay of the initially excited  $S_2$  state, via the  $S_1$  state, to the electronic ground state, accompanied by the lengthening and later scission of the S-CO bond. The initial electronic energy due to photoexcitation is converted to vibrational energy, and at least 3 open-ring structures were identified, some of which may re-form the initial thiophenone molecule. In this work, a key point was that it was possible to identify a range of possible photo products by correlating experimental and theoretical results.

#### 7.4. Dynamics of photo-excited He droplets

Mudrich et al. (2020) studied He nanodroplets and directly probed the excited state with a UV pulse (266 nm) and measured the outgoing photoelectrons. By working at much lower FEL intensity than the maximum available, they produced a low population of excited atoms in each droplet. They concentrated on the case of a single excitation per droplet and were able to follow in detail the rapid ( $< 0.25$  ps)  $1s2p \rightarrow 1s2s$  interband relaxation, the slow ( $\sim 1$  ps) rearrangement of the local environment (bubble formation), and the ultimate bursting of the bubble (several ps). The experimental results were supported by detailed time-dependent density functional theory calculations; note that in this case, the density in question is that of the helium, not of the electrons, and the density functional is a bosonic one, specialized for  $^4\text{He}$  (Ancilotto et al., 2017).

## 8. Theoretical approaches

Many reviews and books are devoted to the theory of atoms and molecules in a radiation field (for example: Manakov et al., 1986; Faisal, 1987; Fedorov, 1998; Lambropoulos et al., 1998; Delone and Krainov, 2000; Joachain et al., 2012). However describing dynamics of many-electron systems interacting with atto- and femtosecond laser pulses is a challenge for theory. Some recent reviews of theoretical approaches for multielectron dynamics in pulsed electromagnetic fields are given in Ishikawa and Sato (2015); Palacios et al. (2015); Palacios and Martín (2020), as well as in the book by Vrakking and Lepine (2019). Here we briefly outline modern theoretical methods in treating photoionization with FELs in the XUV domain. Inevitably, many excellent works on the interaction of radiation pulses in the visible and infrared regions with atoms and molecules will not be covered here. Atomic units are used throughout this section.

### 8.1. Amplitudes and description of physical quantities

In quantum theory a physical quantity ('observable') after a reaction is obtained from the (complex) amplitudes of the corresponding process. Thus, evaluation of the amplitudes is a key element of theory and the approximations used in these evaluations are the most important characteristics of the theoretical approach. Hereafter we limit ourselves to processes where the field may be described classically, and matter is described by quantum mechanics. Such an approach is widely used and justified when the number of photons in a mode of the radiation field is high.

We denote by  $\langle f | \hat{T} | i \rangle$  the transition amplitude from an initial state described at time  $t_0$  by a state vector (wave function)  $|i\rangle$  with a set of quantum numbers  $\{i\}$ , to a final state  $|f\rangle$  with a set of quantum numbers  $\{f\}$ . The  $\hat{T}$ -operator is the infinite time limit of the evolution operator  $\hat{U}(t, t_0)$ , which may be formally written as

$$\hat{T} = \lim_{t \rightarrow \infty} \hat{U}(t, t_0) = \lim_{t \rightarrow \infty} \mathcal{T} \exp \left[ -i \int_{t_0}^t dt' \hat{H}(t') \right]. \quad (15)$$

Here the exponential of an operator is defined in terms of its Taylor series expansion, while  $\mathcal{T}$  is a time-ordering operator, which by definition orders operators in the Taylor series chronologically (Tannor, 2007).

The choice of the sets of quantum numbers  $\{i\}$  and  $\{f\}$  is largely a matter of convenience. Their selection is normally dictated either by conservation laws or by features of the experimental setup. Generally, the system, both in the initial and the final state is in a mixed state, which cannot be described by a single state vector, but rather by the density matrices  $\langle i | \hat{\rho} | i' \rangle$  and  $\langle f | \hat{\rho} | f' \rangle$ , respectively. The density matrix of the final state is found from the density matrix of the initial state in terms of the amplitudes:

$$\langle f | \hat{\rho} | f' \rangle = \sum_{ii'} \langle f | \hat{T} | i \rangle \langle f' | \hat{T} | i' \rangle^* \langle i | \hat{\rho} | i' \rangle. \quad (16)$$

Standard quantum mechanical prescriptions are used to obtain a physical quantity from the known density matrix of the final state, for example, by taking a trace over unobserved quantum numbers and taking diagonal elements for observed characteristics. However this recipe is not always appropriate for mixed states. The concept of efficiency matrix of a detector or system of detectors  $\langle f | \hat{\epsilon} | f' \rangle$  is more general (Devons and Goldfarb, 1957; Ferguson, 1965). The probability to detect a mixed state is then expressed as  $W = \text{Tr} [\hat{\rho} \hat{\epsilon}]$ . Irreducible components of the density matrix of the angular momentum (equivalent terms such as “statistical tensors”, “state multipoles” and some others are used) and the corresponding efficiency tensors of the detector, in combination with the partial-wave amplitudes are especially convenient in treating different vector correlations. Many expressions for the observable quantities in terms of statistical tensors and the amplitudes can be found in Balashov et al. (2000).

The amplitudes  $\langle f | \hat{T} | i \rangle$  define an important quantity, the time delay (sojourn time). A scattered particle is ‘delayed’ in time relative to the free propagating particle. This effect is extensively discussed in the literature (see, e.g., the reviews by Sassoli de Bianchi, 2012; Maquet et al., 2004; Pazourek et al., 2015). In the formulation of Eisenbud (1948), Wigner (1955) and Smith (1960), this EWS time delay in the channel  $|f\rangle$  is expressed in terms of the derivative

$$\tau_f = \frac{d}{dE} \arg \langle f | \hat{T} | i \rangle, \quad (17)$$

where  $E$  is the energy of the particle. The concept of the EWS time delay has been extended to photoionization, as a half collision process (Schultze et al., 2010; Dahlström et al., 2012; Maquet et al., 2004; Pazourek et al., 2015). It is widely used currently in studies of photoprocesses on the attosecond time scale. Section 4.8 of the present review gives more details and further references on time delays in photoionization.

## 8.2. Time-dependent Schrödinger equation (TDSE)

The time evolution of pure states is described, in the nonrelativistic case, by the time-dependent Schrödinger equation (TDSE). In the coordinate representation

$$i \frac{\partial}{\partial t} \Psi(\xi, t) = \hat{H}(\xi, t) \Psi(\xi, t) \quad (18)$$

with the initial condition  $\Psi(\xi, t = t_0) = \Phi_i(\xi)$ . In the present case of an external classical electromagnetic field,

$$\hat{H}(\xi, t) = \hat{H}_0(\xi) + \hat{V}(\xi, t), \quad (19)$$

where  $\hat{H}_0(\xi)$  is the Hamiltonian of the system,  $\hat{V}(\xi, t)$  is its interaction with the field, and  $\xi$  is a set of particle coordinates of the target. In molecular problems,  $\hat{H}_0(\xi)$  is further subdivided into nuclear and electronic parts and electron-nuclei interaction. The Born-Oppenheimer approximation is often applied, which assumes that the electron motion is much faster than the nuclear motion. Moreover, for pulses as short as a few femtoseconds, the nuclei can be treated as fixed in space during the pulse.

In the vast majority of studies the interaction is taken in the long-wave electric dipole (E1) approximation  $\hat{V}(\xi, t) = \mathbf{E}(t) \cdot \mathbf{D}(\xi)$ , where  $\mathbf{E}(t)$  is the electric field,  $\mathbf{D}(\xi) = \sum_j e_j \mathbf{r}_j$  is the electric dipole operator;  $e_j$  and  $\mathbf{r}_j$  are the electric charge and radius vector of the particle  $j$ . In the fixed-nuclei approximation the nuclei are not affected by the external electromagnetic field, the summation is over electrons, and  $e_j = e$ . Another frequently used and physically equivalent formulation of the interaction in terms of the vector potential  $\mathbf{A}(t)$  uses  $\hat{V}(\xi, t) = -\frac{1}{c} \mathbf{A}(t) \cdot \sum_j \mathbf{p}_j$ , where  $\mathbf{p}_j$  is the linear momentum of the particle  $j$ . The TDSE (18) is equivalent to

$$\Psi(\xi, t) = \mathcal{T} \exp \left[ -i \int_{t_0}^t dt' \hat{H}(\xi, t') \right] \Phi_i(\xi) \quad (20)$$

and the amplitude is expressed (see Eq. (15)) as the projection  $\langle f | \hat{T} | i \rangle = \langle f | \Psi(t \rightarrow \infty) \rangle$ . Approximating the evolution operator in Eq. (20), i.e., propagating the wave function in time, is a key problem for solving the TDSE. This problem is on the border of theoretical physics and theory of numerical methods and has been discussed for decades (e.g., Moler and Van Loan, 2003; Bandrauk and Lu, 2013; Han et al., 2019). Not all methods aim to find the wave function  $\Psi(t \rightarrow \infty)$ , for example, the time-dependent density functional theory (DFT). The DFT is applied to calculations of wave packets in continua, in combination with expansion methods (see Section 8.4).

### 8.3. Solution of the TDSE on the space-time grid

Modern computing capabilities make it easy enough to cope with solving the TDSE (18) on the space-time grid for one or two active electrons. Hundreds of papers using this approach have been published since the first such calculations for one- (Kulander, 1987) and two-electron (Smyth et al., 1998; Parker et al., 2001) systems. The three active electron problem has also been solved (Colgan and Pindzola, 2012) and attempts to solve the TDSE on the grid for four electrons have begun (Pindzola et al., 2019). In fact the multidimensional TDSE is solved on the grid, especially for two or more active electrons, not directly, but after expansion of the solution in a complete basis in part of the variables. For example, in atomic problems expansions in spherical harmonics are used,

$$\Psi(\mathbf{r}, t) = \sum_{lm} P_{lm}(r, t) Y_{lm}(\Omega), \quad (21)$$

where  $Y_{lm}(\Omega)$  is a spherical harmonic, for a single active electron, or

$$\Psi(\mathbf{r}_1, \mathbf{r}_2, t) = \sum_{l_1 l_2 LM} P_{l_1 l_2}^{LM}(r_1, r_2, t) Y_{l_1 l_2}^{LM}(\Omega_1, \Omega_2), \quad (22)$$

where  $Y_{l_1 l_2}^{LM}(\Omega_1, \Omega_2)$  is a bipolar spherical harmonic, for two active electrons, etc. Then Eq. (18) reduces to the set of coupled partial differential equations (close-coupling equations) for the radial functions  $P_{lm}(r, t)$  and  $P_{l_1 l_2}^{LM}(r_1, r_2, t)$ , respectively, which are then solved on the one or two dimensional space grids with time propagation. Basis sets were applied to separate part of the variables in prolate spheroidal coordinates for the  $H_2$  molecule (Awasthi et al., 2005; Guan et al., 2011). Two- and three dimensional grids in cylindrical coordinates without basis expansions were used in solving the TDSE for single-electron problems (Kulander, 1987; Yuan and Bandrauk, 2019).

The solution of the TDSE on the grid can be obtained in a wide range of the field frequencies and intensities for pulses with various envelopes and relative carrier-envelope phases. However, direct numerical solution on a space-time grid is a computationally laborious method with rapidly increasing computational cost not only with increasing number of spatial dimensions, but also with the pulse length and field intensity. Furthermore, essential properties of many-electron atoms and molecules are neglected. Only part of them can be taken into account by effective local potentials for the target description. Nevertheless, the method may be useful in simple cases for many-electron atoms too, when the process does not involve the inner shells and the continuum is flat. Appropriate examples are Douguet et al. (2017) and Gryzlova et al. (2018, 2019b), where photoelectron angular distributions in ionization by XUV pulses in the region of intermediate excited states were described.

### 8.4. Expansion methods

In this class of methods, instead of solving Eq. (18) on the space-time grid, the series expansions of the solution in basis functions in the entire space of the variables are applied:

$$\Psi(\xi, t) = \sum_n c_n(t) \phi_n(\xi), \quad (23)$$

where  $\phi_n(\xi)$  is a basis set and  $c_n(t)$  are unknown coefficients. Substitution of Eq. (23) into Eq. (18) reduces the latter to a set of ordinary differential equations (equations of motion) depending on the coefficients  $c_n(t)$ . In practice different basis sets  $\phi_n(\xi)$  are used, giving rise to a variety of methods, which differ by the basis set chosen and technical realization applied. A natural choice is the set of eigenfunctions of the field-free Hamiltonian  $\hat{H}_0(\xi)$ :  $\hat{H}_0(\xi) \phi_n(\xi) = \epsilon_n \phi_n(\xi)$  (Mercouris et al., 1994, 2010, 2016). Further decomposition of the functions  $\phi_n(\xi)$  may be performed, e.g. in B-splines (Martín, 1999; Bachau et al., 2001), Lagrange interpolating polynomials (Artemyev et al., 2015; Müller et al., 2018), or Coulomb-Sturmian functions (Foumouo et al., 2006). The critical points are the choice of states to include in the basis, and the estimate of the number of basis functions necessary to reproduce the essential physics of the problem.

In the time-dependent Feshbach close-coupling method, the wave function is split by the projection operators  $\hat{P}$  and  $\hat{Q}$  ( $\hat{P} + \hat{Q} = \hat{1}$ ,  $\hat{P}^2 = \hat{P}$ ,  $\hat{Q}^2 = \hat{Q}$ ,  $\hat{P}\hat{Q} = \hat{Q}\hat{P} = 0$ ) as

$$\Psi(\xi, t) = \hat{P} \Psi(\xi, t) + \hat{Q} \Psi(\xi, t) \quad (24)$$

with subsequent series expansion of both terms in Eq. (24), similar to Eq. (23). The operators  $\hat{\mathcal{P}}$  and  $\hat{\mathcal{Q}}$  project on two subspaces, coupled by a residual interaction. This approach is successfully used in calculations of molecular photoionization by short pulses beyond the Born-Oppenheimer approximation (Palacios et al., 2015; Palacios and Martín, 2020).

In the “time-dependent configuration-interaction singles method” (Greenman et al., 2010; Hochstuhl and Bonitz, 2012; Karamatskou et al., 2014; Sato et al., 2018c) only the Hartree-Fock ground state and one-particle-one-hole excitations with respect to this state are included in the basis. The corresponding basis functions are built as time-independent Slater determinants. Thus, it includes an essential part of many-electron effects, which is a big step in comparison with the models which use the effective potential. The method was applied to studies of energy- and angle-resolved photoelectron spectra in one-photon and above-threshold ionization of argon following strong XUV irradiation (Karamatskou et al., 2014; Goetz et al., 2016), and the multi-photon process of above-threshold ionization for the light elements in the hard X-ray regime (Tilley et al., 2015). The method can be further improved by inclusion of two-particle-two-hole states in the expansion Eq. (23) (Bauch et al., 2014). The methods based on the expansion Eq. (23) may be characterized as configuration interaction methods with a fixed number of certain stable configurations mixed in a time-dependent way.

The multicofigutaion time-dependent Hartree-Fock (MCTDHF) method is a further extension, where the basis functions in Eq. (23), expressed as Slater determinants, depend on time,  $\phi_n(\xi) = \phi_n(\xi, t)$  through the time-dependent electron orbitals (Beck et al., 2000; Zanghellini et al., 2003; Caillat et al., 2005; Kato and Kono, 2004; Nest, 2009; Alon et al., 2009; Haxton et al., 2011; Haxton and McCurdy, 2015). In this case, equations for  $c_n(t)$  and  $\phi_n(\xi, t)$  are obtained not directly from Eq. (18) but by using the time-dependent variational principle (TDVP) leading to the relation:

$$\delta \langle \Psi(t) | \hat{H}(t) | \Psi(t) \rangle - i \left( \langle \delta \Psi(t) | \frac{\partial \Psi(t)}{\partial t} \rangle - \langle \frac{\partial \Psi(t)}{\partial t} | \delta \Psi(t) \rangle \right) = 0. \quad (25)$$

The MCTDHF method considers all the possible Slater determinants for a given number of orbitals. Thus, though powerful, the computational time for solving the corresponding set of equations for the time-dependent coefficients and orbitals scales factorially with the number of electrons. Therefore this approach is hardly tractable for systems with a large number of electrons. A more flexible method was introduced by Sato and Ishikawa (2013) and by Miyagi and Madsen (2013), where orbital sub-spaces are selected, and are treated in different approximations, for example, time-independent tightly bound core electrons and active electrons to describe the ionization. Various options of this method may be applied (Sato and Ishikawa, 2015). For an extended list of references, see Omiste and Madsen (2019), while more details of this method are given in Section 8.8.

In the time-dependent R-matrix approach (Burke and Burke, 1997), an expansion of the following type is used

$$\Psi(x_1, x_2, \dots, x_{N+1}, t) = \hat{A} \sum_n \phi_n(x_1, x_2, \dots, \Omega_N, \sigma_N) r_{N+1}^{-1} \psi_n(r_{N+1}, t), \quad (26)$$

where  $\hat{A}$  is the antisymmetrization operator,  $x = \{\mathbf{r}, \sigma\}$  denote space ( $\mathbf{r} = \{r, \Omega\}$ ) and spin ( $\sigma$ ) coordinates,  $\phi_n$  is a basis (channel) function formed by coupling of the  $N$ -electron residual state with the angular and spin parts of the outer electron wave function, and  $\psi_n$  is the radial function that describes the electron motion in the  $n$ -th channel. Substitution of Eq. (26) into Eq. (18) gives a set of integro-differential equations for the radial time-dependent functions  $\psi_n$ . A characteristic of the method is partitioning of the configuration space into internal and external (asymptotic) regions. Account is taken of electron correlations and channel coupling in the internal region, and a local long-range atomic potential, together with the laser field, are assumed in the external region. The solutions in the two regions are matched.

The details of the method are presented in the literature, where versions of the time-dependent R-matrix approach are being developed (van der Hart et al., 2007; Guan et al., 2007; Nikolopoulos et al., 2008; Lysaght et al., 2009; Moore et al., 2011; Hutchinson et al., 2013; Feist et al., 2014; Wragg et al., 2015). A simple option for one-electron systems is discussed in Ó Broin and Nikolopoulos (2017). Despite the computational awkwardness, this method uses numerical codes developed over years for stationary R-matrix theory and can be successful in the domain of its applicability (Zatsarinny and Bartschat, 2013), although the boundaries of this domain are still to be established. For many-electron atoms examples of the application of the time-dependent R-matrix method so far include ionization of Ne and Ar (van der Hart et al., 2007, 2008; Guan et al., 2007, 2008; Lysaght et al., 2008; Moore et al., 2011; Hutchin-

son et al., 2013; Chen et al., 2019). The method is under development for molecules (Ó Broin and Nikolopoulos, 2015).

### 8.5. Perturbation theory

It is often assumed that for ionization in the XUV region, perturbation theory (PT) is sufficiently accurate to describe the interaction  $\hat{V}(\xi, t)$ . This assumption is justified in many cases of interest, since the ratio of the ponderomotive electron energy to the photon energy decreases as the inverse cube of the photon frequency. Therefore, while in the IR and visible range for intensities of the order  $10^{13}$ - $10^{14}$  W/cm<sup>2</sup>, the field is considered as strong, and processes take place which cannot be described within the perturbation theory (such as tunneling and high harmonic generation), the lowest possible order PT gives an adequate description of photoionization for these intensities in the XUV. However, at a given intensity, the perturbation theory may become unreliable near resonances.

For pulses with finite time duration, the first and second order PT amplitudes are, respectively, of the form

$$\langle f | \hat{T} | i \rangle_1 = -i \int_{-\infty}^{\infty} dt \exp[i(\epsilon_f - \epsilon_i)t] \langle f | \mathbf{E}(t) \cdot \mathbf{D} | i \rangle, \quad (27)$$

and

$$\begin{aligned} \langle f | \hat{T} | i \rangle_2 &= i^2 \sum_p \int_{-\infty}^{\infty} dt \exp[i(\epsilon_f - \epsilon_p)t] \langle f | \mathbf{E}(t) \cdot \mathbf{D} | p \rangle \\ &\quad \times \int_{-\infty}^t dt' \exp[i(\epsilon_p - \epsilon_i)t'] \langle p | \mathbf{E}(t') \cdot \mathbf{D} | i \rangle, \end{aligned} \quad (28)$$

where the summation is over eigenstates of the field-free Hamiltonian, including integration over the continuum. In practice, most essential near-resonant intermediate states are included in Eq. (28). The advantages of the second order PT are its flexibility in selecting and analysing individual reaction channels, straightforward procedure for improving the target description and low computational cost. The PT amplitudes explicitly show simple tensorial structure, which is very convenient in analytical transformations, especially for treating vector correlations. Comparison with non-perturbative calculations, for example, with the solution of the TDSE, clarifies the domain of applicability of the PT (Grum-Grzhimailo et al., 2015b; Douguet et al., 2016).

In the limit of infinite pulses with constant amplitudes, the time integrals in Eq. (27) and Eq. (28) are taken and become the relationships representing energy conservation. For the second and higher order amplitude in this limit, the summation over the intermediate states can be performed using additional approaches, for example by using Green's function (Manakov et al., 1986; Maquet et al., 1998) or by variational procedures (Gao and Starace, 1989; Machado and Masili, 2004; Douguet et al., 2017). In this limit, developed program packages for the first-order PT amplitudes and characteristics of the atomic electron emission are available, based on an R-matrix approach [RMA-TRX (Berrington et al., 1995); BSR (Zatsarinny, 2006)], multiconfiguration Dirac-Fock [RATIP (Fritzsche, 2001, 2012)], Hartree-Fock [MCHF (Froese-Fischer et al., 1997)] approximations, and the random phase approximation with exchange [ATOM, (Amusia et al., 2016)]. Also for molecules, various methods are used for calculating the first-order amplitudes, for example: approaches based on the DFT with B-splines (Toffoli et al., 2002; Stener et al., 2007), including vibrationally resolved photoionization (Plésiat et al., 2012; Engin et al., 2019); single center methods (Demekhin et al., 2011a); the random phase approximation (Semenov et al., 2000); and the multichannel Schwinger configuration interaction method (Lucchese and McKoy, 1983; Stratmann and Lucchese, 1995).

The first order PT is extensively used in the calculation of few-photon, sequential ionization by FELs, especially the photoelectron angular distributions and angular correlations (Kheifets, 2007; Fritzsche et al., 2008; Gryzlova et al., 2010, 2012, 2014, 2015). When combined with the statistical tensor formalism, it conveniently takes into account polarization of intermediate ionic states. This approach was used in the description of sequential ionization of Ne (Kurka et al., 2009; Rouzée et al., 2011), Ar (Fukuzawa et al., 2010; Gryzlova et al., 2011; Augustin et al., 2018; Gryzlova et al., 2019a), Kr (Fritzsche et al., 2009), and Xe (Fritzsche et al., 2011) in the XUV. The field was reviewed in Grum-Grzhimailo et al. (2016). Non-dipole effects in sequential two-photon double ionization were predicted in the framework of the PT (Grum-Grzhimailo et al., 2012, 2015a) and measured in argon at FERMI (Ilchen et al., 2018).

The photoelectron angular distribution and various types of dichroism for the sidebands in two-photon, two-colour above-threshold atomic ionization were studied within the second order perturbation theory by Grum-Grzhimailo and

Gryzlova (2014) taking account of the full multipole expansion of the radiation field and independently variable polarizations of the XUV and IR radiation beams. The calculations predicted nondipole effects in the sidebands for Ne 1s ionization, in some cases much larger than in the main photoelectron line.

### 8.6. Strong-field-type approximations

The strong-field approximation (SFA) (Keldysh, 1965; Faisal, 1973; Reiss, 1980) has a large number of variations (Lewenstein et al., 1994; Quéré et al., 2005; Maquet and Taïeb, 2007; Kazansky and Kabachnik, 2006; Jiménez Galán et al., 2013; Boll and Fojón, 2014); see also the reviews by Ivanov et al. (2005), and by Karnakov et al. (2015). This approximation assumes that the photoelectron moves as a particle in the electromagnetic field, while the atomic or molecular potential is considered as a perturbation. In most applications, the latter is neglected and the electron is described by the non-relativistic Volkov wave function (Wolkow, 1935)

$$\psi_{\mathbf{p}}(\mathbf{r}, t) = \exp\{i[\mathbf{p} - \mathbf{A}(t)]\mathbf{r} - i\Phi(\mathbf{p}, t)\}, \quad (29)$$

where  $\mathbf{p}$  is the electron momentum,  $\mathbf{A}(t)$  is vector potential of the strong field and

$$\Phi(\mathbf{p}, t) = \frac{1}{2} \int_t^\infty dt' [\mathbf{p} - \mathbf{A}(t')]^2. \quad (30)$$

The SFA is used when the XUV radiation from the FEL ionizing the target is combined with a strong IR field. Interaction of the XUV field with the target is treated in the first-order PT. Therefore, to obtain the amplitude in the SFA, the wave function (Eq. 30) combined with the wave function of the residual ion is substituted in Eq. (27) as the final state  $|f\rangle$ . The domain of applicability of this approach is usually limited to high energies of the outgoing electrons in comparison with the energy of the IR photon. The Coulomb interaction between the photoelectron and the residual ion, which modifies the final state wave function (Coulomb-Volkov approximation) is generally important and may be taken into account. An extensive literature on the effects of the Coulomb field on the ionization process within the strong-field approach is available (see, e.g., Goreslavski et al., 2004; Karnakov et al., 2015, for further references). The SFA is regularly used in description of the sidebands of the main photoelectron line in XUV + IR ionization by atto- and femtosecond pulses (Kazansky et al., 2010, 2011; Jiménez Galán et al., 2013; Picard et al., 2004). It allows significant advances in developing analytical derivations, in particular, closed-form expressions for the angular distributions of photoelectrons in two-colour XUV + IR ionization were obtained (Boll and Fojón, 2016).

### 8.7. Density matrix approach

The time evolution of the density matrix is described by the Liouville equation (Blum, 2012):

$$i \frac{\partial \hat{\rho}(t)}{\partial t} = [\hat{H}(t), \hat{\rho}(t)], \quad (31)$$

which is written here in the operator form with  $\hat{\rho}(t)$  being the density operator. The density matrix formalism consistently takes into account coupling to an external reservoir and relaxation processes. Relaxation is especially important in studies of the inner-shell excitation/ionization by XFELs on the femtosecond time scale. This scale is usually determined by the lifetime of the hole decaying by Auger decay, and competing with photoionization by the XFEL pulse. Furthermore, considering the reservoir with short correlation time, i.e., one which quickly “forgets” its interaction with the system, allows the introduction of the Markov approximation (Blum, 2012; Cohen-Tannoudji et al., 2004; Lambropoulos and Petrosyan, 2007). Together with the rotating wave approximation, it simplifies drastically Eq. (31) up to the master equations for the elements of the density matrix (Zwanzig, 1964; Haake, 1973) and, moreover, eliminates the density matrix elements coupling the continuum states (Hanson et al., 1997). Solutions of the master equations are repeatedly used in treating problems related to the processes generated by FELs (Sun et al., 2010; Nikolopoulos et al., 2011; Middleton and Nikolopoulos, 2012; Rohringer and Santra, 2012). For example, Nikolopoulos (2013) calculated the sequential two-photon double ionization of neon by a FEL pulse and successfully reproduced the angular correlation function of the two emitted electrons, while Nikolopoulos and Lambropoulos (2015) revealed a role of a small admixture of FEL harmonics on photoionization.



After making some additional approximations (Blum, 2012), Eq. (31) transforms into a set of rate equations for population of the levels of the system

$$\frac{dN_n(t)}{dt} = \sum_{n' \neq n} W_{n' \rightarrow n} N_{n'}(t) - N_n(t) \sum_{n' \neq n} W_{n \rightarrow n'}, \quad (32)$$

where  $N_n$  is the population of level  $n$  and  $W_{n \rightarrow n'}$  is the transition rate from level  $n'$  to level  $n$ . Generally,  $W_{n \rightarrow n'}$  is also time dependent, as in the case of photoionization when the rate varies with the field intensity during the pulse. The rate equations is a convenient tool for calculating ionic charge distributions and state populations within and after the pulse. They are extensively used in the description of sequential multiple ionization by XFEL pulses of atoms (for example, Makris et al., 2009; Nakajima and Nikolopoulos, 2002; Son and Santra, 2011, 2012; Lorenz et al., 2012; Lambropoulos and Nikolopoulos, 2013; Lunin et al., 2015; Serkez et al., 2018; Buth et al., 2018) and molecules (Liu et al., 2016; Inhester et al., 2016).

#### 8.8. Real-time *ab initio* simulations: Time-dependent multiconfiguration self-consistent-field method

Here we give a brief description of the time-dependent complete-active-space self-consistent field (TD-CASSCF) method (Sato and Ishikawa, 2013; Sato et al., 2016, 2018a) and the time-dependent occupation-restricted multiple-active-space (TD-ORMAS) method (Sato and Ishikawa, 2015). The dynamics of the laser-driven  $N$ -electron system is described by the TDSE (18)

$$i \frac{\partial \Psi(t)}{\partial t} = \hat{H}(t) \Psi(t), \quad (33)$$

where the time-dependent Hamiltonian is

$$\hat{H}(t) = \hat{H}_1(t) + \hat{H}_2, \quad (34)$$

with the one-electron part

$$\hat{H}_1(t) = \sum_{i=1}^N \hat{h}(\mathbf{r}_i, t) \quad (35)$$

and the two-electron part

$$\hat{H}_2 = \sum_{i=1}^N \sum_{j < i} \frac{1}{|\mathbf{r}_i - \mathbf{r}_j|}. \quad (36)$$

The one-body Hamiltonian  $\hat{h}(\mathbf{r}, t)$  for an atomic system within the dipole approximation is given in the length gauge by,

$$\hat{h}(\mathbf{r}, t) = \frac{\mathbf{p}^2}{2} + \mathbf{E}(t) \cdot \mathbf{r} - \frac{Z}{|\mathbf{r}|}, \quad (37)$$

and in the velocity gauge by,

$$\hat{h}(\mathbf{r}, t) = \frac{\mathbf{p}^2}{2} + \mathbf{A}(t) \cdot \mathbf{p} - \frac{Z}{|\mathbf{r}|}, \quad (38)$$

where  $\mathbf{A}(t) = -\int \mathbf{E}(t) dt$  is the vector potential,  $\mathbf{E}(t)$  is the laser electric field, and  $Z$  the atomic number.

The TD-CASSCF and TD-ORMAS methods belong to a class of *ab initio* approach called the time-dependent multiconfiguration self-consistent field (TD-MCSCF) methods, which express the total electronic wave function in the multiconfiguration expansion:

$$\Psi(x_1, x_2, \dots, x_N, t) = \sum_I C_I(t) \Phi_I(x_1, x_2, \dots, x_N, t), \quad (39)$$

where  $x = \{\mathbf{r}, \sigma\}$ . The electronic configuration  $\Phi_I(x_1, x_2, \dots, x_N, t)$  is a Slater determinant composed of spin orbital functions  $\{\psi_p(\mathbf{r}, t) \times s(\sigma)\}$ , where  $\psi_p(\mathbf{r}, t)$  and  $s(\sigma)$  denote spatial orbitals and spin functions, respectively. The coefficients  $C_I$  and orbitals are both time dependent.

In the TD-CASSCF and TD-ORMAS methods the spatial orbitals are classified into three groups: doubly occupied and time-independent frozen core (FC), doubly occupied and time-dependent dynamical core (DC), and correlated active orbitals. The total wave function is given by:

$$\Psi(t) = \hat{A} \left[ \Phi_{\text{fc}} \Phi_{\text{dc}}(t) \sum_I C_I(t) \Phi_I(t) \right], \quad (40)$$

where  $\hat{A}$  is the antisymmetrization operator,  $\Phi_{\text{fc}}$  and  $\Phi_{\text{dc}}$  the closed-shell determinants formed with numbers  $n_{\text{fc}}$  FC orbitals and  $n_{\text{dc}}$  DC orbitals, respectively, and  $\Phi_I$  the determinants constructed from  $n_a$  active orbitals. Whereas all the possible distributions of active electrons among active orbitals are considered in the TD-CASSCF method, the TD-ORMAS method further subdivides the active orbitals into an arbitrary number of subgroups, specifying the minimum and maximum number of electrons accommodated in each subgroup. This decomposition permits us to significantly reduce the computational cost without sacrificing accuracy in the description of correlated multielectron dynamics.

The equations of motion describing the temporal evolution of the coefficients  $C_I$  and the orbitals  $\psi_p$  are derived using the TDVP Eq. (25) and read, suppressing the argument  $t$  for notational convenience,

$$i \frac{d}{dt} C_I = \sum_J \langle \Phi_I | \hat{H} - \hat{R} | \Phi_J \rangle, \quad (41)$$

$$i \frac{d}{dt} |\psi_p\rangle = \hat{h} |\psi_p\rangle + \hat{Q} \hat{F} |\psi_p\rangle + \sum_q |\psi_q\rangle R_p^q, \quad (42)$$

where  $\hat{Q} = 1 - \sum_q |\psi_q\rangle \langle \psi_q|$  the projector onto the orthogonal complement of the occupied orbital space.  $\hat{F}$  is a non-local operator describing the contribution from the interelectronic Coulomb interaction, defined as,

$$\hat{F} |\psi_p\rangle = \sum_{oqsr} (D^{-1})_p^o P_{or}^{qs} \hat{W}_s^r |\psi_q\rangle, \quad (43)$$

where  $D$  and  $P$  are the one- and two-electron reduced density matrices, and  $\hat{W}_s^r$  is given, in the coordinate space, by,

$$W_s^r(\mathbf{r}) = \int d\mathbf{r}' \frac{\psi_r^*(\mathbf{r}') \psi_s(\mathbf{r}')}{|\mathbf{r} - \mathbf{r}'|}. \quad (44)$$

The matrix element  $R_p^q$  is given by,

$$R_p^q = i \langle \psi_q | \dot{\psi}_p \rangle - h_p^q, \quad (45)$$

with  $h_p^q = \langle \psi_q | \hat{h} | \psi_p \rangle$ . The elements  $R_p^q$  within one orbital subspace (frozen core, dynamical core and each subdivided active space) can be arbitrary Hermitian matrix elements and set to zero. On the other hand, the elements between different orbital subspaces are determined by the TDVP. Their concrete expressions are given in Sato and Ishikawa (2015), where  $iX_p^q = R_p^q + h_p^q$  is used for working variables. The numerical implementation for atoms with the use of infinite-range exterior complex scaling as an efficient absorbing boundary, and the time-dependent surface flux method for extracting angle-resolved photoelectron energy spectra, are described in detail in Sato et al. (2016) and Orimo et al. (2018, 2019).

TD-CASSCF and TD-ORMAS can systematically control the accuracy, until numerical convergence, through the number of orbitals and flexible orbital subspace decomposition. With TD-CASSCF, especially, we can take account of as many electron excitations as we want. Both methods are gauge invariant by virtue of the time-dependent variationally optimized orbitals. Moreover, TD-CASSCF is size extensive while TD-ORMAS is not, which is not relevant to the atomic case. Whereas the computational cost of TD-CASSCF scales factorially with the number of active electrons, TD-ORMAS has the advantage of polynomial cost scaling, enabling even more efficient simulations.

The methods described above and in Section 8.4 are based on the idea of expressing the total wave function as a linear combination. As an alternative, approaches based on the coupled-cluster expansion,

$$\Psi = \exp(\tau_i^a \hat{E}_i^a + \tau_{ij}^{ab} \hat{E}_{ij}^{ab} + \tau_{ijk}^{abc} \hat{E}_{ijk}^{abc} + \dots) \Phi, \quad (46)$$

of the time-dependent wave function  $\Psi(t)$  using time-dependent orbitals for electron dynamics have recently been developed. Here, the operator  $\hat{E}_{ijk\dots}^{abc\dots}$  excites electron(s) from orbital(s)  $i, j, k \dots$ , occupied in the reference determinant  $\Phi$  (hole), to those  $a, b, c \dots$ , not occupied in the reference (particle). Einstein's summation convention is used for the orbital indices. Both amplitudes  $\{\tau_{ijk\dots}^{abc\dots}(t)\}$  and orbitals are propagated in time. The methods are gauge invariant and extensive and scale polynomially with respect to the number of active electrons. Their details are presented, e.g., in Kvaal (2012); Sato et al. (2018b); Pathak et al. (2020a).

### 8.9. Theoretical proposals for XFEL experiments

Above we have reviewed experiments using light from narrow bandwidth FELs, and the powerful theoretical frameworks available to describe them. In addition, theoreticians have made numerous proposals for specific experiments, some of which have been tried, with or without success so far, and some of which are waiting to be attempted. Here we describe a selection of these proposed experiments.

X-Ray Photoelectron Spectroscopy (XPS) probes the chemical environment of individual atoms by measuring the core-level chemical shift, and has been widely used for chemical analysis of various kinds of samples. An obvious new direction for XPS with FELs is time-resolved XPS for probing the temporal evolution of the chemical environment in photoexcited systems. Time-resolved XPS has been extensively employed for solids at FLASH, see, for example, Hellmann et al. (2012), where a monochromatized FEL beam was employed. This approach has, however, not been used widely for gas-phase samples because of the rather low fluence of monochromatized FEL light. Recent developments of XFEL technologies, such as seeded FELs in the soft X-ray regime, and special accelerator modes (e.g. Prat and Reiche (2018)) are changing the situation. Also, the generation of soft X-ray two-colour double FEL pulses, especially attosecond/few-femtosecond double pulses (Duris et al., 2020), are attractive and stimulated renewed interest in time-resolved XPS. Oberli et al. (2019), for example, showed that the  $N\ 1s \rightarrow \pi^*$  transition can induce an isomerization reaction in formamide and that it is possible to observe in real time hydrogen migration by time-resolved XPS, measuring the chemical shifts with the X-ray probe pulse.

Regarding X-ray double pulses, experiments on some other systems have been suggested with other detection schemes. For example, for the glycine molecule, Cooper et al. (2014) showed that the dynamics of a hole arising from ionization in the inner valence region evolves with a timescale in the range of current XFEL capabilities. The proposed pump-probe scheme uses X-rays with photon energy below the K edge of carbon (275–280 eV) that can ionize the inner valence region. A second probe X-ray at the same energy can excite an electron from the core to fill the vacancy in the inner-valence region. The dynamics of the inner valence hole can be tracked by measuring the Auger electrons produced by the subsequent refilling of the core hole as a function of pump-probe delay. Li et al. (2014) studied the dynamics of an electron hole created by photoionization of the valence shell of protonated water clusters  $H^+(H_2O)_n$  and demonstrated that the electron hole is strongly correlated with the protons forming the hydrogen bond network. They showed that it is possible to probe key aspects of the valence electron hole dynamics and the coupled nuclear motion with femtosecond time resolution by resonantly exciting  $1s$  electrons to fill the valence hole. They proposed the use of transient X-ray absorption as a probe. Kuleff et al. (2016) found that when a hole is created in the core, it is stationary, but in response to this hole, interesting electron dynamics takes place, which can lead to intense charge migration in the valence shell. This migration is typically faster than that after the ionization of a valence electron and occurs on a shorter time scale than the natural decay of the core hole by the Auger process, making the subject challenging to experimentalists in attosecond science.

XPS and XTPPS (see Section 5.7) measure energies of single and double core hole states, and Auger and X-ray absorption spectroscopy also measure energetics. Today, more advanced experimental tools, which go beyond measuring photoelectron energies, are in our toolbox. Measurements of electron angular distributions in the molecular frame of reference (molecular-frame photoelectron angular distributions, MFPADs) are performed routinely using synchrotron radiation. Such MFPADs are highly sensitive probes of the electronic and molecular structures. Time-resolved MFPAD measurements are, however, still limited (see, e.g., the review article by Suzuki (2006) for valence photoemission, and Rouzée et al. (2013); Boll et al. (2013); Minemoto et al. (2016) for inner-shell photoemission). There are some instructive theoretical predictions, for example, Arasaki et al. (2011) demonstrated that time-resolved valence-band MFPADs can monitor electron-ion coupling via a conical intersection, whereas Krasniqi et al. (2010) demonstrated time-resolved core-level MFPADs can monitor structural changes of photoexcited molecules. High-repetition rate soft X-ray FELs will certainly make time-resolved core-level MFPAD measurements a tangible reality. Very recently, on the SQS beam line of SASE3 at the European XFEL, Kastirke et al. (2020) succeeded in measuring

O 1s MFPADs of dissociating  $O_2^{2+}$  molecular dications created by the Auger decay that follows O 1s photoionization of neutral  $O_2$  molecules, demonstrating that time-resolved core-level MFPAD measurements are indeed possible when two-colour X-ray double pulses become available (Serkez et al., 2020).

The above described predictions are based on linear spectroscopy or sequential two-photon absorption. For non-linear spectroscopic experiments, perhaps the most prolific theoretical group for devising new ideas for exploiting coherent, intense and short duration X-ray pulses is that of Mukamel and co-authors. In an early review, Mukamel et al. (2009) showed how coherent techniques developed for nuclear magnetic resonance and optical spectroscopy could be applied at shorter wavelengths, in particular with femtosecond and attosecond X-rays. This group has performed theoretical calculations investigating circular dichroism in achiral molecules, where the circular polarization of the light induces dichroism in the excited state (Rouxel et al., 2017), four-wave mixing in molecules (Tanaka and Mukamel, 2002), coherent control of electron transfer (Dorfman et al., 2016), etc. Some of the theoretical approaches and proposed experimental measurements for studying conical intersections in molecules have been summarised in Kowalewski et al. (2017). These include X-ray Hybrid Stimulated Raman Detection: Attosecond Stimulated X-ray Raman Spectroscopy (ASRS), in which a combination of narrow and broadband (attosecond) pulses is used; and the TRUECARs technique (Transient Redistribution of Ultrafast Electronic Coherences in Attosecond Raman Signals: Kowalewski et al., 2015), which also requires narrow and broadband X-ray pulses. In another investigation, Ye et al. (2019) suggested the use of X-rays carrying orbital angular momentum (twisted light, see also Section 4.4) to measure the dichroism of chiral molecules; since the method is based on resonant absorption, narrow bandwidth is required. The four-wave-mixing signals for the CO molecule in the gas phase have been calculated for XUV and core (carbon K edge) excitation (Cho et al., 2018). Many of these experiments are at present beyond the capabilities of present FELs: while phase resolution of a few attoseconds and pulse durations of less than a femtosecond have been demonstrated, they have not been demonstrated for the same beam. Longer pulses with phase control, or shorter pulses without phase control are available.

Ho et al. (2015) studied theoretically the effect of extremely high intensities on resonance-mediated atomic ionization by tender X-rays (few keV). Noble gas targets were considered, and broad band SASE pulses were compared with seeded (narrow band) pulses. At high energies, Kr and Xe absorb many photons and undergo cascade decay by Auger and other processes to produce highly charged states. SASE leads to higher ionization states, basically because the broad bandwidth increases the probability that an intermediate ionic state underwent resonant excitation. Shorter pulses, approaching the lifetime of some excited states, generally leads to less highly charged states because less decay occurs, and channels involving sequential ionization are reduced. However under some circumstances the opposite may occur: if the pulse has a duration shorter than the lifetime of a deep core hole, the atom may undergo excitation of this hole state, followed by ionization of valence and shallower core holes, after which the deep core hole decays. This leads to higher charge states.

Zhang et al. (2016) have suggested using a soft x-ray pump-control scheme with double pulses to investigate molecular wave packets. A core level resonance is excited by the first pulse, and then the second, strong control pulse couples this excited state to a valence excited state. The system is then interrogated by transient X-ray absorption, or by measuring the vibrationally resolved Auger spectrum as a function of the delay between the two pulses. This experiment would be very demanding. Apart from the necessity to create two pulses with well-defined photon energies and durations and relative delays of about 1 fs or less, very high spectroscopic resolution is required.

Khokhlova et al. (2019) have suggested molecular Auger interferometry, which is based on the coherent phase control of Auger dynamics in a two-color  $\omega - 2\omega$  laser field. They showed that, in contrast to atoms, in oriented molecules of certain point groups, the relative  $\omega - 2\omega$  phase modulates the total ionization yield. They derived a simple analytical formula for the extraction of the lifetimes of Auger-active states from a molecular Auger interferogram, circumventing the need for either high-resolution or attosecond spectroscopy. Another innovative idea was put forward by Liu et al. (2019), who have proposed second-harmonic generation using noble gas atoms: this process is normally forbidden in systems containing inversion symmetry.

Proposals have also been put forward to utilise the polarization of the light to gain new insights. Agueny (2020) has proposed using orthogonally polarized beams to investigate attosecond dynamics. Hofbrucker et al. (2018) have proposed an investigation of two-photon, elliptical dichroism. In this experiment, the dichroism is zero if the light polarization is linear or circular, but non-zero for elliptical polarization.

The availability of short-wavelength coherent sources has also prompted interest in coherent *nuclear* excitation (Adams et al., 2013, 2019). Indeed Rabi oscillations, one of the hallmarks of coherent excitation, have been observed

(Haber et al., 2017) with a synchrotron source in combination with a resonant cavity scheme. Nuclear excitations are also of interest for the next-generation of scientific clocks (Masuda et al., 2019; nuClock).

## 9. Perspectives

Short wavelength Free-Electron Lasers have provided scientists with new light sources for experiments requiring intense light, and have expanded the range of available wavelengths from the UV region to soft and hard X-rays. At hard X-ray wavelengths, a major application so far of the transverse coherence has been the measurement of coherent diffraction images of single molecules and nanocrystals, providing fundamental information for structural biology. The absence of longitudinal coherence for SASE sources has meant that there has been little or no exploration of the possibilities of full coherence. Several ideas have been published for controlling the bandwidth of SASE FELs, for example modified self-seeding to produce narrower line width radiation (Prat and Reiche, 2018), or machine methods to enhance the brightness (Prat and Reiche, 2019). For some experiments, a *larger* bandwidth is advantageous and this can also be provided (Prat et al., 2020). For crystallography, large bandwidth increases the probability of finding Bragg reflections, and may have applications in spectroscopy. For example, a spectrographic setup provides a multiplexing advantage, as in transient absorption (Bhattacharjee et al., 2017), and ghost spectroscopy (Driver et al., 2020) exploits correlation techniques to obtain clean data from fluctuating light pulses. We are now at the stage where accelerator physicists can control more and more parameters, not only bandwidth but also pulse duration and polarization.

Experiments in the XUV and soft X-ray range have made the greatest use of the longitudinal coherence properties available at short wavelengths, and we foresee a wide range of interesting developments. In the first instance, many of the techniques developed by optical laser scientists are now available at much shorter wavelengths. Quite a few of these have been tried, or are being tried with short wavelengths: bichromatic experiments, multi-dimensional spectroscopy, STIRAP (STImulated Raman Adiabatic Passage), second harmonic generation (at solid surfaces; Lam et al., 2018), four wave mixing (Bencivenga et al., 2015), Hanbury Brown and Twiss interferometry (Gorobtsov et al., 2018), etc. To date many of these methods have been restricted to bound states by the low photon energy of the laboratory sources used, but FEL light permits the extension into the ionizing region, with all the advantages and disadvantages that this implies. Whenever a non-linear process is involved, then FELs have a significant advantage compared to most laboratory sources, due to their high pulse energy. These optical techniques allow the discovery of molecular coherences not accessible by other methods, and the exploration of non-linear phenomena (Wituschek et al., 2020). The present level of phase control, a few attoseconds, permits the measurement of physical quantities on this time scale by interferometric methods. An immediate goal is to use this capability for the measurement of physical quantities of interest, such as photoemission delays (Cirelli et al., 2018).

An exciting future development will be based on the recently demonstrated capability of a seeded FEL to produce a “sculpted” pulse train, that is, one in which the phase and amplitude of the contributing wavelengths is controlled (Maroju et al., 2020). The reader will recall that attosecond science with laboratory lasers began with the demonstration of attosecond pulse trains, which are still widely used, and was followed by the production of single attosecond pulses: we may expect, or at least hope, for a similar evolution for longitudinally coherent FELs. Regarding this experiment, we note that a crucial breakthrough in permitting the “sculpture” of pulses was the use of intensity correlation methods. This is a form of covariance analysis, which was implemented some time ago for optical lasers (Frasinski et al., 1989), as well as more recently for FELs (Frasinski et al., 2013; Kornilov et al., 2013; You et al., 2020a): we expect to see increasing applications of correlation techniques. A recent example is ghost spectroscopy, or “spooktscopy” (Driver et al., 2020).

In the long term it is possible that FELs will be applied to investigate quantum optical phenomena. The field was inspired by the experiments of Hanbury Brown and Twiss (1956a,b), and Glauber (1963) won a Nobel prize for his insights. A challenge here is to discover and control exotic states of light fields at short wavelengths.

Other novel experiments may become possible due to machine developments. Echo Enabled Harmonic Generation has been demonstrated as a method for providing shorter wavelengths, more stable intensity and a larger choice of wavelengths (Rebernik Ribič et al., 2019), and signifies a marked improvement in seeded FEL performance. There may also be demand for narrowband pulses for precision spectroscopy; transform limited pulses are now possible with a duration of up to a ps. At the other extreme, hard X-ray pulses with a duration of less than 1 fs, and peak power of

over 100 GW can now be generated (Duris et al., 2020), and coherent soft x-ray FEL pulses with a duration of less than 5 fs have been produced.

As discussed in the previous section, theoreticians continue to provide new insights and ideas for new experiments. Accelerator physicists have made rapid progress in improving light sources - shorter pulses, higher peak powers, better stability, etc. This ensures that much new physics will be discovered at short wavelength, coherent FELs in the future.

## 10. List of symbols

Table 2: List of symbols used in this work

name	definition	equations
$c$	speed of light	
$e$	electron charge	
$h; (\hbar)$	Planck's constant; (reduced)	
$i$	imaginary unit	
$A$	asymmetry of angular distribution $W(\vartheta, \varphi)$	5
$A_m$	amplitude of the asymmetry oscillation	5
$\hat{A}$	antisymmetrization operator	26, 40
$\mathbf{A}(t)$	vector potential	20, 29, 30, 38
$\beta_k$	coefficients of Legendre expansion ("beta parameters")	4, 5
$\beta'_k$	coefficients of Legendre expansion ("beta parameters"). $\nu = \{\text{lin, circ}\}$ : light polarization	12
$c_n(t)$	wavefunction expansion coefficients	23
$C_I(t)$	CI expansion coefficients	39, 40
$\mathbf{D}(t)$	electric dipole operator	20, 27, 28
$e_j$	electric charge of particle $j$	20
$E$	particle energy	17
$E(t)$	electric field	1
$\mathbf{E}(t)$	electric field vector	20, 27, 28
$\epsilon_i, \epsilon_p, \epsilon_f$	energies of initial, intermediate, and final state	27, 28
$\eta$	amplitude ratio between FEL harmonics	1
$\eta$	spectral phase	Sec. 4.8
$F(t)$	pulse envelope	1
$\phi$	relative phase between FEL harmonics	1, 5
$\phi_m$	phase at the value of maximum asymmetry	5
$\varphi_q$	absolute phase of FEL $q^{\text{th}}$ harmonic	7, 8, 9
$\Delta\varphi_{q-1,q,q+1}$	phase difference between three consecutive FEL harmonics	9, 10
$\Delta\varphi_{at}$	difference of photoionisation phases	7, 8
$\phi_n(\xi)$	wavefunction expansion basis function	23
$\phi_n(x_1, x_2, \dots, \Omega_N, \sigma_N)$	wavefunction expansion basis function	26
$\Phi_i(\xi)$	initial-condition wavefunction	19
$\Phi(\mathbf{p}, t)$	wavefunction written as a function of time and electron momentum	30
$\Phi_I(\vec{x}_1, \vec{x}_2, \dots, \vec{x}_N, t)$	electronic configuration	39, 40
$\Phi_{fc}, \Phi_{dc}$	frozen core and dynamic core closed-shell determinants	40
$\hat{h}(\mathbf{r}, t)$	one-body Hamiltonian	35, 38
$\hat{H}(t)$	Hamiltonian	15, 25, 31, 33, 34
$\hat{H}_1(t)$	one-electron Hamiltonian	34, 35
$\hat{H}_2(t)$	two-electron Hamiltonian	34, 36
$\hat{H}_0(\xi)$	unperturbed Hamiltonian	19
$H(\xi, t)$	full Hamiltonian	18, 19
$I'(\theta)$	photoelectron angular distribution. $\nu \in \{\text{lin, circ}\}$ : light polarization	12
$J_i, J_f$	total electronic angular momentum of initial atom, and of residual ion	2
$\mathbf{p}$	electron momentum	29, 30, 38
$M_f$	magnetic quantum number of residual ion	2
$N_n(t)$	population of level $n$	32
$\omega$	fundamental FEL frequency	1, 13
$\omega_{\text{NIR}}$	NIR laser frequency	7, 8

Table 2: List of symbols used in this work (continued)

name	definition	equations
$\omega_{UV}$	seed laser frequency	10
$\Omega \equiv (\vartheta, \varphi)$	spherical coordinates	2, 3, 21, 22
$\mathbf{p}_j$	linear momentum of particle $j$	20
$P_k(\cos \vartheta)$	Legendre polynomial of order $k$	4, 12
$P_+, P_-$	probability of ionization in bichromatic fields of same or opposite helicities	14
$P_{q,q+1}$	oscillating component of the sidebands	11
$P_{lm}(r, t)$	one-active-electron radial function	21
$P_{l_1 l_2}^{LM}(r_1, r_2, t)$	two-active-electron radial function	22
$\psi_n(r_{N+1}, t)$	$n$ -th channel radial function	26
$\psi_{\mathbf{p}}$	Volkov wavefunction	29
$\Psi(t)$	wavefunction	25, 33, 40
$\Psi(\xi, t)$	wavefunction	18, 23
$\Psi(x_1, x_2, \dots, x_{N+1}, t)$	wavefunction	26
$\Phi_I(\vec{x}_1, \vec{x}_2, \dots, \vec{x}_N, t)$	electronic wavefunction	39, 40
$\Psi(\mathbf{r}, t)$	one-active-electron wavefunction	21
$\Psi(\mathbf{r}_1, \mathbf{r}_2, t)$	two-active-electron wavefunction	22
$\mathbf{r}$	photoelectron position	29, 30, 38
$\mathbf{r}_j$	position of particle $j$	20, 35, 36
$r_1, r_2, \dots, r_{N+1}$	radial coordinates	26
$\hat{\rho}, \hat{\rho}(t)$	density operator	16, 31
$\rho$	number density of excited states	Sec. 3.2
$S_{q,q+2}$	intensity of the sideband between the $q^{\text{th}}$ and $(q+2)^{\text{th}}$ harmonics (HHG)	7
$S_{q,q+1}^{(\pm)}$	intensity of the sidebands between the $q^{\text{th}}$ and $(q+1)^{\text{th}}$ harmonics (FEL)	8, 11
$\sigma$	spin coordinate	26, 39
$\tau$	delay between NIR and FEL harmonics	7, 8
$\tau_f$	EWS time delay in the channel $ f\rangle$	17
$T$	temporal evolution operator, infinite time limit	2, 15
$\langle f T i\rangle_n$	$n^{\text{th}}$ order transition amplitudes ( $n = 1, 2$ )	2, 27, 28
$U(t, t_0)$	temporal evolution operator	15
$V(\xi, t)$	external-field perturbation Hamiltonian	18, 19
$W(\vartheta, \varphi)$	differential ionization probability	2
$W^{(i)}(\vartheta, \varphi)$	first-harmonic ( $i = 1$ ), second-harmonic ( $i = 2$ ), and cross-term ( $i = 12$ ) contributions to $W(\vartheta, \varphi)$	2
$W_0$	isotropic component of $W(\vartheta, \varphi)$	4
$W_{n \rightarrow n'}$	transition rate from level $n'$ to level $n$	32
$x_1, x_2, \dots, x_N$	particle coordinates (space + spin)	26, 39
$\xi$	particle coordinates	19, 23
$Y_{lm}(\Omega)$	spherical harmonic	21
$Y_{l_1 l_2}^{LM}(\Omega_1, \Omega_2)$	bipolar spherical harmonic	22
$Z$	atomic number	38

## 11. Acknowledgements

KU acknowledges the Ministry of Education, Culture, Sports, Science, and Technology of Japan (MEXT) for funding via the X-ray Free Electron Laser Utilization Research Project, the X-ray Free Electron Laser Priority Strategy Program and the Dynamic Alliance for Open Innovation Bridging Human, Environment and Materials program, and the IMRAM program of Tohoku University. GS acknowledges funding from the Deutsche Forschungsgemeinschaft



(DFG, German Research Foundation) Projekt: 429805582. ANG acknowledges funding from the Russian Foundation for Basic Research under the Project No. 20-52-12023.

## References

- Adams, B., Aeppli, G., Allison, T., Baron, A.Q.R., Bucksbaum, P., Chumakov, A.I., Corder, C., Cramer, S.P., DeBeer, S., Ding, Y., Evers, J., Frisch, J., Fuchs, M., Grübel, G., Hastings, J.B., Heyl, C.M., Holberg, L., Huang, Z., Ishikawa, T., Kaldun, A., Kim, K.J., Kolodziej, T., Krzywinski, J., Li, Z., Liao, W.T., Lindberg, R., Madsen, A., Maxwell, T., Monaco, G., Nelson, K., Pálffy, A., Porat, G., Qin, W., Raubenheimer, T., Reis, D.A., Röhlberger, R., Santra, R., Schoenlein, R., Schünemann, V., Shpyrko, O., Shvyd'ko, Y., Shwartz, S., Singer, A., Sinha, S.K., Sutton, M., Tamasaku, K., Wille, H.C., Yabashi, M., Ye, J., Zhu, D., 2019. Scientific opportunities with an X-ray free-electron laser oscillator. *arXiv:1903.09317*.
- Adams, B.W., Buth, C., Cavaletto, S.M., Evers, J., Harman, Z., Keitel, C.H., Pálffy, A., Picón, A., Röhlberger, R., Rostovtsev, Y., Tamasaku, K., 2013. X-ray quantum optics. *J. Mod. Opt.* 60, 2–21. doi:10.1080/09500340.2012.752113.
- Afanasev, A., Carlson, C.E., Schmiegelow, C.T., Schulz, J., Schmidt-Kaler, F., Solyanik, M., 2018. Experimental verification of position-dependent angular-momentum selection rules for absorption of twisted light by a bound electron. *New J. Phys.* 20, 023032. doi:10.1088/1367-2630/aaa63d.
- Agueny, H., 2020. Quantum control and characterization of ultrafast ionization with orthogonal two-color laser pulses. *Sci. Rep.* 10, 239. doi:10.1038/s41598-019-57125-z.
- Allaria, E., Appio, R., Badano, L., Barletta, W.A., Bassanese, S., Biedron, S.G., Borgia, A., Busetto, E., Castronovo, D., Cinquegrana, P., Cleva, S., Cocco, D., Cornacchia, M., Craievich, P., Cudin, I., D'Auria, G., Dal Forno, M., Danailov, M.B., De Monte, R., De Ninno, G., Delgiusto, P., Demidovich, A., Di Mitri, S., Diviacco, B., Fabris, A., Fabris, R., Fawley, W., Ferianis, M., Ferrari, E., Ferry, S., Froehlich, L., Furlan, P., Gaio, G., Gelmetti, F., Giannessi, L., Giannini, M., Gobessi, R., Ivanov, R., Karantzoulis, E., Lonza, M., Lutman, A., Mahieu, B., Milloch, M., Milton, S.V., Musardo, M., Nikolov, I., Noe, S., Parmigiani, F., Penco, G., Petronio, M., Pivetta, L., Predonzani, M., Rossi, F., Rumiz, L., Salom, A., Scafuri, C., Serpico, C., Sigalotti, P., Spampinati, S., Spezzani, C., Svandrik, M., Svetina, C., Tazzari, S., Trovo, M., Umer, R., Vascotto, A., Veronese, M., Visintini, R., Zaccaria, M., Zangrando, D., Zangrando, M., 2012a. Highly coherent and stable pulses from the FERMI seeded free-electron laser in the extreme ultraviolet. *Nat. Photonics* 6, 699–704. doi:10.1038/nphoton.2012.233.
- Allaria, E., Battistoni, A., Bencivenga, F., Borghes, R., Callegari, C., Capotondi, F., Castronovo, D., Cinquegrana, P., Cocco, D., Coreno, M., Craievich, P., Cucini, R., D'Amico, F., Danailov, M.B., Demidovich, A., De Ninno, G., Di Cicco, A., Di Fonzo, S., Di Fraia, M., Di Mitri, S., Diviacco, B., Fawley, W.M., Ferrari, E., Filippini, A., Froehlich, L., Gessini, A., Giangrisostomi, E., Giannessi, L., Giuressi, D., Grazioli, C., Gunnella, R., Ivanov, R., Mahieu, B., Mahne, N., Masciovecchio, C., Nikolov, I.P., Passos, G., Pedersoli, E., Penco, G., Principi, E., Raimondi, L., Sergo, R., Sigalotti, P., Spezzani, C., Svetina, C., Trovò, M., Zangrando, M., 2012b. Tunability experiments at FERMI@Elettra free electron laser. *New J. Phys.* 14, 113009. doi:10.1088/1367-2630/14/11/113009.
- Allaria, E., Bencivenga, F., Borghes, R., Capotondi, F., Castronovo, D., Charalambous, P., Cinquegrana, P., Danailov, M.B., De Ninno, G., Demidovich, A., Di Mitri, S., Diviacco, B., Fausti, D., Fawley, W.M., Ferrari, E., Froehlich, L., Gauthier, D., Gessini, A., Giannessi, L., Ivanov, R., Kiskinova, M., Kurdi, G., Mahieu, B., Mahne, N., Nikolov, I., Masciovecchio, C., Pedersoli, E., Penco, G., Raimondi, L., Serpico, C., Sigalotti, P., Spampinati, S., Spezzani, C., Svetina, C., Trovò, M., Zangrando, M., 2013a. Two-colour pump-probe experiments with a twin-pulse-seed extreme ultraviolet free-electron laser. *Nat. Commun.* 4, 2476. doi:10.1038/ncomms3476.
- Allaria, E., Castronovo, D., Cinquegrana, P., Craievich, P., Dal Forno, M., Danailov, M.B., D'Auria, G., Demidovich, A., De Ninno, G., Di Mitri, S., Diviacco, B., Fawley, W.M., Ferianis, M., Ferrari, E., Froehlich, L., Gaio, G., Gauthier, D., Giannessi, L., Ivanov, R., Mahieu, B., Mahne, N., Nikolov, I., Parmigiani, F., Penco, G., Raimondi, L., Scafuri, C., Serpico, C., Sigalotti, P., Spampinati, S., Spezzani, C., Svandrik, M., Svetina, C., Trovo, M., Veronese, M., Zangrando, D., Zangrando, M., 2013b. Two-stage seeded soft-X-ray free-electron laser. *Nat. Photonics* 7, 913–918. doi:10.1038/nphoton.2013.277.
- Alon, O.E., Streltsov, A.I., Cederbaum, L.S., 2009. Many-body theory for systems with particle conversion: Extending the multiconfigurational time-dependent Hartree method. *Phys. Rev. A* 79, 022503. doi:10.1103/PhysRevA.79.022503.
- Amann, J., Berg, W., Blank, V., Decker, F.J., Ding, Y., Emma, P., Feng, Y., Frisch, J., Fritz, D., Hastings, J., Huang, Z., Krzywinski, J., Lindberg, R., Loos, H., Lutman, A., Nuhn, H.D., Ratner, D., Rzepiela, J., Shu, D., Shvyd'ko, Y., Spampinati, S., Stoupin, S., Terentyev, S., Trakhtenberg, E., Walz, D., Welch, J., Wu, J., Zholents, A., Zhu, D., 2012. Demonstration of self-seeding in a hard-X-ray free-electron laser. *Nat. Photonics* 6, 693–698. doi:10.1038/nphoton.2012.180.
- Amusia, M.Y., Semenov, S.K., Chernysheva, L.V., 2016. ATOM-M: algorithms and programs for the study of atomic and molecular processes. Nauka, St. Petersburg, Russia. In Russian.
- Ancilotto, F., Barranco, M., Coppens, F., Eloranta, J., Halberstadt, N., Hernandez, A., Mateo, D., Pi, M., 2017. Density functional theory of doped superfluid liquid helium and nanodroplets. *Int. Rev. Phys. Chem.* 36, 621–707. doi:10.1080/0144235x.2017.1351672.
- Arasaki, Y., Wang, K., McKoy, V., Takatsuka, K., 2011. Monitoring the effect of a control pulse on a conical intersection by time-resolved photoelectron spectroscopy. *Phys. Chem. Chem. Phys.* 13, 8681–8689. doi:10.1039/c0cp02302g.
- Artemyev, A.N., Müller, A.D., Hochstuhl, D., Demekhin, P.V., 2015. Photoelectron circular dichroism in the multiphoton ionization by short laser pulses. I. propagation of single-active-electron wave packets in chiral pseudo-potentials. *J. Chem. Phys.* 142, 244105. doi:10.1063/1.4922690.
- Attar, A.R., Bhattacharjee, A., Pemmaraju, C.D., Schnorr, K., Closser, K.D., Prendergast, D., Leone, S.R., 2017. Femtosecond x-ray spectroscopy of an electrocyclic ring-opening reaction. *Science* 356, 54–59. doi:10.1126/science.aaj2198.
- Attwood, D., Sakdinawat, A., 2016. X-Rays and Extreme Ultraviolet Radiation. Cambridge University Press. doi:10.1017/cbo9781107477629.
- Aue, W.P., Bartholdi, E., Ernst, R.R., 1976. Two-dimensional spectroscopy. application to nuclear magnetic resonance. *J. Chem. Phys.* 64, 2229–2246. doi:10.1063/1.432450.
- Augustin, S., Schulz, M., Schmid, G., Schnorr, K., Gryzlova, E.V., Lindenblatt, H., Meister, S., Liu, Y.F., Trost, F., Fechner, L., Grum-Grzhimailo, A.N., Burkov, S.M., Braune, M., Treusch, R., Gisselbrecht, M., Schröter, C.D., Pfeifer, T., Moshhammer, R., 2018. Signatures of autoionization in the angular electron distribution in two-photon double ionization of Ar. *Phys. Rev. A* 98, 033408. doi:10.1103/PhysRevA.98.033408.

- Awasthi, M., Vanne, Y.V., Saenz, A., 2005. Non-perturbative solution of the time-dependent Schrödinger equation describing H<sub>2</sub> in intense short laser pulses. *J. Phys. B* 38, 3973–3985. doi:10.1088/0953-4075/38/22/005.
- Ayvazyan, V., Baboi, N., Bähr, J., Balandin, V., Beutner, B., Brandt, A., Bohnet, I., Bolzmann, A., Brinkmann, R., Brovko, O.I., Carneiro, J.P., Casalbuoni, S., Castellano, M., Castro, P., Catani, L., Chiadroni, E., Choroba, S., Cianchi, A., Delsim-Hashemi, H., Di Pirro, G., Dohlus, M., Düsterer, S., Edwards, H.T., Faatz, B., Fateev, A.A., Feldhaus, J., Flöttmann, K., Frisch, J., Fröhlich, L., Garvey, T., Gensch, U., Golubeva, N., Grabosch, H.J., Grigoryan, B., Grimm, O., Hahn, U., Han, J.H., Hartrott, M.V., Honkavaara, K., Hüning, M., Ischebeck, R., Jaeschke, E., Jablonka, M., Kammering, R., Katalev, V., Keitel, B., Khodyachykh, S., Kim, Y., Kocharyan, V., Körfer, M., Kollwe, M., Kostin, D., Krämer, D., Krassilnikov, M., Kube, G., Lilje, L., Limberg, T., Lipka, D., Löhl, F., Luong, M., Magne, C., Menzel, J., Michelato, P., Miltchev, V., Minty, M., Möller, W.D., Monaco, L., Müller, W., Nagl, M., Napoly, O., Nicolosi, P., Nölle, D., Nuñez, T., Oppelt, A., Pagani, C., Paparella, R., Petersen, B., Petrosyan, B., Pflüger, J., Piot, P., Plönjes, E., Poletto, L., Proch, D., Pugachov, D., Rehlich, K., Richter, D., Riemann, S., Ross, M., Rossbach, J., Sachwitz, M., Saldin, E.L., Sandner, W., Schlarb, H., Schmidt, B., Schmitz, M., Schmüser, P., Schneider, J.R., Schneidmiller, E.A., Schreiber, H.J., Schreiber, S., Shabunov, A.V., Sertore, D., Setzer, S., Simrock, S., Sombrowski, E., Staykov, L., Steffen, B., Stephan, F., Stulle, F., Sytchev, K.P., Thom, H., Tiedtke, K., Tischer, M., Treusch, R., Trines, D., Tsakov, I., Vardanyan, A., Wanzenberg, R., Weiland, T., Weise, H., Wendt, M., Will, I., Winter, A., Wittenburg, K., Yurkov, M.V., Zagorodnov, I., Zambolin, P., Zapfe, K., 2006. First operation of a free-electron laser generating GW power radiation at 32 nm wavelength. *Eur. Phys. J. D* 37, 297–303. doi:10.1140/epjd/e2005-00308-1.
- Ayvazyan, V., Baboi, N., Schneider, J.R., Schneidmiller, E.A., Schreiber, H.J., Schreiber, S., Sertore, D., Setzer, S., Simrock, S., Sobierajski, R., Sonntag, B., Steeg, B., Stephan, F., Sytchev, K.P., Tiedtke, K., Tonutti, M., Treusch, R., Trines, D., Türke, D., Verzilov, V., Wanzenberg, R., Weiland, T., Weise, H., Wendt, M., Wilhelm, T., Will, I., Wittenburg, K., Wolff, S., Yurkov, M.V., Zapfe, K., Bohnet, I., Brinkmann, R., Castellano, M., Castro, P., Catani, L., Choroba, S., Cianchi, A., Dohlus, M., Edwards, H.T., Faatz, B., Fateev, A.A., Feldhaus, J., Flöttmann, K., Gamp, A., Garvey, T., Genz, H., Gerth, C., Gretchko, V., Grigoryan, B., Hahn, U., Hessler, C., Honkavaara, K., Hüning, M., Ischebeck, R., Jablonka, M., Kamps, T., Körfer, M., Krassilnikov, M., Krzywinski, J., Liepe, M., Liero, A., Limberg, T., Loos, H., Luong, M., Magne, C., Menzel, J., Michelato, P., Minty, M., Müller, U.C., Nölle, D., Novokhatski, A., Pagani, C., Peters, F., Pflüger, J., Piot, P., Plucinski, L., Rehlich, K., Reyzl, I., Richter, A., Rossbach, J., Saldin, E.L., Sandner, W., Schlarb, H., Schmidt, G., Schmüser, P., 2002. A new powerful source for coherent VUV radiation: Demonstration of exponential growth and saturation at the TTF free-electron laser. *Eur. Phys. J. D* 20, 149–156. doi:10.1140/epjd/e2002-00121-4.
- Bachau, H., Cormier, E., Decleva, P., Hansen, J.E., Martin, F., 2001. Applications of B-splines in atomic and molecular physics. *Rep. Prog. Phys.* 64, 1815–1942. doi:10.1088/0034-4885/64/12/205.
- Bahr, J., Gaupp, A., Gudat, W., Mast, M., Molter, K., Peatman, W.B., Scheer, M., Schroeter, T., Wang, C., 1992. Circularly polarized synchrotron radiation from the crossed undulator at BESSY. *Rev. Sci. Instrum.* 63, 339–342. doi:10.1063/1.1142750.
- Balashov, V.V., Grum-Grzhimailo, A.N., Kabachnik, N.M., 2000. Polarization and Correlation Phenomena in Atomic Collisions. A Practical Theory Course. *Physics of Atoms and Molecules*, Kluwer Academic/Plenum Publishers, New York Boston Dordrecht London Moscow. doi:10.1007/978-1-4757-3228-3.
- Bandrauk, A.D., Lu, H., 2013. Exponential propagators (integrators) for the time-dependent Schrödinger equation. *J. Theor. Comp. Chem.* 12, 1340001. doi:10.1142/S0219633613400014.
- Baranova, N.B., Beterov, I.M., Zel'Dovich, B.Y., Ryabtsev, I.I., Chudinov, A.N., Shul'ginov, A.A., 1992. Observation of an interference of one- and two-photon ionization of the sodium 4s state. *JETP Lett.* 55, 439–444. URL: [http://www.jetpletters.ac.ru/ps/1275/article\\_19280.shtml](http://www.jetpletters.ac.ru/ps/1275/article_19280.shtml).
- Barron, L.D., 2004. *Molecular Light Scattering and Optical Activity*. Cambridge University Press. doi:10.1017/cbo9780511535468.
- Bartels, R., Backus, S., Zeek, E., Misoguti, L., Vdovin, G., Christov, I.P., Murnane, M.M., Kapteyn, H.C., 2000. Shaped-pulse optimization of coherent emission of high-harmonic soft X-rays. *Nature* 406, 164–166. doi:10.1038/35018029.
- Bauch, S., Sørensen, L.K., Madsen, L.B., 2014. Time-dependent generalized-active-space configuration-interaction approach to photoionization dynamics of atoms and molecules. *Phys. Rev. A* 90, 062508. doi:10.1103/PhysRevA.90.062508.
- Beck, M., Jačkle, A., Worth, G., Meyer, H.D., 2000. The multiconfiguration time-dependent Hartree (MCTDH) method: a highly efficient algorithm for propagating wavepackets. *Phys. Rep.* 324, 1–105. doi:10.1016/S0370-1573(99)00047-2.
- Bencivenga, F., Cucini, R., Capotondi, F., Battistoni, A., Mincigrucchi, R., Giangrisostomi, E., Gessini, A., Manfredda, M., Nikolov, I.P., Pedersoli, E., Principi, E., Svetina, C., Parisse, P., Casolari, F., Danailov, M.B., Kiskinova, M., Masciovecchio, C., 2015. Four-wave mixing experiments with extreme ultraviolet transient gratings. *Nature* 520, 205–208. doi:10.1038/nature14341.
- Berrah, N., Bozek, J., Costello, J., Düsterer, S., Fang, L., Feldhaus, J., Fukuzawa, H., Hoener, M., Jiang, Y., Johnsson, P., Kennedy, E., Meyer, M., Moshammer, R., Radcliffe, P., Richter, M., Rouzée, A., Rudenko, A., Sorokin, A., Tiedtke, K., Ueda, K., Ullrich, J., Vrakking, M., 2010. Non-linear processes in the interaction of atoms and molecules with intense EUV and X-ray fields from SASE free electron lasers (FELs). *J. Mod. Opt.* 57, 1015–1040. doi:10.1080/09500340.2010.487946.
- Berrah, N., Fang, L., Murphy, B., Osipov, T., Ueda, K., Kukk, E., Feifel, R., van der Meulen, P., Salen, P., Schmidt, H.T., Thomas, R.D., Larsson, M., Richter, R., Prince, K.C., Bozek, J.D., Bostedt, C., Wada, S., Piancastelli, M.N., Tashiro, M., Ehara, M., 2011. Double-core-hole spectroscopy for chemical analysis with an intense x-ray femtosecond laser. *Proceedings of the National Academy of Sciences* 108, 16912–16915. doi:10.1073/pnas.1111380108.
- Berrah, N., Sanchez-Gonzalez, A., Jurek, Z., Obaid, R., Xiong, H., Squibb, R.J., Osipov, T., Lutman, A., Fang, L., Barillot, T., Bozek, J.D., Cryan, J., Wolf, T.J.A., Rolles, D., Coffee, R., Schnorr, K., Augustin, S., Fukuzawa, H., Motomura, K., Niebuhr, N., Frasiniski, L.J., Feifel, R., Schulz, C.P., Toyota, K., Son, S.K., Ueda, K., Pfeifer, T., Marangos, J.P., Santra, R., 2019. Femtosecond-resolved observation of the fragmentation of buckminsterfullerene following X-ray multiphoton ionization. *Nat. Phys.* 15, 1279–1283. doi:10.1038/s41567-019-0665-7.
- Berrington, K.A., Eissner, W.B., Norrington, P.H., 1995. RMATRX1: Belfast atomic R-matrix codes. *Comput. Phys. Commun.* 92, 290–420. doi:10.1016/0010-4655(95)00123-8.
- Beutler, H., 1935. Über Absorptionsserien von Argon, Krypton und Xenon zu Termen zwischen den beiden Ionisierungsgrenzen  $2P_3^{2/0}$  und  $2P_1^{2/0}$ . *Z. Phys.* 93, 177–196. doi:10.1007/bf01365116.
- Bhattacharjee, A., Pemmaraju, C.D., Schnorr, K., Attar, A.R., Leone, S.R., 2017. Ultrafast intersystem crossing in acetylacetone via femtosecond X-ray transient absorption at the carbon K-edge. *J. Am. Chem. Soc.* 139, 16576–16583. doi:10.1021/jacs.7b07532.

- Blum, K., 2012. Density Matrix Theory and Applications. volume 64 of *Springer Series on Atomic, Optical, and Plasma Physics*. Third ed., Springer-Verlag, Berlin, Heidelberg. doi:10.1007/978-3-642-20561-3.
- Boll, D.I.R., Fojón, O.A., 2014. Interferences and asymmetries in laser-assisted photoionization of diatomic molecules. *Phys. Rev. A* 90, 053414. doi:10.1103/PhysRevA.90.053414.
- Boll, D.I.R., Fojón, O.A., 2016. Atomic RABBIT-like experiments framed as diatomic molecules. *J. Phys. B* 49, 185601. doi:10.1088/0953-4075/49/18/185601.
- Boll, R., Anielski, D., Bostedt, C., Bozek, J.D., Christensen, L., Coffee, R., De, S., Declava, P., Epp, S.W., Erk, B., Foucar, L., Krasniqi, F., Küpper, J., Rouzée, A., Rudek, B., Rudenko, A., Schorb, S., Stapelfeldt, H., Stener, M., Stern, S., Teichert, S., Trippel, S., Vrakking, M.J.J., Ullrich, J., Rolles, D., 2013. Femtosecond photoelectron diffraction on laser-aligned molecules: Towards time-resolved imaging of molecular structure. *Phys. Rev. A* 88, 061402. doi:10.1103/PhysRevA.88.061402.
- Bonifacio, R., Casagrande, F., Cerchioni, G., de Salvo Souza, L., Pierini, P., Piovella, N., 1990a. Physics of the high-gain FEL and superradiance. *Nuovo Cimento* 13, 1–69. doi:10.1007/BF02770850.
- Bonifacio, R., De Salvo, L., Pierini, P., Piovella, N., Pellegrini, C., 1994. Spectrum, temporal structure, and fluctuations in a high-gain free-electron laser starting from noise. *Phys. Rev. Lett.* 73, 70–73. doi:10.1103/PhysRevLett.73.70.
- Bonifacio, R., De Salvo Souza, L., Pierini, P., Scharlemann, E.T., 1990b. Generation of XUV light by resonant frequency tripling in a two-wiggler FEL amplifier. *Nucl. Instrum. Methods Phys. Res. A* 296, 787–790. doi:10.1016/0168-9002(90)91307-w.
- Bostedt, C., Boutet, S., Fritz, D.M., Huang, Z., Lee, H.J., Lemke, H.T., Robert, A., Schlotter, W.F., Turner, J.J., Williams, G.J., 2016. Linac Coherent Light Source: The first five years. *Rev. Mod. Phys.* 88, 015007. doi:10.1103/RevModPhys.88.015007.
- Bostedt, C., Chapman, H.N., Costello, J.T., López-Urrutia, J.R.C., Düsterer, S., Epp, S.W., Feldhaus, J., Föhlisch, A., Meyer, M., Möller, T., Moshhammer, R., Richter, M., Sokolowski-Tinten, K., Sorokin, A., Tiedtke, K., Ullrich, J., Wurth, W., 2009. Experiments at FLASH. *Nucl. Instrum. Methods Phys. Res. A* 601, 108–122. doi:10.1016/j.nima.2008.12.202. special issue in honour of Prof. Kai Siegbahn.
- Burke, P.G., Burke, V.M., 1997. Time-dependent R-matrix theory of multiphoton processes. *J. Phys. B* 30, L383–L391. doi:10.1088/0953-4075/30/11/002.
- Buth, C., Beerwerth, R., Obaid, R., Berrah, N., Cederbaum, L.S., Fritzsche, S., 2018. Neon in ultrashort and intense x-rays from free electron lasers. *J. Phys. B* 51, 055602. doi:10.1088/1361-6455/aaa39a.
- Caillat, J., Zanghellini, J., Kitzler, M., Koch, O., Kreuzer, W., Scrinzi, A., 2005. Correlated multielectron systems in strong laser fields: A multiconfiguration time-dependent Hartree-Fock approach. *Phys. Rev. A* 71, 012712. doi:10.1103/PhysRevA.71.012712.
- Carpeggiani, P.A., Gryzlova, E.V., Reduzzi, M., Dubrouil, A., Faccialá, D., Negro, M., Ueda, K., Burkov, S.M., Frassetto, F., Stienkemeier, F., Ovcharenko, Y., Meyer, M., Plekan, O., Finetti, P., Prince, K.C., Callegari, C., Grum-Grzhimailo, A.N., Sansone, G., 2019. Complete reconstruction of bound and unbound electronic wavefunctions in two-photon double ionization. *Nat. Phys.* 15, 170–177. doi:10.1038/s41567-018-0340-4.
- Cederbaum, L.S., Tarantelli, F., Sgamellotti, A., Schirmer, J., 1986. On double vacancies in the core. *J. Chem. Phys.* 85, 6513–6523. doi:10.1063/1.451432.
- Cederbaum, L.S., Zobeley, J., Tarantelli, F., 1997. Giant intermolecular decay and fragmentation of clusters. *Phys. Rev. Lett.* 79, 4778–4781. doi:10.1103/PhysRevLett.79.4778.
- Chen, M.C., Arpin, P., Popmintchev, T., Gerrity, M., Zhang, B., Seaberg, M., Popmintchev, D., Murnane, M.M., Kapteyn, H.C., 2010. Bright, coherent, ultrafast soft X-ray harmonics spanning the water window from a tabletop light source. *Phys. Rev. Lett.* 105, 173901. doi:10.1103/PhysRevLett.105.173901.
- Chen, Y.J., Pabst, S., Karamatskou, A., Santra, R., 2015. Theoretical characterization of the collective resonance states underlying the xenon giant dipole resonance. *Phys. Rev. A* 91, 032503. doi:10.1103/PhysRevA.91.032503.
- Chen, Z., Zhang, L., Wang, Y., Zatsarinny, O., Bartschat, K., Morishita, T., Lin, C.D., 2019. Pulse-duration dependence of the double-to-single ionization ratio of Ne by intense 780-nm and 800-nm laser fields: Comparison of simulations with experiments. *Phys. Rev. A* 99, 043408. doi:10.1103/PhysRevA.99.043408.
- Cho, D., Rouxel, J.R., Kowalewski, M., Saurabh, P., Lee, J.Y., Mukamel, S., 2018. Phase cycling RT-TDDFT simulation protocol for nonlinear XUV and x-ray molecular spectroscopy. *J. Phys. Chem. Lett.* 9, 1072–1078. doi:10.1021/acs.jpcllett.8b00061.
- Cirelli, C., Marante, C., Heuser, S., Petersson, C.L.M., Galán, Á.J., Argenti, L., Zhong, S., Busto, D., Isinger, M., Nandi, S., Maclot, S., Rading, L., Johnsson, P., Gisselbrecht, M., Lucchini, M., Gallmann, L., Dahlström, J.M., Lindroth, E., L’Huillier, A., Martín, F., Keller, U., 2018. Anisotropic photoemission time delays close to a Fano resonance. *Nat. Commun.* 9, 955. doi:10.1038/s41467-018-03009-1.
- Codling, K., Madden, R.P., 1971. Resonances in the photoionization continuum of Kr and Xe. *Phys. Rev. A* 4, 2261–2263. doi:10.1103/PhysRevA.4.2261.
- Coffee, R.N., Cryan, J.P., Duris, J., Helml, W., Li, S., Marinelli, A., 2019. Development of ultrafast capabilities for X-ray free-electron lasers at the linac coherent light source. *Philos. Trans. R. Soc. A* 377, 20180386. doi:10.1098/rsta.2018.0386.
- Cohen-Tannoudji, C., Dupont-Roc, J., Grynberg, G., 2004. *Atom-Photon Interactions*. John Wiley & Sons, Ltd. doi:10.1002/9783527617197.
- Colgan, J., Pindzola, M.S., 2012. Angular distributions for the complete photofragmentation of the Li atom. *Phys. Rev. Lett.* 108, 053001. doi:10.1103/PhysRevLett.108.053001.
- Colson, W., 1981. The nonlinear wave equation for higher harmonics in free-electron lasers. *IEEE J. Quantum Electron.* 17, 1417–1427. doi:10.1109/jqe.1981.1071273.
- Colson, W.B., 1977. One-body electron dynamics in a free electron laser. *Phys. Lett. A* 64, 190–192. doi:10.1016/0375-9601(77)90712-5.
- Colson, W.B., Dattoli, G., Ciocci, F., 1985. Angular-gain spectrum of free-electron lasers. *Phys. Rev. A* 31, 828–842. doi:10.1103/PhysRevA.31.828.
- Colson, W.B., Sessler, A.M., 1985. Free electron lasers. *Annu. Rev. Nucl. Part. Sci.* 35, 25–54. doi:10.1146/annurev.ns.35.120185.000325.
- Cooper, B., Averbukh, V., 2013. Single-photon laser-enabled Auger spectroscopy for measuring attosecond electron-hole dynamics. *Phys. Rev. Lett.* 111, 083004. doi:10.1103/PhysRevLett.111.083004.
- Cooper, B., Kolorenč, P., Frasinski, L.J., Averbukh, V., Marangos, J.P., 2014. Analysis of a measurement scheme for ultrafast hole dynamics by few femtosecond resolution X-ray pump-probe Auger spectroscopy. *Faraday Discuss.* 171, 93–111. doi:10.1039/c4fd00051j.

- Cousin, S.L., Silva, F., Teichmann, S., Hemmer, M., Buades, B., Biegert, J., 2014. High-flux table-top soft x-ray source driven by sub-2-cycle, CEP stable, 1.85- $\mu\text{m}$  1-kHz pulses for carbon K-edge spectroscopy. *Opt. Lett.* 39, 5383. doi:10.1364/ol.39.005383.
- Dahlström, J.M., L'Huillier, A., Maquet, A., 2012. Introduction to attosecond delays in photoionization. *J. Phys. B* 45, 183001. doi:10.1088/0953-4075/45/18/183001.
- Danailov, M.B., Cinquegrana, P., Demidovich, A.A., Ivanov, R., Nikolov, I., Sigalotti, P., 2011. Design and first experience with the FERMI seed laser, in: *Proceedings of the 33rd International Free Electron Laser Conference (FEL 2011)*, Shanghai, China, FEL'11/EPS-AG. p. 183. URL: <https://accelconf.web.cern.ch/FEL2011/papers/tuoc4.pdf>.
- De Ninno, G., Gauthier, D., Mahieu, B., Rebernik Ribič, P., Allaria, E., Cinquegrana, P., Danailov, M.B., Demidovich, A., Ferrari, E., Giannessi, L., Penco, G., Sigalotti, P., Stupar, M., 2015. Single-shot spectro-temporal characterization of XUV pulses from a seeded free-electron laser. *Nat. Commun.* 6, 8075. doi:10.1038/ncomms9075.
- De Ninno, G., Wätzel, J., Rebernik Ribič, P., Allaria, E., Coreno, M., Danailov, M.B., David, C., Demidovich, A., Di Fraia, M., Giannessi, L., Hansen, K., Krušič, Š., Manfreda, M., Meyer, M., Mihelič, A., Mirian, N., Plekan, O., Ressel, B., Rösner, B., Simoncig, A., Spampinati, S., Stupar, M., Žitnik, M., Zangrando, M., Callegari, C., Berakdar, J., 2020. Photoelectric effect with a twist. *Nat. Photon.* In press.
- Decking, W., Abeghyan, S., Abramian, P., Abramsky, A., Aguirre, A., Albrecht, C., Alou, P., Altarelli, M., Altmann, P., Amyan, K., Anashin, V., Apostolov, E., Appel, K., Auguste, D., Ayvazyan, V., Baark, S., Babies, F., Baboi, N., Bak, P., Balandin, V., Baldinger, R., Baranasic, B., Barbanotti, S., Belikov, O., Belokurov, V., Belova, L., Belyakov, V., Berry, S., Bertucci, M., Beutner, B., Block, A., Blöcher, R., Böckmann, T., Bohm, C., Böhnert, M., Bondar, V., Bondarchuk, E., Bonezzi, M., Borowiec, P., Bösch, C., Bösenberg, U., Bosotti, A., Bösplflug, R., Bousoville, M., Boyd, E., Bozhko, Y., Brand, A., Branlard, J., Briechele, S., Brinker, F., Brinker, S., Brinkmann, R., Brockhauser, S., Brovko, O., Brück, H., Brüdgam, A., Butkowski, L., Büttner, T., Calero, J., Castro-Carballo, E., Cattalanotto, G., Charrier, J., Chen, J., Cherepenko, A., Cheskidov, V., Chiodini, M., Chong, A., Choroba, S., Chorowski, M., Churanov, D., Cichalewski, W., Clausen, M., Clement, W., Cloué, C., Cobos, J.A., Coppola, N., Cunis, S., Czuba, K., Czwalińska, M., D'Almagne, B., Dammann, J., Danared, H., de Zubiurre Wagner, A., Delfs, A., Delfs, T., Dietrich, F., Dietrich, T., Dohlus, M., Dommach, M., Donat, A., Dong, X., Doynikov, N., Dressel, M., Duda, M., Duda, P., Eckoldt, H., Ehsan, W., Eidam, J., Eints, F., Engling, C., Englisch, U., Ermakov, A., Escherich, K., Eschke, J., Saldin, E., Faesing, M., Fallou, A., Felber, M., Fenner, M., Fernandes, B., Fernández, J.M., Feucker, S., Filippakopoulos, K., Floettmann, K., Fogel, V., Fontaine, M., Francés, A., Martin, I.F., Freund, W., Freyermuth, T., Friedland, M., Fröhlich, L., Fusetti, M., Fydrich, J., Gallas, A., García, O., Garcia-Tabares, L., Geloni, G., Gerasimova, N., Gerth, C., Geßler, P., Gharibyan, V., Gloor, M., Głowinkowski, J., Goessel, A., Gołębiewski, Z., Golubeva, N., Grabowski, W., Graeff, W., Grebentsov, A., Grecki, M., Grevsmuehl, T., Gross, M., Grosse-Wortmann, U., Grünert, J., Grunewald, S., Grzegory, P., Feng, G., Guler, H., Gusev, G., Gutierrez, J.L., Hagge, L., Hamburg, M., Hanneken, R., Harms, E., Hartl, I., Hauberg, A., Hauf, S., Hauschildt, J., Hauser, J., Havlicek, J., Hedqvist, A., Heidbrook, N., Hellberg, F., Henning, D., Hensler, O., Hermann, T., Hidvégi, A., Hierholzer, M., Hintz, H., Hoffmann, F., Hoffmann, M., Hoffmann, M., Holler, Y., Hüning, M., Ignatenko, A., Ilchen, M., Iluk, A., Iversen, J., Iversen, J., Izquierdo, M., Jachmann, L., Jardon, N., Jastrow, U., Jensch, K., Jensen, J., Ježabek, M., Jidda, M., Jin, H., Johannson, N., Jonas, R., Kaabi, W., Kaefer, D., Kammering, R., Kapitzka, H., Karabekyan, S., Karstensen, S., Kasprzak, K., Katalev, V., Keese, D., Keil, B., Kholopov, M., Killenberger, M., Kitaev, B., Klimchenko, Y., Klos, R., Knebel, L., Koch, A., Koepke, M., Köhler, S., Köhler, W., Kohlstrunk, N., Konopkova, Z., Konstantinov, A., Kook, W., Koprek, W., Körfer, M., Korth, O., Kosarev, A., Kosiński, K., Kostin, D., Kot, Y., Kotarba, A., Kozak, T., Kozak, V., Kramert, R., Krasilnikov, M., Krasnov, A., Krause, B., Kravchuk, L., Krebs, O., Kretschmer, R., Kreutzkamp, J., Kröplin, O., Krzysik, K., Kube, G., Kuehn, H., Kujala, N., Kulikov, V., Kuzminych, V., Civita, D.L., Lacroix, M., Lamb, T., Lancetov, A., Larsson, M., Pinvidic, D.L., Lederer, S., Lensch, T., Lenz, D., Leuschner, A., Levenhagen, F., Li, Y., Liebing, J., Lilje, L., Limberg, T., Lipka, D., List, B., Liu, J., Liu, S., Lorbeer, B., Lorkiewicz, J., Lu, H.H., Ludwig, F., Machau, K., Maciocha, W., Madec, C., Magueur, C., Maiano, C., Maksimova, I., Malcher, M., Maltezopoulos, T., Mamoshkina, E., Manschwetus, B., Marcellini, F., Marinkovic, G., Martinez, T., Martirosyan, H., Maschmann, W., Maslov, M., Matheisen, A., Mavric, U., Meißner, J., Meissner, K., Messerschmidt, M., Meyners, N., Michalski, G., Michelato, P., Mildner, N., Moe, M., Moglia, F., Mohr, C., Mohr, S., Möller, W., Mommerz, M., Monaco, L., Montiel, C., Moretti, M., Morozov, I., Morozov, P., Mross, D., Mueller, J., Müller, C., Müller, J., Müller, K., Munilla, J., Münnich, A., Muratov, V., Napoly, O., Näser, B., Nefedov, N., Neumann, R., Neumann, R., Ngada, N., Noelle, D., Obier, F., Okunev, I., Oliver, J.A., Omet, M., Oppelt, A., Ottmar, A., Oublaïd, M., Pagani, C., Paparella, R., Paramonov, V., Peitzmann, C., Penning, J., Perus, A., Peters, F., Petersen, B., Petrov, A., Petrov, I., Pfeiffer, S., Pflüger, J., Philipp, S., Pinaud, Y., Pierini, P., Pivovarov, S., Planas, M., Pławski, E., Pohl, M., Polinski, J., Popov, V., Prat, S., Prenting, J., Priebe, G., Prysichelski, H., Przygoda, K., Pyata, E., Racky, B., Rathjen, A., Ratuschni, W., Regnaud-Camperderros, S., Rehlich, K., Reschke, D., Robson, C., Roeber, J., Roggli, M., Rothenburg, J., Rusiński, E., Rybaniec, R., Sahling, H., Salmani, M., Samoylova, L., Sanzone, D., Saretzki, F., Sawlanski, O., Schaffran, J., Schlarb, H., Schlösser, M., Schlott, V., Schmidt, C., Schmidt-Foehre, F., Schmitz, M., Schmökel, M., Schnautz, T., Schneidmiller, E., Scholz, M., Schöneburg, B., Schultze, J., Schulz, C., Schwarz, A., Sekutowicz, J., Sellmann, D., Semenov, E., Serkez, S., Sertore, D., Shehzad, N., Shemarykin, P., Shi, L., Sienkiewicz, M., Sikora, D., Sikorski, M., Silenzi, A., Simon, C., Singer, W., Singer, X., Sinn, H., Sinram, K., Skvorodnev, N., Smirnov, P., Sommer, T., Sorokin, A., Stadler, M., Steckel, M., Steffen, B., Steinhilber, N., Stephan, F., Stodulski, M., Stolper, M., Sulimov, A., Susen, R., Świerblewski, J., Sydo, C., Syresin, E., Sytchev, V., Szuba, J., Tesch, N., Thie, J., Thiebault, A., Tiedtke, K., Tischhauser, D., Tolkiehn, J., Tomin, S., Tonisch, F., Toral, F., Torbin, I., Trapp, A., Treyer, D., Trowitzsch, G., Trublet, T., Tschentscher, T., Ullrich, F., Vannoni, M., Varela, P., Varghese, G., Vashchenko, G., Vasic, M., Vazquez-Velez, C., Verguet, A., Vilcins-Czvitkovits, S., Villanueva, R., Visentin, B., Viti, M., Vogel, E., Volobuev, E., Wagner, R., Walker, N., Wamsat, T., Weddig, H., Weichert, G., Weise, H., Wendorf, R., Werner, M., Wichmann, R., Wiebers, C., Wieneck, M., Wilksen, T., Will, I., Winkelmann, L., Winkowski, M., Wittenburg, K., Witzig, A., Wlk, P., Wohlenberg, T., Wojciechowski, M., Wolff-Fabris, F., Wrochna, G., Wrona, K., Yakopov, M., Yang, B., Yang, F., Yurkov, M., Zagorodnov, I., Zalden, P., Zavadtsev, A., Zavadtsev, D., Zhirnov, A., Zhukov, A., Ziemann, V., Zolotov, A., Zolotukhina, N., Zummack, F., Zybin, D., 2020. A MHz-repetition-rate hard x-ray free-electron laser driven by a superconducting linear accelerator. *Nature Photonics* 14, 391–397. doi:10.1038/s41566-020-0607-z.
- Delone, N.B., Krainov, V.P., 2000. *Multiphoton Processes in Atoms*. Springer, Berlin Heidelberg. doi:10.1007/978-3-642-57208-1.
- Demekhin, P.V., Ehresmann, A., Sukhorukov, V., 2011a. Single center method: A computational tool for ionization and electronic excitation studies of molecules. *J. Chem. Phys.* 134, 024113. doi:10.1063/1.3526026.
- Demekhin, P.V., Gokhberg, K., Jabbari, G., Kopelke, S., Kuleff, A.I., Cederbaum, L.S., 2013. Overcoming blockade in producing doubly excited dimers by a single intense pulse and their decay. *J. Phys. B* 46, 021001. doi:10.1088/0953-4075/46/2/021001.

- Demekhin, P.V., Stoychev, S.D., Kuleff, A.I., Cederbaum, L.S., 2011b. Exploring interatomic coulombic decay by free electron lasers. *Phys. Rev. Lett.* 107, 273002. doi:10.1103/PhysRevLett.107.273002.
- Devons, S., Goldfarb, L.J.B., 1957. Angular correlations, in: Flügge, S. (Ed.), *Kernreaktionen III / Nuclear Reactions III*. Springer-Verlag, Berlin Heidelberg, volume 42 of *Handbuch der Physik*. chapter 5, pp. 362–554. doi:10.1007/978-3-642-45878-1\_5.
- Di Fraia, M., Plekan, O., Callegari, C., Prince, K.C., Giannessi, L., Allaria, E., Badano, L., De Ninno, G., Trovò, M., Diviacco, B., Gauthier, D., Mirian, N., Penco, G., Rebernik Ribič, P., Spampinati, S., Spezzani, C., Gaio, G., Orimo, Y., Tugs, O., Sato, T., Ishikawa, K.L., Carpeggiani, P.A., Csizmadia, T., Füle, M., Sansone, G., Kumar Maroju, P., D’Elia, A., Mazza, T., Meyer, M., Gryzlova, E.V., Grum-Grzhimailo, A.N., You, D., Ueda, K., 2019. Complete characterization of phase and amplitude of bichromatic extreme ultraviolet light. *Phys. Rev. Lett.* 123, 213904. doi:10.1103/PhysRevLett.123.213904.
- Ding, C., Xiong, W., Fan, T., Hickstein, D.D., Popmintchev, T., Zhang, X., Walls, M., Murnane, M.M., Kapteyn, H.C., 2014. High flux coherent super-continuum soft X-ray source driven by a single-stage, 10 mJ, Ti:sapphire amplifier-pumped OPA. *Opt. Express* 22, 6194. doi:10.1364/oe.22.006194.
- Ding, T., Rebholz, M., Aufleger, L., Hartmann, M., Meyer, K., Stooß, V., Magunia, A., Wachs, D., Birk, P., Mi, Y., Borisova, G.D., da Costa Castanheira, C., Rupprecht, P., Loh, Z.H., Attar, A.R., Gaumnitz, T., Roling, S., Butz, M., Zacharias, H., Düsterer, S., Treusch, R., Cavaletto, S.M., Ott, C., Pfeifer, T., 2019. Nonlinear coherence effects in transient-absorption ion spectroscopy with stochastic extreme-ultraviolet free-electron laser pulses. *Phys. Rev. Lett.* 123, 103001. doi:10.1103/PhysRevLett.123.103001.
- Diviacco, B., Bracco, R., Millo, D., Musardo, M.M., 2011. Phase shifters for the FERMI@Elettra undulators, in: Petit-Jean-Genaz, C. (Ed.), *Proceedings of the 2nd International Conference on Particle Accelerators (IPAC 2011)*, San Sebastián, Spain, IPAC’11 EPS-AG, Geneva, Switzerland. p. 3278. URL: <https://accelconf.web.cern.ch/AccelConf/IPAC2011/papers/thpc164.pdf>.
- Domke, M., Schulz, K., Remmers, G., Gutiérrez, A., Kaindl, G., Wintgen, D., 1995. Interferences in photoexcited double-excitation series of He. *Phys. Rev. A* 51, R4309–R4312. doi:10.1103/PhysRevA.51.R4309.
- Domke, M., Schulz, K., Remmers, G., Kaindl, G., Wintgen, D., 1996. High-resolution study of  $1P^o$  double-excitation states in helium. *Phys. Rev. A* 53, 1424–1438. doi:10.1103/PhysRevA.53.1424.
- Dorfman, K.E., Zhang, Y., Mukamel, S., 2016. Coherent control of long-range photoinduced electron transfer by stimulated X-ray Raman processes. *Proc. Natl. Acad. Sci. U.S.A.* 113, 10001–10006. doi:10.1073/pnas.1610729113.
- Douguet, N., Grum-Grzhimailo, A.N., Gryzlova, E.V., Staroselskaya, E.I., Venzke, J., Bartschat, K., 2016. Photoelectron angular distributions in bichromatic atomic ionization induced by circularly polarized VUV femtosecond pulses. *Phys. Rev. A* 93, 033402. doi:10.1103/PhysRevA.93.033402.
- Douguet, N., Gryzlova, E.V., Staroselskaya, E.I., Bartschat, K., Grum-Grzhimailo, A.N., 2017. Photoelectron angular distribution in two-pathway ionization of neon with femtosecond XUV pulses. *Eur. Phys. J. D* 71, 105. doi:10.1140/epjd/e2017-70695-7.
- Driver, T., Li, S., Champenois, E.G., Duris, J., Ratner, D., Lane, T.J., Rosenberger, P., Al-Haddad, A., Averbukh, V., Barnard, T., Berrah, N., Bostedt, C., Bucksbaum, P.H., Coffee, R., DiMauro, L.F., Fang, L., Garratt, D., Gatton, A., Guo, Z., Hartmann, G., Haxton, D., Helml, W., Huang, Z., LaForge, A., Kamalov, A., Kling, M.F., Knurr, J., Lin, M.F., Lutman, A.A., MacArthur, J.P., Marangos, J.P., Nantel, M., Natan, A., Obaid, R., O’Neal, J.T., Shivaram, N.H., Schori, A., Walter, P., Wang, A.L., Wolf, T.J.A., Marinelli, A., Cryan, J.P., 2020. Attosecond transient absorption spectroscopy: a ghost imaging approach to ultrafast absorption spectroscopy. *Phys. Chem. Chem. Phys.* 22, 2704–2712. doi:10.1039/c9cp03951a.
- Dubrouil, A., Reduzzi, M., Devetta, M., Feng, C., Hummert, J., Finetti, P., Plekan, O., Grazioli, C., Di Fraia, M., Lyamayev, V., La Forge, A., Katzy, R., Stienkemeier, F., Ovcharenko, Y., Coreno, M., Berrah, N., Motomura, K., Mondal, S., Ueda, K., Prince, K.C., Callegari, C., Kuleff, A.I., Demekhin, P.V., Sansone, G., 2015. Two-photon resonant excitation of interatomic coulombic decay in neon dimers. *J. Phys. B* 48, 204005. doi:10.1088/0953-4075/48/20/204005.
- Duris, J., Li, S., Driver, T., Champenois, E.G., MacArthur, J.P., Lutman, A.A., Zhang, Z., Rosenberger, P., Aldrich, J.W., Coffee, R., Coslovich, G., Decker, F.J., Glowia, J.M., Hartmann, G., Helml, W., Kamalov, A., Knurr, J., Krzywinski, J., Lin, M.F., Marangos, J.P., Nantel, M., Natan, A., O’Neal, J.T., Shivaram, N., Walter, P., Wang, A.L., Welch, J.J., Wolf, T.J.A., Xu, J.Z., Kling, M.F., Bucksbaum, P.H., Zholents, A., Huang, Z., Cryan, J.P., Marinelli, A., 2020. Tunable isolated attosecond X-ray pulses with gigawatt peak power from a free-electron laser. *Nat. Photonics* 14, 30–36. doi:10.1038/s41566-019-0549-5.
- Einstein, A., 1905. Über einen die Erzeugung und Verwandlung des Lichtes betreffenden heuristischen Gesichtspunkt. *Ann. Phys.* 322, 132–148. doi:10.1002/andp.19053220607.
- Eisenbud, L., 1948. Formal properties of nuclear collisions. Ph.D. thesis. Princeton University. Princeton, NJ, U.S.A.
- Emma, C., Lutman, A., Guet, M.W., Krzywinski, J., Marinelli, A., Wu, J., Pellegrini, C., 2017. Experimental demonstration of fresh bunch self-seeding in an X-ray free electron laser. *Appl. Phys. Lett.* 110, 154101. doi:10.1063/1.4980092.
- Emma, P., Akre, R., Arthur, J., Bionta, R., Bostedt, C., Bozek, J., Brachmann, A., Bucksbaum, P., Coffee, R., Decker, F.J., Ding, Y., Dowell, D., Edstrom, S., Fisher, A., Frisch, J., Gilevich, S., Hastings, J., Hays, G., Hering, P., Huang, Z., Iverson, R., Loos, H., Messerschmidt, M., Miahnahri, A., Moeller, S., Nuhn, H.D., Pile, G., Ratner, D., Rzepiela, J., Schultz, D., Smith, T., Stefan, P., Tompkins, H., Turner, J., Welch, J., White, W., Wu, J., Yocky, G., Galayda, J., 2010. First lasing and operation of an ångström-wavelength free-electron laser. *Nat. Photonics* 4, 641–647. doi:10.1038/nphoton.2010.176.
- Engin, S., González-Vázquez, J., Maliyar, G.G., Milosavljević, A.R., Ono, T., Nandi, S., Iablonskyi, D., Kooser, K., Bozek, J.D., Declava, P., Kukk, E., Ueda, K., Martín, F., 2019. Full-dimensional theoretical description of vibrationally resolved valence-shell photoionization of H<sub>2</sub>O. *Struct. Dyn.* 6, 054101. doi:10.1063/1.5106431.
- Erk, B., Boll, R., Trippel, S., Anielski, D., Foucar, L., Rudek, B., Epp, S.W., Coffee, R., Carron, S., Schorb, S., Ferguson, K.R., Swiggers, M., Bozek, J.D., Simon, M., Marchenko, T., Kupper, J., Schlichting, I., Ullrich, J., Bostedt, C., Rolles, D., Rudenko, A., 2014. Imaging charge transfer in iodomethane upon x-ray photoabsorption. *Science* 345, 288–291. doi:10.1126/science.1253607.
- Ernst, R.R., Wokaun, A., Bodenhausen, G., 1990. *Principles of Nuclear Magnetic Resonance in One and Two Dimensions*. Oxford University Press, Oxford, UK.
- Faatz, B., Braune, M., Hensler, O., Honkavaara, K., Kammering, R., Kuhlmann, M., Ploenjes, E., Roensch-Schulenburg, J., Schneidmiller, E., Schreiber, S., Tiedtke, K., Tischer, M., Treusch, R., Vogt, M., Wurth, W., Yurkov, M., Zemella, J., 2017. The FLASH facility: Advanced options

- for FLASH2 and future perspectives. *Appl. Sci.* 7, 1114. doi:10.3390/app7111114.
- Faisal, F.H.M., 1973. Multiple absorption of laser photons by atoms. *J. Phys.* B 6, L89–L92. doi:10.1088/0022-3700/6/4/011.
- Faisal, F.H.M., 1987. *Theory of Multiphoton Processes*. Plenum Press, New York. doi:10.1007/978-1-4899-1977-9.
- Fano, U., 1935. Sullo spettro di assorbimento dei gas nobili presso il limite dello spettro d'arco. *Il Nuovo Cimento* 12, 154–161. doi:10.1007/bf02958288. In Italian; translated into English as Fano et al. (2005).
- Fano, U., 1961. Effects of configuration interaction on intensities and phase shifts. *Phys. Rev.* 124, 1866–1878. doi:10.1103/PhysRev.124.1866.
- Fano, U., Pupillo, G., Zannoni, A., Clark, C., 2005. On the absorption spectrum of noble gases at the arc spectrum limit. *J. Res. Nat. Inst. Stand. Technol.* 110, 583. doi:10.6028/jres.110.083. English translation of Fano (1935).
- Fedorov, M.V., 1998. *Atomic and Free Electrons in a Strong Light Field*. World Scientific. doi:10.1142/3320.
- Feist, J., Nagele, S., Pazourek, R., Persson, E., Schneider, B.I., Collins, L.A., Burgdörfer, J., 2009. Probing electron correlation via attosecond xuv pulses in the two-photon double ionization of helium. *Phys. Rev. Lett.* 103, 063002. doi:10.1103/PhysRevLett.103.063002.
- Feist, J., Zatsarinny, O., Nagele, S., Pazourek, R., Burgdörfer, J., Guan, X., Bartschat, K., Schneider, B.I., 2014. Time delays for attosecond streaking in photoionization of neon. *Phys. Rev. A* 89, 033417. doi:10.1103/PhysRevA.89.033417.
- Feldhaus, J., Arthur, J., Hastings, J.B., 2005. X-ray free-electron lasers. *J. Phys.* B 38, S799–S819. doi:10.1088/0953-4075/38/9/023.
- Feldhaus, J., Krikunova, M., Meyer, M., Möller, T., Moshhammer, R., Rudenko, A., Tschentscher, T., Ullrich, J., 2013. AMO science at the FLASH and european XFEL free-electron laser facilities. *J. Phys.* B 46, 164002. doi:10.1088/0953-4075/46/16/164002.
- Feldhaus, J., Saldin, E.L., Schneider, J.R., Schneidmiller, E.A., Yurkov, M.V., 1997. Possible application of X-ray optical elements for reducing the spectral bandwidth of an X-ray SASE FEL. *Opt. Commun.* 140, 341–352. doi:10.1016/s0030-4018(97)00163-6.
- Feng, C., Deng, H.X., 2018. Review of fully coherent free-electron lasers. *Nucl. Sci. Tech.* 29. doi:10.1007/s41365-018-0490-1.
- Feng, T., Heilmann, A., Bock, M., Ehrentraut, L., Witting, T., Yu, H., Stiel, H., Eisebitt, S., Schürer, M., 2020. 27 W 2.1 $\mu$ m OPCPA system for coherent soft X-ray generation operating at 10 kHz. *Opt. Express* 28, 8724. doi:10.1364/oe.386588.
- Ferguson, A.J., 1965. *Angular correlation method in gamma ray spectroscopy*. North Holland, Amsterdam.
- Ferguson, K.R., Bucher, M., Gorkhover, T., Boutet, S., Fukuzawa, H., Koglin, J.E., Kumagai, Y., Lutman, A., Marinelli, A., Messerschmidt, M., Nagaya, K., Turner, J., Ueda, K., Williams, G.J., Bucksbaum, P.H., Bostedt, C., 2016. Transient lattice contraction in the solid-to-plasma transition. *Sci. Adv.* 2, e1500837. doi:10.1126/sciadv.1500837.
- Ferrari, E., Roussel, E., Buck, J., Callegari, C., Cucini, R., De Ninno, G., Diviacco, B., Gauthier, D., Giannessi, L., Glaser, L., Hartmann, G., Penco, G., Scholz, F., Seltmann, J., Shevchuk, I., Viefhaus, J., Zangrando, M., Allaria, E.M., 2019. Free electron laser polarization control with interfering crossed polarized fields. *Phys. Rev. Accel. Beams* 22, 080701. doi:10.1103/PhysRevAccelBeams.22.080701.
- Ferrari, E., Spezzani, C., Fortuna, F., Delaunay, R., Vidal, F., Nikolov, I., Cinquegrana, P., Diviacco, B., Gauthier, D., Penco, G., Ribič, P.R., Roussel, E., Trovò, M., Moussy, J.B., Pincelli, T., Lounis, L., Manfreda, M., Pedersoli, E., Capotondi, F., Svetina, C., Mahne, N., Zangrando, M., Raimondi, L., Demidovich, A., Giannessi, L., De Ninno, G., Danailov, M.B., Allaria, E., Sacchi, M., 2016. Widely tunable two-colour seeded free-electron laser source for resonant-pump resonant-probe magnetic scattering. *Nat. Commun.* 7, 10343. doi:10.1038/ncomms10343.
- Feyer, V., Prince, K.C., Coreno, M., Melandri, S., Maris, A., Evangelisti, L., Caminati, W., Giuliano, B.M., Kjaergaard, H.G., Carravetta, V., 2018. Quantum effects for a proton in a low-barrier, double-well potential: Core level photoemission spectroscopy of acetylacetone. *J. Phys. Chem. Lett.* 9, 521–526. doi:10.1021/acs.jpcllett.7b03175.
- Finetti, P., Höppner, H., Allaria, E., Callegari, C., Capotondi, F., Cinquegrana, P., Coreno, M., Cucini, R., Danailov, M.B., Demidovich, A., De Ninno, G., Di Fraia, M., Feifel, R., Ferrari, E., Fröhlich, L., Gauthier, D., Golz, T., Grazioli, C., Kai, Y., Kurdi, G., Mahne, N., Manfreda, M., Medvedev, N., Nikolov, I.P., Pedersoli, E., Penco, G., Plekan, O., Prandolini, M.J., Prince, K.C., Raimondi, L., Rebernik, P., Riedel, R., Roussel, E., Sigalotti, P., Squibb, R., Stojanovic, N., Stranges, S., Svetina, C., Tanikawa, T., Teubner, U., Tkachenko, V., Tolek, S., Zangrando, M., Ziaja, B., Tavella, F., Giannessi, L., 2017. Pulse duration of seeded free-electron lasers. *Phys. Rev. X* 7, 021043. doi:10.1103/PhysRevX.7.021043.
- Foumouo, E., Kamta, G.L., Edah, G., Piraux, B., 2006. Theory of multiphoton single and double ionization of two-electron atomic systems driven by short-wavelength electric fields: An *ab initio* treatment. *Phys. Rev. A* 74, 063409. doi:10.1103/PhysRevA.74.063409.
- Frasinski, L.J., 2016. Covariance mapping techniques. *J. Phys. B: At., Mol. Opt. Phys.* 49, 152004. doi:10.1088/0953-4075/49/15/152004.
- Frasinski, L.J., Codling, K., Hatherly, P.A., 1989. Covariance mapping: A correlation method applied to multiphoton multiple ionization. *Science* 246, 1029–1031. doi:10.1126/science.246.4933.1029.
- Frasinski, L.J., Zhaunerchyk, V., Mücke, M., Squibb, R.J., Siano, M., Eland, J.H.D., Linusson, P., v.d. Meulen, P., Salén, P., Thomas, R.D., Larsson, M., Foucar, L., Ullrich, J., Motomura, K., Mondal, S., Ueda, K., Osipov, T., Fang, L., Murphy, B.F., Berrah, N., Bostedt, C., Bozek, J.D., Schorb, S., Messerschmidt, M., Glowia, J.M., Cryan, J.P., Coffee, R.N., Takahashi, O., Wada, S., Piancastelli, M.N., Richter, R., Prince, K.C., Feifel, R., 2013. Dynamics of hollow atom formation in intense x-ray pulses probed by partial covariance mapping. *Phys. Rev. Lett.* 111, 073002. doi:10.1103/PhysRevLett.111.073002.
- Friedman, A., Gover, A., Kurizki, G., Ruschin, S., Yariv, A., 1988. Spontaneous and stimulated emission from quasifree electrons. *Rev. Mod. Phys.* 60, 471–535. doi:10.1103/RevModPhys.60.471.
- Fritzsche, S., 2001. Utilities for the RATIP package. *Comput. Phys. Commun.* 141, 163–174. doi:10.1016/s0010-4655(01)00400-3.
- Fritzsche, S., 2012. The RATIP program for relativistic calculations of atomic transition, ionization and recombination properties. *Comput. Phys. Commun.* 183, 1525–1559. doi:10.1016/j.cpc.2012.02.016.
- Fritzsche, S., Grum-Grzhimailo, A.N., Gryzlova, E.V., Kabachnik, N.M., 2008. Angular distributions and angular correlations in sequential two-photon double ionization of atoms. *J. Phys. B* 41, 165601. doi:10.1088/0953-4075/41/16/165601.
- Fritzsche, S., Grum-Grzhimailo, A.N., Gryzlova, E.V., Kabachnik, N.M., 2009. Sequential two-photon double ionization of Kr atoms. *J. Phys. B* 42, 145602. doi:10.1088/0953-4075/42/14/145602.
- Fritzsche, S., Grum-Grzhimailo, A.N., Gryzlova, E.V., Kabachnik, N.M., 2011. Sequential two-photon double ionization of the 4d shell in xenon. *J. Phys. B* 44, 175602. doi:10.1088/0953-4075/44/17/175602.
- Froese-Fischer, C., Brage, T., Jönsson, P., 1997. *Computational Atomic Structure: An MCHF Approach*. CRC Press. doi:10.1201/9781315139982.
- Fukuzawa, H., Gryzlova, E.V., Motomura, K., Yamada, A., Ueda, K., Grum-Grzhimailo, A.N., Strakhova, S.I., Nagaya, K., Sugishima, A.,

- Mizoguchi, Y., Iwayama, H., Yao, M., Saito, N., Piseri, P., Mazza, T., Devetta, M., Coreno, M., Nagasono, M., Tono, K., Yabashi, M., Ishikawa, T., Ohashi, H., Kimura, H., Togashi, T., Senba, Y., 2010. Photoelectron spectroscopy of sequential three-photon double ionization of Ar irradiated by EUV free-electron laser pulses. *J. Phys. B* 43, 111001. doi:10.1088/0953-4075/43/11/111001.
- Fukuzawa, H., Son, S.K., Motomura, K., Mondal, S., Nagaya, K., Wada, S., Liu, X.J., Feifel, R., Tachibana, T., Ito, Y., Kimura, M., Sakai, T., Matsunami, K., Hayashita, H., Kajikawa, J., Johnsson, P., Siano, M., Kuk, E., Rudek, B., Erk, B., Foucar, L., Robert, E., Miron, C., Tono, K., Inubushi, Y., Hatsui, T., Yabashi, M., Yao, M., Santra, R., Ueda, K., 2013. Deep inner-shell multiphoton ionization by intense X-ray free-electron laser pulses. *Phys. Rev. Lett.* 110, 173005. doi:10.1103/PhysRevLett.110.173005.
- Fukuzawa, H., Takashi, T., Kuk, E., Motomura, K., Wada, S., Nagaya, K., Ito, Y., Nishiyama, T., Nicolas, C., Kumagai, Y., Iablonsky, D., Mondal, S., Tachibana, T., You, D., Yamada, S., Sakakibara, Y., Asa, K., Sato, Y., Sakai, T., Matsunami, K., Umamoto, T., Kariyazono, K., Kajimoto, S., Sotome, H., Johnsson, P., Schöffler, M.S., Kastirke, G., Kooser, K., Liu, X.J., Asavei, T., Neagu, L., Molodtsov, S., Ochiai, K., Kanno, M., Yamazaki, K., Owada, S., Ogawa, K., Katayama, T., Togashi, T., Tono, K., Yabashi, M., Ghosh, A., Gokhberg, K., Cederbaum, L.S., Kuleff, A.I., Fukumura, H., Kishimoto, N., Rudenko, A., Miron, C., Kono, H., Ueda, K., 2019. Real-time observation of X-ray-induced intramolecular and interatomic electronic decay in CH<sub>2</sub>I<sub>2</sub>. *Nat. Commun.* 10, 2186. doi:10.1038/s41467-019-10060-z.
- Fukuzawa, H., Ueda, K., 2020. X-ray induced ultrafast dynamics in atoms, molecules and clusters: experimental studies at an X-ray free-electron laser facility SACLAL and modelling. *Advances in Physics: X* doi:10.1080/23746149.2020.1785327. in press.
- Gao, B., Starace, A.F., 1989. Variational principle for high-order perturbations with application to multiphoton processes for the H atom. *Phys. Rev. A* 39, 4550–4560. doi:10.1103/PhysRevA.39.4550.
- Gauthier, D., Allaria, E., Coreno, M., Cudin, I., Dacasa, H., Danailov, M.B., Demidovich, A., di Mitri, S., Diviacco, B., Ferrari, E., Finetti, P., Frassetto, F., Garzella, D., Künzel, S., Leroux, V., Mahieu, B., Mahne, N., Meyer, M., Mazza, T., Miotti, P., Penco, G., Raimondi, L., Rebernik Ribič, P., Richter, R., Roussel, E., Schulz, S., Sturari, L., Svetina, C., Trovò, M., Walker, P.A., Zangrando, M., Callegari, C., Fajardo, M., Poletto, L., Zeitoun, P., Giannessi, L., de Ninno, G., 2016a. Chirped pulse amplification in an extreme-ultraviolet free-electron laser. *Nat. Commun.* 7, 13688. doi:10.1038/ncomms13688.
- Gauthier, D., Rebernik Ribič, P., De Ninno, G., Allaria, E., Cinquegrana, P., Danailov, M.B., Demidovich, A., Ferrari, E., Giannessi, L., 2016b. Generation of phase-locked pulses from a seeded free-electron laser. *Phys. Rev. Lett.* 116, 024801. doi:10.1103/PhysRevLett.116.024801.
- Gauthier, D., Rebernik Ribič, P., De Ninno, G., Allaria, E., Cinquegrana, P., Danailov, M.B., Demidovich, A., Ferrari, E., Giannessi, L., Mahieu, B., Penco, G., 2015. Spectrotemporal shaping of seeded free-electron laser pulses. *Phys. Rev. Lett.* 115, 114801. doi:10.1103/PhysRevLett.115.114801.
- Geloni, G., 2016. Self-seeded free-electron lasers, in: Jaeschke, E.J., Khan, S., Schneider, J.R., Hastings, J.B. (Eds.), *Synchrotron Light Sources and Free-Electron Lasers*. Springer International Publishing, pp. 161–193. doi:10.1007/978-3-319-14394-1\_4.
- Geloni, G., Kocharyan, V., Saldin, E., 2011. A novel self-seeding scheme for hard X-ray FELs. *J. Mod. Opt.* 58, 1391–1403. doi:10.1080/09500340.2011.586473.
- Giannessi, L., Allaria, E., Prince, K.C., Callegari, C., Sansone, G., Ueda, K., Morishita, T., Liu, C.N., Grum-Grzhimailo, A.N., Gryzlova, E.V., Douguet, N., Bartschat, K., 2018. Coherent control schemes for the photoionization of neon and helium in the Extreme Ultraviolet spectral region. *Sci. Rep.* 8, 7774. doi:10.1038/s41598-018-25833-7.
- Giannessi, L., Bellaveglia, M., Chiodroni, E., Cianchi, A., Couprie, M.E., Del Franco, M., Di Pirro, G., Ferrario, M., Gatti, G., Labat, M., Marcus, G., Mostacci, A., Petralia, A., Petrillo, V., Quattromini, M., Rau, J.V., Spampinati, S., Surrenti, V., 2013. Superradiant cascade in a seeded free-electron laser. *Phys. Rev. Lett.* 110, 044801. doi:10.1103/PhysRevLett.110.044801.
- Ginzburg, V., 1947. On the radiation of microradiowaves and their absorption in the air. *Izv. Akad. Nauk SSSR, Ser. Fiz.* 11, 165.
- Glauber, R.J., 1963. The quantum theory of optical coherence. *Phys. Rev.* 130, 2529–2539. doi:10.1103/PhysRev.130.2529.
- Goetz, R.E., Karamatskou, A., Santra, R., Koch, C.P., 2016. Quantum optimal control of photoelectron spectra and angular distributions. *Phys. Rev. A* 93, 013413. doi:10.1103/PhysRevA.93.013413.
- Gordon, J.P., Zeiger, H.J., Townes, C.H., 1954. Molecular microwave oscillator and new hyperfine structure in the microwave spectrum of NH<sub>3</sub>. *Phys. Rev.* 95, 282–284. doi:10.1103/PhysRev.95.282.
- Gordon, J.P., Zeiger, H.J., Townes, C.H., 1955. The maser—new type of microwave amplifier, frequency standard, and spectrometer. *Phys. Rev.* 99, 1264–1274. doi:10.1103/PhysRev.99.1264.
- Gordon, R.J., Rice, S.A., 1997. Active control of the dynamics of atoms and molecules. *Annu. Rev. Phys. Chem.* 48, 601–641. doi:10.1146/annurev.physchem.48.1.601.
- Goreslavski, S.P., Paulus, G.G., Popruzhenko, S.V., Shvetsov-Shilovski, N.I., 2004. Coulomb asymmetry in above-threshold ionization. *Phys. Rev. Lett.* 93, 233002. doi:10.1103/PhysRevLett.93.233002.
- Gorkhover, T., Schorb, S., Coffee, R., Adolph, M., Foucar, L., Rupp, D., Aquila, A., Bozek, J.D., Epp, S.W., Erk, B., Gumprecht, L., Holmgaard, L., Hartmann, A., Hartmann, R., Hauser, G., Holl, P., Hömke, A., Johnsson, P., Kimmel, N., Kühnel, K., Messerschmidt, M., Reich, C., Rouzée, A., Rudek, B., Schmidt, C., Schulz, J., Soltau, H., Stern, S., Weidenspointner, G., White, B., Küpper, J., Strüder, L., Schlichting, I., Ullrich, J., Rolles, D., Rudenko, A., Möller, T., Bostedt, C., 2016. Femtosecond and nanometre visualization of structural dynamics in superheated nanoparticles. *Nat. Photonics* 10, 93–97. doi:10.1038/nphoton.2015.264.
- Gorobtsov, O.Y., Mercurio, G., Capotondi, F., Skopintsev, P., Lazarev, S., Zaluzhnyy, I.A., Danailov, M.B., Dell'Angela, M., Manfreda, M., Pedersoli, E., Giannessi, L., Kiskinova, M., Prince, K.C., Wurth, W., Vartanyants, I.A., 2018. Seeded X-ray free-electron laser generating radiation with laser statistical properties. *Nat. Commun.* 9, 4498. doi:10.1038/s41467-018-06743-8.
- Goswami, D., 2003. Optical pulse shaping approaches to coherent control. *Phys. Rep.* 374, 385–481. doi:10.1016/s0370-1573(02)00480-5.
- Goulielmakis, E., 2004. Direct measurement of light waves. *Science* 305, 1267–1269. doi:10.1126/science.1100866.
- Greene, C.H., Zare, R.N., 1982. Photofragment alignment and orientation. *Annu. Rev. Phys. Chem.* 33, 119–150. doi:10.1146/annurev.pc.33.100182.001003.
- Greenman, L., Ho, P.J., Pabst, S., Kamarchik, E., Mazziotti, D.A., Santra, R., 2010. Implementation of the time-dependent configuration-interaction singles method for atomic strong-field processes. *Phys. Rev. A* 82, 023406. doi:10.1103/PhysRevA.82.023406.
- Grum-Grzhimailo, A.N., Douguet, N., Meyer, M., Bartschat, K., 2019. Two-color XUV plus near-IR multiphoton near-threshold ionization of the helium ion by circularly polarized light in the vicinity of the 3*p* resonance. *Phys. Rev. A* 100, 033404. doi:10.1103/PhysRevA.100.033404.

- Grum-Grzhimailo, A.N., Gryzlova, E.V., 2014. Nondipole effects in the angular distribution of photoelectrons in two-photon two-color above-threshold atomic ionization. *Phys. Rev. A* 89, 043424. doi:10.1103/PhysRevA.89.043424.
- Grum-Grzhimailo, A.N., Gryzlova, E.V., Fritzsche, S., Kabachnik, N.M., 2016. Photoelectron angular distributions and correlations in sequential double and triple atomic ionization by free electron lasers. *J. Mod. Opt.* 60, 334–357. doi:10.1080/09500340.2015.1047805.
- Grum-Grzhimailo, A.N., Gryzlova, E.V., Kuzmina, E.I., Chetverkina, A.S., Strakhova, S.I., 2015a. Two-color above-threshold and two-photon sequential double ionization beyond the dipole approximation. *J. Phys. Conf. Ser.* 601, 012012. doi:10.1088/1742-6596/601/1/012012.
- Grum-Grzhimailo, A.N., Gryzlova, E.V., Meyer, M., 2012. Non-dipole effects in the angular distribution of photoelectrons in sequential two-photon atomic double ionization. *J. Phys. B* 45, 215602. doi:10.1088/0953-4075/45/21/215602.
- Grum-Grzhimailo, A.N., Gryzlova, E.V., Staroselskaya, E.I., Venzke, J., Bartschat, K., 2015b. Interfering one-photon and two-photon ionization by femtosecond VUV pulses in the region of an intermediate resonance. *Phys. Rev. A* 91, 063418. doi:10.1103/PhysRevA.91.063418.
- Grum-Grzhimailo, A.N., Meyer, M., 2009. Magnetic dichroism in atomic core level photoemission. *Eur. Phys. J ST* 169, 43–50. doi:10.1140/epjst/e2009-00971-2.
- Gruson, V., Barreau, L., Jiménez-Galan, Á., Risoud, F., Caillaud, J., Maquet, A., Carré, B., Lepetit, F., Hergott, J.F., Ruchon, T., Argenti, L., Taïeb, R., Martín, F., Salières, P., 2016. Attosecond dynamics through a Fano resonance: Monitoring the birth of a photoelectron. *Science* 354, 734–738. doi:10.1126/science.1251888.
- Gryzlova, E.V., Grum-Grzhimailo, A.N., Fritzsche, S., Kabachnik, N.M., 2010. Angular correlations between two electrons emitted in the sequential two-photon double ionization of atoms. *J. Phys. B* 43, 225602. doi:10.1088/0953-4075/43/22/225602.
- Gryzlova, E.V., Grum-Grzhimailo, A.N., Kabachnik, N.M., Fritzsche, S., 2012. Angular distributions and correlations in sequential three-photon triple atomic ionization. *J. Phys. Conf. Ser.* 388, 012031. doi:10.1088/1742-6596/388/1/012031.
- Gryzlova, E.V., Grum-Grzhimailo, A.N., Kiselev, M.D., Burkov, S.M., 2019a. Two-photon sequential double ionization of argon in the region of Rydberg autoionizing states of Ar<sup>+</sup>. *Eur. Phys. J D* 73, 93. doi:10.1140/epjd/e2019-90678-x.
- Gryzlova, E.V., Grum-Grzhimailo, A.N., Kuzmina, E.I., Strakhova, S.I., 2014. Sequential two-photon double ionization of noble gases by circularly polarized XUV radiation. *J. Phys. B* 47, 195601. doi:10.1088/0953-4075/47/19/195601.
- Gryzlova, E.V., Grum-Grzhimailo, A.N., Staroselskaya, E.I., Douguet, N., Bartschat, K., 2018. Quantum coherent control of the photoelectron angular distribution in bichromatic-field ionization of atomic neon. *Phys. Rev. A* 97, 013420. doi:10.1103/PhysRevA.97.013420.
- Gryzlova, E.V., Grum-Grzhimailo, A.N., Staroselskaya, E.I., Strakhova, S.I., 2015. Similarity between the angular distributions of the first- and second-step electrons in sequential two-photon atomic double ionization. *J. Electron Spectrosc. Relat. Phenom.* 204, 277–283. doi:10.1016/j.elspec.2015.08.016.
- Gryzlova, E.V., Ma, R., Fukuzawa, H., Motomura, K., Yamada, A., Ueda, K., Grum-Grzhimailo, A.N., Kabachnik, N.M., Strakhova, S.I., Rouzée, A., Hundermark, A., Vrakking, M.J.J., Johnsson, P., Nagaya, K., Yase, S., Mizoguchi, Y., Yao, M., Nagasono, M., Tono, K., Togashi, T., Senba, Y., Ohashi, H., Yabashi, M., Ishikawa, T., 2011. Doubly resonant three-photon double ionization of Ar atoms induced by an EUV free-electron laser. *Phys. Rev. A* 84, 063405. doi:10.1103/PhysRevA.84.063405.
- Gryzlova, E.V., Popova, M.M., Grum-Grzhimailo, A.N., Staroselskaya, E.I., Douguet, N., Bartschat, K., 2019b. Coherent control of the photoelectron angular distribution in ionization of neon by a circularly polarized bichromatic field in the resonance region. *Phys. Rev. A* 100, 063417. doi:10.1103/PhysRevA.100.063417.
- Guan, X., Bartschat, K., Schneider, B.I., 2011. Breakup of the aligned H<sub>2</sub> molecule by xuv laser pulses: A time-dependent treatment in prolate spheroidal coordinates. *Phys. Rev. A* 83, 043403. doi:10.1103/PhysRevA.83.043403.
- Guan, X., Noble, C.J., Zatsarinny, O., Bartschat, K., Schneider, B.I., 2008. Time-dependent R-matrix calculations for multiphoton ionization of argon atoms in strong laser pulses. *Phys. Rev. A* 78, 053402. doi:10.1103/PhysRevA.78.053402.
- Guan, X., Zatsarinny, O., Bartschat, K., Schneider, B.I., Feist, J., Noble, C.J., 2007. General approach to few-cycle intense laser interactions with complex atoms. *Phys. Rev. A* 76, 053411. doi:10.1103/PhysRevA.76.053411.
- Haake, F., 1973. Statistical treatment of open systems by generalized master equations, in: Höhler, G. (Ed.), *Quantum Statistics in Optical and Solid-State Physics*. Springer-Verlag. volume 66 of *Springer Tracts in Modern Physics*, pp. 98–168. doi:10.1007/978-3-662-40468-3\_2.
- Haber, J., Kong, X., Strohm, C., Willing, S., Gollwitzer, J., Bocklage, L., Ruffer, R., Pálffy, A., Röhlberger, R., 2017. Rabi oscillations of X-ray radiation between two nuclear ensembles. *Nat. Photonics* 11, 720–725. doi:10.1038/s41566-017-0013-3.
- Haber, L.H., Doughty, B., Leone, S.R., 2009. Continuum phase shifts and partial cross sections for photoionization from excited states of atomic helium measured by high-order harmonic optical pump-probe velocity map imaging. *Phys. Rev. A* 79, 031401. doi:10.1103/PhysRevA.79.031401.
- Haber, L.H., Doughty, B., Leone, S.R., 2010. Time-resolved photoelectron angular distributions and cross-section ratios of two-colour two-photon above threshold ionization of helium. *Molecular Physics* 108, 1241–1251. doi:10.1080/00268976.2010.483133.
- Halavanau, A., Decker, F.J., Emma, C., Sheppard, J., Pellegrini, C., 2019. Very high brightness and power LCLS-II hard X-ray pulses. *J. Synchrotron Radiat.* 26, 635–646. doi:10.1107/s1600577519002492.
- Han, J., Zhang, L., E, W., 2019. Solving many-electron Schrödinger equation using deep neural networks. *J. Comp. Phys.* 399, 108929. doi:10.1016/j.jcp.2019.108929.
- Hanbury Brown, R., Twiss, R.Q., 1956a. Correlation between photons in two coherent beams of light. *Nature* 177, 27–29. doi:10.1038/177027a0.
- Hanbury Brown, R., Twiss, R.Q., 1956b. A test of a new type of stellar interferometer on Sirius. *Nature* 178, 1046–1048. doi:10.1038/1781046a0.
- Hanson, L.G., Zhang, J., Lambropoulos, P., 1997. Manifestations of atomic and core resonances in photoelectron energy spectra. *Phys. Rev. A* 55, 2232–2244. doi:10.1103/PhysRevA.55.2232.
- Harries, J.R., Iwayama, H., Kuma, S., Iizawa, M., Suzuki, N., Azuma, Y., Inoue, I., Owada, S., Togashi, T., Tono, K., Yabashi, M., Shigemasa, E., 2018. Superfluorescence, free-induction decay, and four-wave mixing: Propagation of free-electron laser pulses through a dense sample of helium ions. *Phys. Rev. Lett.* 121, 263201. doi:10.1103/PhysRevLett.121.263201.
- van der Hart, H.W., Lysaght, M.A., Burke, P.G., 2007. Time-dependent multielectron dynamics of Ar in intense short laser pulses. *Phys. Rev. A* 76, 043405. doi:10.1103/PhysRevA.76.043405.
- van der Hart, H.W., Lysaght, M.A., Burke, P.G., 2008. Momentum distributions of electrons ejected during ultrashort laser interactions with multielectron atoms described using the R-matrix basis sets. *Phys. Rev. A* 77, 065401. doi:10.1103/PhysRevA.77.065401.



- Haxton, D.J., Lawler, K.V., McCurdy, C.W., 2011. Multiconfiguration time-dependent Hartree-Fock treatment of electronic and nuclear dynamics in diatomic molecules. *Phys. Rev. A* 83, 063416. doi:10.1103/PhysRevA.83.063416.
- Haxton, D.J., McCurdy, C.W., 2015. Two methods for restricted configuration spaces within the multiconfiguration time-dependent Hartree-Fock method. *Phys. Rev. A* 91, 012509. doi:10.1103/PhysRevA.91.012509.
- Hellmann, S., Sohr, C., Beye, M., Rohwer, T., Sorgenfrei, F., Marczyński-Bühlow, M., Kalläne, M., Redlin, H., Hennies, F., Bauer, M., Föhlich, A., Kipp, L., Wurth, W., Rossnagel, K., 2012. Time-resolved x-ray photoelectron spectroscopy at FLASH. *New J. Phys.* 14, 013062. doi:10.1088/1367-2630/14/1/013062.
- Helml, W., Grguraš, I., Juranić, P., Düsterer, S., Mazza, T., Maier, A., Hartmann, N., Ilchen, M., Hartmann, G., Patthey, L., Callegari, C., Costello, J., Meyer, M., Coffee, R., Cavalieri, A., Kienberger, R., 2017. Ultrashort free-electron laser X-ray pulses. *Applied Sciences* 7, 915. doi:10.3390/app7090915.
- Helml, W., Maier, A.R., Schweinberger, W., Grguraš, I., Radcliffe, P., Doumy, G., Roedig, C., Gagnon, J., Messerschmidt, M., Schorb, S., Bostedt, C., Grüner, F., DiMauro, L.F., Cubaynes, D., Bozek, J.D., Tschentscher, T., Costello, J.T., Meyer, M., Coffee, R., Düsterer, S., Cavalieri, A.L., Kienberger, R., 2014. Measuring the temporal structure of few-femtosecond free-electron laser X-ray pulses directly in the time domain. *Nature Photonics* 8, 950–957. doi:10.1038/nphoton.2014.278.
- Hemsing, E., Halavanau, A., Zhang, Z., 2020. Statistical theory of a self-seeded free electron laser with noise pedestal growth. *Phys. Rev. Accel. Beams* 23, 010701. doi:10.1103/PhysRevAccelBeams.23.010701.
- Hemsing, E., Marcus, G., Fawley, W.M., Schoenlein, R.W., Coffee, R., Dakovski, G., Hastings, J., Huang, Z., Ratner, D., Raubenheimer, T., Penn, G., 2019. Soft x-ray seeding studies for the SLAC Linac Coherent Light Source II. *Phys. Rev. Accel. Beams* 22, 110701. doi:10.1103/PhysRevAccelBeams.22.110701.
- Heyl, C.M., Arnold, C.L., Couairon, A., L'Huillier, A., 2016. Introduction to macroscopic power scaling principles for high-order harmonic generation. *J. Phys. B* 50, 013001. doi:10.1088/1361-6455/50/1/013001.
- Hikosaka, Y., Fushitani, M., Matsuda, A., Tseng, C.M., Hishikawa, A., Shigemasa, E., Nagasono, M., Tono, K., Togashi, T., Ohashi, H., Kimura, H., Senba, Y., Yabashi, M., Ishikawa, T., 2010. Multiphoton double ionization of Ar in intense extreme ultraviolet laser fields studied by shot-by-shot photoelectron spectroscopy. *Phys. Rev. Lett.* 105, 133001. doi:10.1103/PhysRevLett.105.133001.
- Hikosaka, Y., Kaneyasu, T., Fujimoto, M., Iwayama, H., Katoh, M., 2019. Coherent control in the extreme ultraviolet and attosecond regime by synchrotron radiation. *Nat. Commun.* 10, 4988. doi:10.1038/s41467-019-12978-w.
- Hishikawa, A., Fushitani, M., Hikosaka, Y., Matsuda, A., Liu, C.N., Morishita, T., Shigemasa, E., Nagasono, M., Tono, K., Togashi, T., Ohashi, H., Kimura, H., Senba, Y., Yabashi, M., Ishikawa, T., 2011. Enhanced nonlinear double excitation of He in intense extreme ultraviolet laser fields. *Phys. Rev. Lett.* 107, 243003. doi:10.1103/PhysRevLett.107.243003.
- Ho, P.J., Bostedt, C., Schorb, S., Young, L., 2014. Theoretical tracking of resonance-enhanced multiple ionization pathways in X-ray free-electron laser pulses. *Phys. Rev. Lett.* 113, 253001. doi:10.1103/PhysRevLett.113.253001.
- Ho, P.J., Kanter, E.P., Young, L., 2015. Resonance-mediated atomic ionization dynamics induced by ultraintense x-ray pulses. *Phys. Rev. A* 92, 063430. doi:10.1103/PhysRevA.92.063430.
- Hochstuhl, D., Bonitz, M., 2012. Time-dependent restricted-active-space configuration-interaction method for the photoionization of many-electron atoms. *Phys. Rev. A* 86, 053424. doi:10.1103/PhysRevA.86.053424.
- Hofbrucker, J., Volotka, A.V., Fritzsche, S., 2018. Maximum elliptical dichroism in atomic two-photon ionization. *Phys. Rev. Lett.* 121, 053401. doi:10.1103/PhysRevLett.121.053401.
- Hofstetter, M., Schultze, M., Fieß, M., Dennhardt, B., Guggenmos, A., Gagnon, J., Yakovlev, V.S., Goulielmakis, E., Kienberger, R., Gullikson, E.M., Krausz, F., Kleineberg, U., 2011. Attosecond dispersion control by extreme ultraviolet multilayer mirrors. *Opt. Express* 19, 1767–1776. doi:10.1364/OE.19.001767.
- Hogle, C.W., Tong, X.M., Martin, L., Murnane, M.M., Kapteyn, H.C., Ranitovic, P., 2015. Attosecond coherent control of single and double photoionization in argon. *Phys. Rev. Lett.* 115, 173004. doi:10.1103/PhysRevLett.115.173004.
- Holzmeier, F., Bello, R.Y., Hervé, M., Achner, A., Baumann, T.M., Meyer, M., Finetti, P., Di Fraia, M., Gauthier, D., Roussel, E., Plekan, O., Richter, R., Prince, K.C., Callegari, C., Bachau, H., Palacios, A., Martín, F., Dowek, D., 2018. Control of H<sub>2</sub> dissociative ionization in the nonlinear regime using vacuum ultraviolet free-electron laser pulses. *Phys. Rev. Lett.* 121, 103002. doi:10.1103/PhysRevLett.121.103002.
- Hong, K.H., Lai, C.J., Gkortsas, V.M., Huang, S.W., Moses, J., Granados, E., Bhardwaj, S., Kärtner, F.X., 2012. High-order harmonic generation in Xe, Kr, and Ar driven by a 2.1- $\mu\text{m}$  source: High-order harmonic spectroscopy under macroscopic effects. *Phys. Rev. A* 86, 043412. doi:10.1103/physreva.86.043412.
- Hong, K.H., Lai, C.J., Siqueira, J.P., Krogen, P., Moses, J., Chang, C.L., Stein, G.J., Zapata, L.E., Kärtner, F.X., 2014. Multi-mJ, kHz, 2.1 $\mu\text{m}$  optical parametric chirped-pulse amplifier and high-flux soft x-ray high-harmonic generation. *Opt. Lett.* 39, 3145. doi:10.1364/ol.39.003145.
- Hutchinson, S., Lysaght, M.A., van der Hart, H.W., 2013. Anisotropy parameters in two-color two-photon above-threshold ionization. *Phys. Rev. A* 88, 023424. doi:10.1103/PhysRevA.88.023424.
- Iablonskyi, D., Nagaya, K., Fukuzawa, H., Motomura, K., Kumagai, Y., Mondal, S., Tachibana, T., Takanashi, T., Nishiyama, T., Matsunami, K., Johnsson, P., Piseri, P., Sansone, G., Dubrouil, A., Reduzzi, M., Carpeggiani, P., Vozzi, C., Devetta, M., Negro, M., Callegari, F., Trabattini, A., Castrovilli, M.C., Faccialá, D., Ovcharenko, Y., Möller, T., Mudrich, M., Stienkemeier, F., Coreno, M., Alagia, M., Schütte, B., Berrah, N., Kuleff, A.I., Jabbari, G., Callegari, C., Plekan, O., Finetti, P., Spezzani, C., Ferrari, E., Allaria, E., Penco, G., Serpico, C., De Nino, G., Nikolov, I., Diviacco, B., Di Mitri, S., Giannessi, L., Prince, K.C., Ueda, K., 2016. Slow interatomic coulombic decay of multiply excited neon clusters. *Phys. Rev. Lett.* 117, 276806. doi:10.1103/PhysRevLett.117.276806.
- Iablonskyi, D., Ueda, K., Ishikawa, K.L., Kheifets, A.S., Carpeggiani, P., Reduzzi, M., Ahmadi, H., Comby, A., Sansone, G., Csizmadia, T., Kuehn, S., Ovcharenko, E., Mazza, T., Meyer, M., Fischer, A., Callegari, C., Plekan, O., Finetti, P., Allaria, E., Ferrari, E., Roussel, E., Gauthier, D., Giannessi, L., Prince, K.C., 2017. Observation and control of laser-enabled Auger decay. *Phys. Rev. Lett.* 119, 073203. doi:10.1103/PhysRevLett.119.073203.
- Ilchen, M., Douguet, N., Mazza, T., Rafipoor, A.J., Callegari, C., Finetti, P., Plekan, O., Prince, K.C., Demidovich, A., Grazioli, C., Avaldi, L., Bolognesi, P., Coreno, M., Di Fraia, M., Devetta, M., Ovcharenko, Y., Düsterer, S., Ueda, K., Bartschat, K., Grum-Grzhimailo, A.N., Bozhevolnov, A.V., Kazansky, A.K., Kabachnik, N.M., Meyer, M., 2017. Circular dichroism in multiphoton ionization of resonantly excited

- He<sup>+</sup> ions. Phys. Rev. Lett. 118, 013002. doi:10.1103/PhysRevLett.118.013002.
- Ilchen, M., Hartmann, G., Gryzlova, E.V., Achner, A., Allaria, E., Beckmann, A., Braune, M., Buck, J., Callegari, C., Coffee, R.N., Cucini, R., Danailov, M., De Fanis, A., Demidovich, A., Ferrari, E., Finetti, P., Glaser, L., Knie, A., Lindahl, A.O., Plekan, O., Mahne, N., Mazza, T., Raimondi, L., Roussel, E., Seltmann, F.S.J., Shevchuk, I., Svetina, C., Walter, P., Zangrando, M., Viefhaus, J., Grum-Grzhimailo, A.N., Meyer, M., 2018. Symmetry breakdown of electron emission in extreme ultraviolet photoionization of argon. Nat. Commun. 8, 4659. doi:10.1038/s41467-018-07152-7.
- Inhester, L., Hanasaki, K., Hao, Y., Son, S.K., Santra, R., 2016. X-ray multiphoton ionization dynamics of a water molecule irradiated by an x-ray free-electron laser pulse. Phys. Rev. A 94, 023422. doi:10.1103/PhysRevA.94.023422.
- Inoue, I., Osaka, T., Hara, T., Tanaka, T., Inagaki, T., Fukui, T., Goto, S., Inubushi, Y., Kimura, H., Kinjo, R., Ohashi, H., Togawa, K., Tono, K., Yamaga, M., Tanaka, H., Ishikawa, T., Yabashi, M., 2019. Generation of narrow-band X-ray free-electron laser via reflection self-seeding. Nat. Photonics 13, 319–322. doi:10.1038/s41566-019-0365-y.
- Ishikawa, K.L., Kawazura, Y., Ueda, K., 2010. Two-photon ionization of atoms by ultrashort laser pulses. J. Mod. Opt. 57, 999–1007. doi:10.1080/09500340903511703.
- Ishikawa, K.L., Kazansky, A.K., Kabachnik, N.M., Ueda, K., 2014. Theoretical study of pulse delay effects in the photoelectron angular distribution of near-threshold EUV + IR two-photon ionization of atoms. Phys. Rev. A 90, 023408. doi:10.1103/PhysRevA.90.023408.
- Ishikawa, K.L., Midorikawa, K., 2005. Above-threshold double ionization of helium with attosecond intense soft x-ray pulses. Phys. Rev. A 72, 013407. doi:10.1103/PhysRevA.72.013407.
- Ishikawa, K.L., Sato, T., 2015. A review on *ab initio* approaches for multielectron dynamics. IEEE J. Sel. Top. Quantum Electron. 21, 8700916. doi:10.1109/JSTQE.2015.2438827.
- Ishikawa, K.L., Ueda, K., 2012. Competition of resonant and nonresonant paths in resonance-enhanced two-photon single ionization of He by an ultrashort extreme-ultraviolet pulse. Phys. Rev. Lett. 108, 033003. doi:10.1103/PhysRevLett.108.033003.
- Ishikawa, K.L., Ueda, K., 2013. Photoelectron angular distribution and phase in two-photon single ionization of H and He by a femtosecond and attosecond extreme-ultraviolet pulse. Applied Sciences 3, 189–213. doi:10.3390/app3010189.
- Ishikawa, T., Aoyagi, H., Asaka, T., Asano, Y., Azumi, N., Bizen, T., Ego, H., Fukami, K., Fukui, T., Furukawa, Y., Goto, S., Hanaki, H., Hara, T., Hasegawa, T., Hatsui, T., Higashiya, A., Hirono, T., Hosoda, N., Ishii, M., Inagaki, T., Inubushi, Y., Itoga, T., Joti, Y., Kago, M., Kameshima, T., Kimura, H., Kirihara, Y., Kiyomichi, A., Kobayashi, T., Kondo, C., Kudo, T., Maesaka, H., Maréchal, X.M., Masuda, T., Matsubara, S., Matsumoto, T., Matsushita, T., Matsui, S., Nagasono, M., Nariyama, N., Ohashi, H., Ohata, T., Ohshima, T., Ono, S., Otake, Y., Saji, C., Sakurai, T., Sato, T., Sawada, K., Seike, T., Shirasawa, K., Sugimoto, T., Suzuki, S., Takahashi, S., Takebe, H., Takeshita, K., Tamasaku, K., Tanaka, H., Tanaka, R., Tanaka, T., Togashi, T., Togawa, K., Tokuhisa, A., Tomizawa, H., Tono, K., Wu, S., Yabashi, M., Yamaga, M., Yamashita, A., Yanagida, K., Zhang, C., Shintake, T., Kitamura, H., Kumagai, N., 2012. A compact x-ray free-electron laser emitting in the sub-ångström region. Nat. Photonics 6, 540–544. doi:10.1038/nphoton.2012.141.
- Ivanov, M.Y., Spanner, M., Smirnova, O., 2005. Anatomy of strong field ionization. J. Mod. Opt. 52, 165–184. doi:10.1080/0950034042000275360.
- Jahnke, T., 2015. Interatomic and intermolecular Coulombic decay: the coming of age story. J. Phys. B 48, 082001. doi:10.1088/0953-4075/48/8/082001.
- Jiang, Y.H., Rudenko, A., Herrwerth, O., Foucar, L., Kurka, M., Kühnel, K.U., Lezius, M., Kling, M.F., van Tilborg, J., Belkacem, A., Ueda, K., Düsterer, S., Treusch, R., Schröter, C.D., Moshhammer, R., Ullrich, J., 2010. Ultrafast extreme ultraviolet induced isomerization of acetylene cations. Phys. Rev. Lett. 105, 263002. doi:10.1103/PhysRevLett.105.263002.
- Jiménez Galán, A., Argenti, L., Martín, F., 2013. The soft-photon approximation in infrared-laser-assisted atomic ionization by extreme-ultraviolet attosecond-pulse trains. New J. Phys. 15, 113009. doi:10.1088/1367-2630/15/11/113009.
- Joachain, C.J., Kylstra, N.J., Potvliege, R.M., 2012. Atoms in Intense Laser Fields. Cambridge University Press. doi:10.1017/cbo9780511993459.
- Jonas, D.M., 2003. Two-dimensional femtosecond spectroscopy. Annu. Rev. Phys. Chem. 54, 425–463. doi:10.1146/annurev.physchem.54.011002.103907.
- Kaldun, A., Blättermann, A., Stooß, V., Donsa, S., Wei, H., Pazourek, R., Nagele, S., Ott, C., Lin, C.D., Burgdörfer, J., Pfeifer, T., 2016. Observing the ultrafast buildup of a Fano resonance in the time domain. Science 354, 738–741. doi:10.1126/science.aah6972.
- Kaneyasu, T., Hikosaka, Y., Fujimoto, M., Iwayama, H., Katoh, M., 2019. Controlling the orbital alignment in atoms using cross-circularly polarized extreme ultraviolet wave packets. Phys. Rev. Lett. 123, 233401. doi:10.1103/PhysRevLett.123.233401.
- Kaneyasu, T., Hikosaka, Y., Fujimoto, M., Konomi, T., Katoh, M., Iwayama, H., Shigemasa, E., 2017. Limitations in photoionization of helium by an extreme ultraviolet optical vortex. Phys. Rev. A 95, 023413. doi:10.1103/PhysRevA.95.023413.
- Kang, H.S., Min, C.K., Heo, H., Kim, C., Yang, H., Kim, G., Nam, I., Baek, S.Y., Choi, H.J., Mun, G., Park, B.R., Suh, Y.J., Shin, D.C., Hu, J., Hong, J., Jung, S., Kim, S.H., Kim, K., Na, D., Park, S.S., Park, Y.J., Han, J.H., Jung, Y.G., Jeong, S.H., Lee, H.G., Lee, S., Lee, S., Lee, W.W., Oh, B., Suh, H.S., Parc, Y.W., Park, S.J., Kim, M.H., Jung, N.S., Kim, Y.C., Lee, M.S., Lee, B.H., Sung, C.W., Mok, I.S., Yang, J.M., Lee, C.S., Shin, H., Kim, J.H., Kim, Y., Lee, J.H., Park, S.Y., Kim, J., Park, J., Eom, I., Rah, S., Kim, S., Nam, K.H., Park, J., Park, J., Kim, S., Kwon, S., Park, S.H., Kim, K.S., Hyun, H., Kim, S.N., Kim, S., Hwang, S.m., Kim, M.J., Lim, C.y., Yu, C.J., Kim, B.S., Kang, T.H., Kim, K.W., Kim, S.H., Lee, H.S., Lee, H.S., Park, K.H., Koo, T.Y., Kim, D.E., Ko, I.S., 2017. Hard X-ray free-electron laser with femtosecond-scale timing jitter. Nat. Photonics 11, 708–713. doi:10.1038/s41566-017-0029-8.
- Karamatskou, A., Pabst, S., Chen, Y.J., Santra, R., 2014. Calculation of photoelectron spectra within the time-dependent configuration-interaction singles scheme. Phys. Rev. A 89, 033415. doi:10.1103/PhysRevA.89.033415.
- Karnakov, B.M., Mur, V.D., Popuzhenko, S.V., Popov, V.S., 2015. Current progress in developing the nonlinear ionization theory of atoms and ions. Physics-Uspekhi 58, 3–32. doi:10.3367/ufne.0185.201501b.0003.
- Kastirke, G., et al., 2020. Photoelectron diffraction imaging of a molecular breakup using an X-ray free-electron laser. Phys. Rev. X 10, 021052. URL: <https://journals.aps.org/prx/accepted/3e079K1fY5616308f3c282754576ab2113a3a587f>.
- Kato, T., Kono, H., 2004. Time-dependent multiconfiguration theory for electronic dynamics of molecules in an intense laser field. Chem. Phys. Lett. 392, 533–540. doi:10.1016/j.cpl.2004.05.106.

- Kazansky, A.K., Grigorieva, A.V., Kabachnik, N.M., 2011. Circular dichroism in laser-assisted short-pulse photoionization. *Phys. Rev. Lett.* 107, 253002. doi:10.1103/PhysRevLett.107.253002.
- Kazansky, A.K., Kabachnik, N.M., 2006. Calculations of the double differential cross section for attosecond laser-assisted photoionization of atoms. *J. Phys. B* 39, 5173–5186. doi:10.1088/0953-4075/39/24/014.
- Kazansky, A.K., Kabachnik, N.M., 2007. Theoretical description of atomic photoionization by an attosecond XUV pulse in a strong laser field: effects of rescattering and orbital polarization. *J. Phys. B* 40, 2163–2177. doi:10.1088/0953-4075/40/11/017.
- Kazansky, A.K., Sazhina, I.P., Kabachnik, N.M., 2010. Angle-resolved electron spectra in short-pulse two-color XUV+IR photoionization of atoms. *Phys. Rev. A* 82, 033420. doi:10.1103/PhysRevA.82.033420.
- Keldysh, L.V., 1965. Ionization in the field of a strong electromagnetic wave. *Sov. Phys. JETP* 20, 1307–1314. URL: <http://www.jetp.ac.ru/cgi-bin/e/index/e/20/5/p1307?a=list>.
- Kheifets, A.S., 2007. Sequential two-photon double ionization of noble gas atoms. *J. Phys. B* 40, F313–F318. doi:10.1088/0953-4075/40/22/F02.
- Khokhlova, M.A., Cooper, B., Ueda, K., Prince, K.C., Kolorenč, P., Ivanov, M.Y., Averbukh, V., 2019. Molecular Auger interferometry. *Phys. Rev. Lett.* 122, 233001. doi:10.1103/PhysRevLett.122.233001.
- Kim, K.J., Huang, Z., Lindberg, R., 2017. *Synchrotron Radiation and Free-Electron Lasers*. Cambridge University Press. doi:10.1017/9781316677377.
- Kleine, C., Ekimova, M., Goldsztejn, G., Raabe, S., Strüber, C., Ludwig, J., Yarlagadda, S., Eisebitt, S., Vrakking, M.J.J., Elsaesser, T., Nibbering, E.T.J., Rouzée, A., 2019. Soft X-ray absorption spectroscopy of aqueous solutions using a table-top femtosecond soft X-ray source. *J. Phys. Chem. Lett.* 10, 52–58. doi:10.1021/acs.jpcllett.8b03420.
- Kondratenko, A.M., Saldin, E.L., 1979. Generation of coherent radiation by relativistic electron beam in an undulator. *Dokl. Akad. Nauk SSSR* 249, 843–847. URL: <http://mi.mathnet.ru/dan43196>.
- Kondratenko, A.M., Saldin, E.L., 1980. Generation of coherent radiation by a relativistic electron beam in an undulator. *Part. Accel.* 10, 207–216. URL: <https://cds.cern.ch/record/1107977>.
- Kornilov, O., Eckstein, M., Rosenblatt, M., Schulz, C.P., Motomura, K., Rouzée, A., Klei, J., Foucar, L., Siano, M., Lübcke, A., Schapper, F., Johnsson, P., Holland, D.M.P., Schlathöler, T., Marchenko, T., Düsterer, S., Ueda, K., Vrakking, M.J.J., Frasinski, L.J., 2013. Coulomb explosion of diatomic molecules in intense XUV fields mapped by partial covariance. *J. Phys. B* 46, 164028. doi:10.1088/0953-4075/46/16/164028.
- Kosloff, R., Rice, S.A., Gaspard, P., Tersigni, S., Tannor, D.J., 1997. Wavepacket dancing: Achieving chemical sensitivity by shaping light pulses. *Chem. Phys.* 48, 601–641. doi:10.1016/0301-0104(89)90012-8.
- Kotur, M., Guénot, D., Jiménez-Galán, Á., Kroon, D., Larsen, E.W., Louisy, M., Bengtsson, S., Miranda, M., Mauritsson, J., Arnold, C.L., Canton, S.E., Gisselbrecht, M., Carette, T., Dahlström, J.M., Lindroth, E., Maquet, A., Argenti, L., Martín, F., L’Huillier, A., 2016. Spectral phase measurement of a Fano resonance using tunable attosecond pulses. *Nat. Commun.* 7, 10566. doi:10.1038/ncomms10566.
- Kowalewski, M., Bennett, K., Dorfman, K.E., Mukamel, S., 2015. Catching conical intersections in the act: Monitoring transient electronic coherences by attosecond stimulated x-ray Raman signals. *Phys. Rev. Lett.* 115, 193003. doi:10.1103/PhysRevLett.115.193003.
- Kowalewski, M., Fingerhut, B.P., Dorfman, K.E., Bennett, K., Mukamel, S., 2017. Simulating coherent multidimensional spectroscopy of nonadiabatic molecular processes: From the infrared to the X-ray regime. *Chem. Rev.* 117, 12165–12226. doi:10.1021/acs.chemrev.7b00081.
- Krasniqi, F., Najjari, B., Strüder, L., Rolles, D., Voitkiv, A., Ullrich, J., 2010. Imaging molecules from within: Ultrafast angstrom-scale structure determination of molecules via photoelectron holography using free-electron lasers. *Phys. Rev. A* 81, 033411. doi:10.1103/PhysRevA.81.033411.
- Krausz, F., Ivanov, M., 2009. Attosecond physics. *Rev. Mod. Phys.* 81, 163–234. doi:10.1103/RevModPhys.81.163.
- Kroll, T., Kern, J., Kubin, M., Ratner, D., Gul, S., Fuller, F.D., Löchel, H., Krzywinski, J., Lutman, A., Ding, Y., Dakovski, G.L., Moeller, S., Turner, J.J., Alonso-Mori, R., Nordlund, D.L., Rehanek, J., Weniger, C., Firsov, A., Brzhezinskaya, M., Chatterjee, R., Lassalle-Kaiser, B., Sierra, R.G., Laksmono, H., Hill, E., Borovik, A., Erko, A., Föhlisch, A., Mitzner, R., Yachandra, V.K., Yano, J., Wernet, P., Bergmann, U., 2016. X-ray absorption spectroscopy using a self-seeded soft X-ray free-electron laser. *Opt. Express* 24, 22469. doi:10.1364/oe.24.022469.
- Kulander, K.C., 1987. Multiphoton ionization of hydrogen: A time-dependent theory. *Phys. Rev. A* 35, 445–447. doi:10.1103/PhysRevA.35.445.
- Kuleff, A.I., Gokhberg, K., Kopelke, S., Cederbaum, L.S., 2010. Ultrafast interatomic electronic decay in multiply excited clusters. *Phys. Rev. Lett.* 105, 043004. doi:10.1103/PhysRevLett.105.043004.
- Kuleff, A.I., Kryzhevoi, N.V., Pernpointner, M., Cederbaum, L.S., 2016. Core ionization initiates subfemtosecond charge migration in the valence shell of molecules. *Phys. Rev. Lett.* 117, 093002. doi:10.1103/PhysRevLett.117.093002.
- Kumagai, Y., Fukuzawa, H., Motomura, K., Iablonskyi, D., Nagaya, K., Wada, S.i., Ito, Y., Takanashi, T., Sakakibara, Y., You, D., Nishiyama, T., Asa, K., Sato, Y., Umemoto, T., Kariyazono, K., Kukk, E., Kooser, K., Nicolas, C., Miron, C., Asavei, T., Neagu, L., Schöffler, M.S., Kastirke, G., Liu, X.j., Owada, S., Katayama, T., Togashi, T., Tono, K., Yabashi, M., Golubev, N.V., Gokhberg, K., Cederbaum, L.S., Kuleff, A.I., Ueda, K., 2018. Following the birth of a nanoplasma produced by an ultrashort hard-x-ray laser in xenon clusters. *Phys. Rev. X* 8, 031034. doi:10.1103/PhysRevX.8.031034.
- Kurka, M., Rudenko, A., Foucar, L., Kühnel, K.U., Jiang, Y.H., Ergler, T., Havermeier, T., Smolarski, M., Schössler, S., Cole, K., Schöffler, M., Dörner, R., Gensch, M., Düsterer, S., Treusch, R., Fritzsche, S., Grum-Grzhimailo, A.N., Gryzlova, E.V., Kabachnik, N.M., Schröter, C.D., Moshhammer, R., Ullrich, J., 2009. Two-photon double ionization of Ne by free-electron laser radiation: a kinematically complete experiment. *J. Phys. B* 42, 141002. doi:10.1088/0953-4075/42/14/141002.
- Kvaal, S., 2012. Ab initio quantum dynamics using coupled-cluster. *J. Chem. Phys.* 136, 194109. doi:10.1063/1.4718427.
- Lablanquie, P., Grozdanov, T.P., Žitnik, M., Carniato, S., Selles, P., Andric, L., Palaudoux, J., Penent, F., Iwayama, H., Shigemasa, E., Hikosaka, Y., Soejima, K., Nakano, M., Suzuki, I.H., Ito, K., 2011. Evidence of single-photon two-site core double ionization of C<sub>2</sub>H<sub>2</sub> molecules. *Phys. Rev. Lett.* 107, 193004. doi:10.1103/PhysRevLett.107.193004.
- LaForge, A.C., Drabbels, M., Brauer, N.B., Coreno, M., Devetta, M., Di Fraia, M., Finetti, P., Grazioli, C., Katzy, R., Lyamayev, V., Mazza, T., Mudrich, M., O’Keeffe, P., Ovcharenko, Y., Piseri, P., Plekan, O., Prince, K.C., Richter, R., Stranges, S., Callegari, C., Möller, T., Stienkemeier,

- F., 2014. Collective autoionization in multiply-excited systems: A novel ionization process observed in helium nanodroplets. *Sci. Rep.* 4, 3621. doi:10.1038/srep03621.
- Lam, R.K., Raj, S.L., Pascal, T.A., Pemmaraju, C.D., Foglia, L., Simoncig, A., Fabris, N., Miotti, P., Hull, C.J., Rizzuto, A.M., Smith, J.W., Mincigrucci, R., Masciovecchio, C., Gessini, A., Allaria, E., De Ninno, G., Diviacco, B., Roussel, E., Spampinati, S., Penco, G., Di Mitri, S., Trovò, M., Danailov, M., Christensen, S.T., Sokaras, D., Weng, T.C., Coreno, M., Poletto, L., Drisdell, W.S., Prendergast, D., Giannessi, L., Principi, E., Nordlund, D., Saykally, R.J., Schwartz, C.P., 2018. Soft X-ray second harmonic generation as an interfacial probe. *Phys. Rev. Lett.* 120, 023901. doi:10.1103/PhysRevLett.120.023901.
- Lambropoulos, P., Maragakis, P., Zhang, J., 1998. Two-electron atoms in strong fields. *Phys. Rep.* 305, 203–293. doi:10.1016/s0370-1573(98)00027-1.
- Lambropoulos, P., Nikolopoulos, G.M., 2013. Multiple ionization under strong XUV to X-ray radiation. *Eur. Phys. J. Special Topics* 222, 2067–2084. doi:10.1140/epjst/e2013-01987-7.
- Lambropoulos, P., Petrosyan, D., 2007. *Fundamentals of Quantum Optics and Quantum Information*. Springer, Berlin Heidelberg. doi:10.1007/978-3-540-34572-5.
- Leitner, T., Josefsson, I., Mazza, T., Miedema, P.S., Schröder, H., Beye, M., Kunnus, K., Schreck, S., Düsterer, S., Föhlisch, A., Meyer, M., Odelius, M., Wernet, P., 2018. Time-resolved electron spectroscopy for chemical analysis of photodissociation: Photoelectron spectra of Fe(CO)<sub>5</sub>, Fe(CO)<sub>4</sub>, and Fe(CO)<sub>3</sub>. *J. Chem. Phys.* 149, 044307. doi:10.1063/1.5035149.
- Lewenstein, M., Balcou, P., Ivanov, M.Y., L’Huillier, A., Corkum, P.B., 1994. Theory of high-harmonic generation by low-frequency laser fields. *Phys. Rev. A* 49, 2117–2132. doi:10.1103/PhysRevA.49.2117.
- Li, S., Guo, Z., Coffee, R.N., Hegazy, K., Huang, Z., Natan, A., Osipov, T., Ray, D., Marinelli, A., Cryan, J.P., 2018. Characterizing isolated attosecond pulses with angular streaking. *Opt. Express* 26, 4531–4547. doi:10.1364/OE.26.004531.
- Li, Z., El-Amine Madjet, M., Vendrell, O., Santra, R., 2014. Core-level transient absorption spectroscopy as a probe of electron hole relaxation in photoionized H<sup>+</sup>(H<sub>2</sub>O)<sub>*n*</sub>. *Faraday Discuss.* 171, 457–470. doi:10.1039/c4fd00078a.
- Liekhus-Schmaltz, C.E., Tenney, I., Osipov, T., Sanchez-Gonzalez, A., Berrah, N., Boll, R., Bomme, C., Bostedt, C., Bozek, J.D., Carron, S., Coffee, R., Devin, J., Erk, B., Ferguson, K.R., Field, R.W., Foucar, L., Frasiniski, L.J., Glowina, J.M., Gühr, M., Kamalov, A., Krzywinski, J., Li, H., Marangos, J.P., Martinez, T.J., McFarland, B.K., Miyabe, S., Murphy, B., Natan, A., Rolles, D., Rudenko, A., Siano, M., Simpson, E.R., Spector, L., Swiggers, M., Walke, D., Wang, S., Weber, T., Bucksbaum, P.H., Petrovic, V.S., 2015. Ultrafast isomerization initiated by X-ray core ionization. *Nat. Commun.* 6, 8199. doi:10.1038/ncoms9199.
- Liu, J.C., Berrah, N., Cederbaum, L.S., Cryan, J.P., Glowina, J.M., Schafer, K.J., Buth, C., 2016. Rate equations for nitrogen molecules in ultrashort and intense x-ray pulses. *J. Phys. B* 49, 075602. doi:10.1088/0953-4075/49/7/075602.
- Liu, J.C., Miron, C., Ågren, H., Polyutov, S., Gel’mukhanov, F., 2019. Resonant x-ray second-harmonic generation in atomic gases. *Phys. Rev. A* 100, 063403. doi:10.1103/PhysRevA.100.063403.
- López-Martens, R., Varjú, K., Johnsson, P., Mauritsson, J., Mairesse, Y., Salières, P., Gaarde, M.B., Schafer, K.J., Persson, A., Svanberg, S., Wahlström, C.G., L’Huillier, A., 2005. Amplitude and phase control of attosecond light pulses. *Phys. Rev. Lett.* 94, 033001. doi:10.1103/PhysRevLett.94.033001.
- Lorenz, U., Kabachnik, N.M., Weckert, E., Vartanyants, I.A., 2012. Impact of ultrafast electronic damage in single-particle x-ray imaging experiments. *Phys. Rev. E* 86, 051911. doi:10.1103/PhysRevE.86.051911.
- Lucchese, R.R., McKoy, V., 1983. Padé-approximant corrections to general variational expressions of scattering theory: Application to 5σ photoionization of carbon monoxide. *Phys. Rev. A* 28, 1382–1394. doi:10.1103/PhysRevA.28.1382.
- Lunin, V.Y., Grum-Grzhimailo, A.N., Gryzlova, E.V., Sinityn, D.O., Petrova, T.E., Lunina, N.L., Balabaev, N.K., Tereshkina, K.B., Stepanov, A.S., Krupnyanski, Y.F., 2015. Efficient calculation of diffracted intensities in the case of nonstationary scattering by biological macromolecules under XFEL pulses. *Acta Cryst. D* 71, 293–303. doi:10.1107/S1399004714025450.
- Lysaght, M.A., Burke, P.G., van der Hart, H.W., 2008. Ultrafast laser-driven excitation dynamics in Ne: An *ab initio* time-dependent R-matrix approach. *Phys. Rev. Lett.* 101, 253001. doi:10.1103/PhysRevLett.101.253001.
- Lysaght, M.A., van der Hart, H.W., Burke, P.G., 2009. Time-dependent R-matrix theory for ultrafast atomic processes. *Phys. Rev. A* 79, 053411. doi:10.1103/PhysRevA.79.053411.
- Ma, R., Motomura, K., Ishikawa, K.L., Mondal, S., Fukuzawa, H., Yamada, A., Ueda, K., Nagaya, K., Yase, S., Mizoguchi, Y., Yao, M., Rouze, A., Hundermark, A., Vrakking, M.J.J., Johnsson, P., Nagasono, M., Tono, K., Togashi, T., Senba, Y., Ohashi, H., Yabashi, M., Ishikawa, T., 2013. Photoelectron angular distributions for the two-photon ionization of helium by ultrashort extreme ultraviolet free-electron laser pulses. *J. Phys. B* 46, 164018. doi:10.1088/0953-4075/46/16/164018.
- Machado, A.M., Masili, M., 2004. Variationally stable calculations for molecular systems: Polarizabilities and two-photon ionization cross section for the hydrogen molecule. *J. Chem. Phys.* 120, 7505–7511. doi:10.1063/1.1687677.
- Madden, R.P., Codling, K., 1963. New autoionizing atomic energy levels in He, Ne, and Ar. *Phys. Rev. Lett.* 10, 516–518. doi:10.1103/PhysRevLett.10.516.
- Madden, R.P., Ederer, D.L., Codling, K., 1969. Resonances in the photo-ionization continuum of Ar I (20–150 eV). *Phys. Rev.* 177, 136–151. doi:10.1103/PhysRev.177.136.
- Madey, J.M.J., 1971. Stimulated emission of Bremsstrahlung in a periodic magnetic field. *J. Appl. Phys.* 42, 1906–1913. doi:10.1063/1.1660466.
- Madey, J.M.J., 2014. Wilson prize article: From vacuum tubes to lasers and back again. *Phys. Rev. ST Accel. Beams* 17, 074901. doi:10.1103/PhysRevSTAB.17.074901.
- Madey, J.M.J., Schwettman, H.A., Fairbank, W.M., 1973. A free electron laser. *IEEE Trans. Nucl. Sci.* 20, 980–983. doi:10.1109/tns.1973.4327304.
- Maeda, K., Ueda, K., Ito, K., 1993. High-resolution measurement for photoabsorption cross sections in the autoionization regions of Ar, Kr and Xe. *J. Phys. B* 26, 1541–1555. doi:10.1088/0953-4075/26/9/003.
- Maiman, T.H., 1960. Stimulated optical radiation in ruby. *Nature* 187, 493–494. doi:10.1038/187493a0.
- Makris, M.G., Lambropoulos, P., Mihelič, A., 2009. Theory of multiphoton multielectron ionization of xenon under strong 93-eV radiation. *Phys. Rev. Lett.* 102, 033002. doi:10.1103/PhysRevLett.102.033002.

- Manakov, N.L., Ovsiannikov, V.D., Rapoport, L.P., 1986. Atoms in a laser field. *Phys. Rep.* 141, 320–433. doi:10.1016/s0370-1573(86)80001-1.
- Maquet, A., Caillat, J., Taïeb, R., 2004. Attosecond delays in photoionization: time and quantum mechanics. *J. Phys. B* 47, 204004. doi:10.1088/0953-4075/47/20/204004.
- Maquet, A., Taïeb, R., 2007. Two-colour IR+XUV spectroscopies: the “soft-photon approximation”. *J. Mod. Opt.* 54, 1847–1857. doi:10.1080/09500340701306751.
- Maquet, A., Vénier, V., Marian, T.A., 1998. The Coulomb Green’s function and multiphoton calculations. *J. Phys. B* 31, 3743–3764. doi:10.1088/0953-4075/31/17/004.
- Marcus, G., Fawley, W.M., Bohler, D., Ding, Y., Feng, Y., Hemsing, E., Huang, Z., Krzywinski, J., Lutman, A., Ratner, D., 2019. Experimental observations of seed growth and accompanying pedestal contamination in a self-seeded, soft x-ray free-electron laser. *Phys. Rev. Accel. Beams* 22, 080702. doi:10.1103/PhysRevAccelBeams.22.080702.
- Maroju, P.K., Grazioli, C., Di Fraia, M., Moiola, M., Ertel, D., Ahmadi, H., Plekan, O., Finetti, P., Allaria, E., Giannessi, L., De Ninno, G., Spezzani, C., Penco, G., Spampinati, S., Demidovich, A., Danailov, M.B., Borghes, R., Kourousias, G., Sanches Dos Reis, C.E., BillÅl, F., Lutman, A.A., Squibb, R.J., Feifel, R., Carpeggiani, P., Reduzzi, M., Mazza, T., Meyer, M., Bengtsson, S., Ibrakovic, N., Simpson, E.R., Mauritsson, J., Csizmadia, T., Dumergue, M., Kühn, S., Nandiga Gopalakrishna, H., You, D., Ueda, K., Labeye, M., Bækhoj, J.E., Schafer, K.J., Gryzlova, E.V., Grum-Grzhimailo, A.N., Prince, K.C., Callegari, C., Sansone, G., 2020. Attosecond pulse shaping using a seeded free-electron laser. *Nature* 578, 386–391. doi:10.1038/s41586-020-2005-6.
- Martín, F., 1999. Ionization and dissociation using B-splines: photoionization of the hydrogen molecule. *J. Phys. B* 32, R197–R231. doi:10.1088/0953-4075/32/16/201.
- Masuda, T., Yoshimi, A., Fujieda, A., Fujimoto, H., Haba, H., Hara, H., Hiraki, T., Kaino, H., Kasamatsu, Y., Kitao, S., Konashi, K., Miyamoto, Y., Okai, K., Okubo, S., Sasao, N., Seto, M., Schumm, T., Shigekawa, Y., Suzuki, K., Stellmer, S., Tamasaku, K., Uetake, S., Watanabe, M., Watanabe, T., Yasuda, Y., Yamaguchi, A., Yoda, Y., Yokokita, T., Yoshimura, M., Yoshimura, K., 2019. X-ray pumping of the <sup>229</sup>Th nuclear clock isomer. *Nature* 573, 238–242. doi:10.1038/s41586-019-1542-3.
- Matthews, D.L., Hagelstein, P.L., Rosen, M.D., Eckart, M.J., Ceglio, N.M., Hazi, A.U., Medeck, H., MacGowan, B.J., Trebes, J.E., Whitten, B.L., Campbell, E.M., Hatcher, C.W., Hawryluk, A.M., Kauffman, R.L., Pleasance, L.D., Rambach, G., Scofield, J.H., Stone, G., Weaver, T.A., 1985. Demonstration of a soft X-ray amplifier. *Phys. Rev. Lett.* 54, 110–113. doi:10.1103/physrevlett.54.110.
- Mazza, T., Gryzlova, E.V., Grum-Grzhimailo, A.N., Kazansky, A.K., Kabachnik, N.M., Meyer, M., 2015a. Dichroism in the photoionisation of atoms at XUV free-electron lasers. *J. Electr. Spectr. Rel. Phenom.* 204, 313–321. doi:10.1016/j.elspec.2015.08.011.
- Mazza, T., Ilchen, M., Rafipoor, A.J., Callegari, C., Finetti, P., Plekan, O., Prince, K.C., Richter, R., Danailov, M.B., Demidovich, A., De Ninno, G., Grazioli, C., Ivanov, R., Mahne, N., Raimondi, L., Svetina, C., Avaldi, L., Bolognesi, P., Coreno, M., O’Keeffe, P., Di Fraia, M., Devetta, M., Ovcharenko, Y., Möller, T., Lyamayev, V., Stienkemeier, F., Düsterer, S., Ueda, K., Costello, J.T., Kazansky, A.K., Kabachnik, N.M., Meyer, M., 2014. Determining the polarization state of an extreme ultraviolet free-electron laser beam using atomic circular dichroism. *Nat. Commun.* 5, 3648. doi:10.1038/ncomms4648.
- Mazza, T., Ilchen, M., Rafipoor, A.J., Callegari, C., Finetti, P., Plekan, O., Prince, K.C., Richter, R., Demidovich, A., Grazioli, C., Avaldi, L., Bolognesi, P., Coreno, M., O’Keeffe, P., Di Fraia, M., Devetta, M., Ovcharenko, Y., Lyamayev, V., Düsterer, S., Ueda, K., Costello, J.T., Gryzlova, E.V., Strakhova, S.I., Grum-Grzhimailo, A.N., Bozhevolnov, A.V., Kazansky, A.K., Kabachnik, N.M., Meyer, M., 2016. Angular distribution and circular dichroism in the two-colour XUV + NIR above-threshold ionization of helium. *J. Mod. Opt.* 63, 367–382. doi:10.1080/09500340.2015.1119897.
- Mazza, T., Karamatskou, A., Ilchen, M., Bakhtiarzadeh, S., Rafipoor, A.J., O’Keeffe, P., Kelly, T.J., Walsh, N., Costello, J.T., Meyer, M., Santra, R., 2015b. Sensitivity of nonlinear photoionization to resonance substructure in collective excitation. *Nat. Commun.* 6, 6799. doi:10.1038/ncomms7799.
- Meister, S., Lindenblatt, H., Trost, F., Schnorr, K., Augustin, S., Braune, M., Treusch, R., Pfeifer, T., Moshhammer, R., 2020. Atomic, molecular and cluster science with the reaction microscope endstation at FLASH2. *Appl. Sci.* 10, 2953. doi:10.3390/app10082953.
- Mercouris, T., Komninos, Y., Dionissopoulou, S., Nicolaides, C.A., 1994. Computation of strong-field multiphoton processes in polyelectronic atoms: State-specific method and applications to H and Li<sup>-</sup>. *Phys. Rev. A* 50, 4109–4121. doi:10.1103/PhysRevA.50.4109.
- Mercouris, T., Komninos, Y., Nicolaides, C.A., 2010. The state-specific expansion approach to the solution of the polyelectronic time-dependent Schrödinger equation for atoms and molecules in unstable states, in: Nicolaides, C.A., Brändas, E. (Eds.), *Unstable States in the Continuous Spectra, Part I: Analysis, Concepts, Methods, and Results*. Academic Press. volume 60 of *Advances in Quantum Chemistry*. chapter 6, pp. 333–405. doi:10.1016/s0065-3276(10)60006-8.
- Mercouris, T., Komninos, Y., Nicolaides, C.A., 2016. EUV two-photon-ionization cross sections of helium from the solution of the time-dependent Schrödinger equation, and comparison with measurements using free-electron lasers. *Phys. Rev. A* 94, 063406. doi:10.1103/PhysRevA.94.063406.
- Meyer, M., Costello, J.T., Düsterer, S., Li, W.B., Radcliffe, P., 2010. Two-colour experiments in the gas phase. *J. Phys. B* 43, 194006. doi:10.1088/0953-4075/43/19/194006.
- Meyer, M., Cubaynes, D., O’Keeffe, P., Luna, H., Yeates, P., Kennedy, E.T., Costello, J.T., Orr, P., Taïeb, R., Maquet, A., Düsterer, S., Radcliffe, P., Redlin, H., Azima, A., Plönjes, E., Feldhaus, J., 2006. Two-color photoionization in xuv free-electron and visible laser fields. *Phys. Rev. A* 74, 011401. doi:10.1103/PhysRevA.74.011401.
- Meyer, M., Radcliffe, P., Tschentscher, T., Costello, J.T., Cavalieri, A.L., Grguras, I., Maier, A.R., Kienberger, R., Bozek, J., Bostedt, C., Schorb, S., Coffee, R., Messerschmidt, M., Roedig, C., Sistrunk, E., Di Mauro, L.F., Doumy, G., Ueda, K., Wada, S., Düsterer, S., Kazansky, A.K., Kabachnik, N.M., 2012. Angle-resolved electron spectroscopy of laser-assisted Auger decay induced by a few-femtosecond X-ray pulse. *Phys. Rev. Lett.* 108, 063007. doi:10.1103/PhysRevLett.108.063007.
- Miao, J., Ishikawa, T., Robinson, I.K., Murnane, M.M., 2015. Beyond crystallography: Diffractive imaging using coherent x-ray light sources. *Science* 348, 530–535. doi:10.1126/science.aaa1394.
- Middleton, D., Nikolopoulos, L., 2012. Effects of autoionising states on the single and double ionisation yields of neon with soft X-ray fields. *J. Mod. Optics* 59, 1653–1663. doi:10.1080/09500340.2012.737481.

- Milne, C., Schietinger, T., Aiba, M., Alarcon, A., Alex, J., Anghel, A., Arsov, V., Beard, C., Beaud, P., Bettoni, S., Bopp, M., Brands, H., Brönnimann, M., Brunnenkant, I., Calvi, M., Citterio, A., Craievich, P., Csatari Divall, M., Dällenbach, M., D'Amico, M., Dax, A., Deng, Y., Dietrich, A., Dinapoli, R., Divall, E., Dordevic, S., Ebner, S., Emy, C., Fitze, H., Flechsig, U., Follath, R., Frei, F., Gärtner, F., Ganter, R., Garvey, T., Geng, Z., Gorgisyan, I., Gough, C., Hauff, A., Hauri, C., Hiller, N., Humar, T., Hunziker, S., Ingold, G., Ischebeck, R., Janousch, M., Juranic, P., Jurcevic, M., Kaiser, M., Kalantari, B., Kalt, R., Keil, B., Kittel, C., Knopp, G., Koprek, W., Lemke, H., Lippuner, T., Llorente Sancho, D., Löhl, F., Lopez-Cuenca, C., Märki, F., Marcellini, F., Marinkovic, G., Martiel, I., Menzel, R., Mozzanica, A., Nass, K., Orlandi, G., Ozkan Loch, C., Panepucci, E., Paraliiev, M., Patterson, B., Pedrini, B., Pedrozzi, M., Pollet, P., Pradervand, C., Prat, E., Radi, P., Raguin, J.Y., Redford, S., Rehanek, J., Réhault, J., Reiche, S., Ringele, M., Rittmann, J., Rivkin, L., Romann, A., Ruat, M., Ruder, C., Sala, L., Schebacher, L., Schilcher, T., Schlott, V., Schmidt, T., Schmitt, B., Shi, X., Stadler, M., Stingelin, L., Sturzenegger, W., Szlachetko, J., Thattil, D., Treyer, D., Trisorio, A., Tron, W., Vetter, S., Vicario, C., Voulot, D., Wang, M., Zamofing, T., Zellweger, C., Zennaro, R., Zimoch, E., Abela, R., Patthey, L., Braun, H.H., 2017. SwissFEL: The swiss X-ray free electron laser. *Appl. Sci.* 7, 720. doi:10.3390/app7070720.
- Milton, S.V., Gluskin, E., Arnold, N.D., Benson, C., Berg, W., Biedron, S.G., Borland, M., Chae, Y.C., Dejus, R.J., Den Hartog, P.K., Deriy, B., Erdmann, M., Eidelman, Y.I., Hahne, M.W., Huang, Z., Kim, K.J., Lewellen, J.W., Li, Y., Lumpkin, A.H., Makarov, O., Moog, E.R., Nassiri, A., Sajaev, V., Soliday, R., Tieman, B.J., Trakhtenberg, E.M., Travish, G., Vasserman, I.B., Vinokurov, N.A., Wang, X.J., Wiemerslage, G., Yang, B.X., 2001. Exponential gain and saturation of a self-amplified spontaneous emission free-electron laser. *Science* 292, 2037–2041. doi:10.1126/science.1059955.
- Milton, S.V., Gluskin, E., Biedron, S.G., Dejus, R.J., Den Hartog, P.K., Galayda, J.N., Kim, K.J., Lewellen, J.W., Moog, E.R., Sajaev, V., Sereno, N.S., Travish, G., Vinokurov, N.A., Arnold, N.D., Benson, C., Berg, W., Biggs, J.A., Borland, M., Carwardine, J.A., Chae, Y.C., Decker, G., Deriy, B.N., Erdmann, M.J., Friedsam, H., Gold, C., Grelick, A.E., Hahne, M.W., Harkay, K.C., Huang, Z., Lessner, E.S., Lill, R.M., Lumpkin, A.H., Makarov, O.A., Markovich, G.M., Meyer, D., Nassiri, A., Noonan, J.R., Pasky, S.J., Pile, G., Smith, T.L., Soliday, R., Tieman, B.J., Trakhtenberg, E.M., Trento, G.F., Vasserman, I.B., Walters, D.R., Wang, X.J., Wiemerslage, G., Xu, S., Yang, B.X., 2000. Observation of self-amplified spontaneous emission and exponential growth at 530 nm. *Phys. Rev. Lett.* 85, 988–991. doi:10.1103/PhysRevLett.85.988.
- Min, C.K., Nam, I., Yang, H., Kim, G., Shim, C.H., Ko, J.H., Cho, M.H., Heo, H., Oh, B., Suh, Y.J., Kim, M.J., Na, D., Kim, C., Kim, Y., Chun, S.H., Lee, J.H., Kim, J., Kim, S., Eom, I., Kim, S.N., Koo, T.Y., Rah, S., Shvyd'ko, Y., Shu, D., Kim, K.J., Terentyev, S., Blank, V., Kang, H.S., 2019. Hard x-ray self-seeding commissioning at PAL-XFEL. *J. Synchrotron Radiat.* 26, 1101–1109. doi:10.1107/s1600577519005460.
- Minemoto, S., Teramoto, T., Akagi, H., Fujikawa, T., Majima, T., Nakajima, K., Niki, K., Owada, S., Sakai, H., Togashi, T., Tono, K., Tsuru, S., Wada, K., Yabashi, M., Yoshida, S., Yagishita, A., 2016. Structure determination of molecules in an alignment laser field by femtosecond photoelectron diffraction using an X-ray free-electron laser. *Sci. Rep.* 6, 38654. doi:10.1038/srep38654.
- Miyagi, H., Madsen, L.B., 2013. Time-dependent restricted-active-space self-consistent-field theory for laser-driven many-electron dynamics. *Phys. Rev. A* 87, 062511. doi:10.1103/PhysRevA.87.062511.
- Miyauchi, N., Adachi, J., Yagishita, A., Sako, T., Koike, F., Sato, T., Iwasaki, A., Okino, T., Yamanouchi, K., Midorikawa, K., Yamakawa, K., Kannari, F., Nakano, H., Nagasono, M., Tono, K., Yabashi, M., Ishikawa, T., Togashi, T., Ohashi, H., Kimura, H., Senba, Y., 2011. Three-photon double ionization of Ar studied by photoelectron spectroscopy using an extreme ultraviolet free-electron laser: manifestation of resonance states of an intermediate Ar<sup>+</sup> ion. *J. Phys. B* 44, 071001. doi:10.1088/0953-4075/44/7/071001.
- Moler, C., Van Loan, C., 2003. Nineteen dubious ways to compute the exponential of a matrix, twenty five years later. *SIAM Review* 45, 3–49. doi:10.1137/S00361445024180.
- Mondal, S., Fukuzawa, H., Motomura, K., Tachibana, T., Nagaya, K., Sakai, T., Matsunami, K., Yase, S., Yao, M., Wada, S., Hayashita, H., Saito, N., Callegari, C., Prince, K.C., Miron, C., Nagasono, M., Togashi, T., Yabashi, M., Ishikawa, K.L., Kazansky, A.K., Kabachnik, N.M., Ueda, K., 2014. Pulse-delay effects in the angular distribution of near-threshold EUV + IR two-photon ionization of Ne. *Phys. Rev. A* 89, 013415. doi:10.1103/PhysRevA.89.013415.
- Mondal, S., Fukuzawa, H., Motomura, K., Tachibana, T., Nagaya, K., Sakai, T., Matsunami, K., Yase, S., Yao, M., Wada, S., Hayashita, H., Saito, N., Callegari, C., Prince, K.C., O'Keeffe, P., Bolognesi, P., Avaldi, L., Miron, C., Nagasono, M., Togashi, T., Yabashi, M., Ishikawa, K.L., Sazhina, I.P., Kazansky, A.K., Kabachnik, N.M., Ueda, K., 2013. Photoelectron angular distributions in infrared one-photon and two-photon ionization of FEL-pumped Rydberg states of helium. *J. Phys. B* 46, 205601. doi:10.1088/0953-4075/46/20/205601.
- Moore, L.R., Lysaght, M.A., Nikolopoulos, L.A.A., Parker, J.S., van der Hart, H.W., Taylor, K.T., 2011. The RMT method for many-electron atomic systems in intense short-pulse laser light. *J. Mod. Opt.* 58, 1132–1140. doi:10.1080/09500340.2011.559315.
- Motomura, K., Fukuzawa, H., Foucar, L., Liu, X.J., Prümper, G., Ueda, K., Saito, N., Iwayama, H., Nagaya, K., Murakami, H., Yao, M., Belkacem, A., Nagasono, M., Higashiya, A., Yabashi, M., Ishikawa, T., Ohashi, H., Kimura, H., 2009. Multiple ionization of atomic argon irradiated by EUV free-electron laser pulses at 62 nm: evidence of sequential electron strip. *J. Phys. B* 42, 221003. doi:10.1088/0953-4075/42/22/221003.
- Motz, H., 1951. Applications of the radiation from fast electron beams. *J. Appl. Phys.* 22, 527–535. doi:10.1063/1.1700002.
- Motz, H., Thon, W., Whitehurst, R.N., 1953. Experiments on radiation by fast electron beams. *J. Appl. Phys.* 24, 826–833. doi:10.1063/1.1721389.
- Mourou, G., 2019. Nobel lecture: Extreme light physics and application. *Rev. Mod. Phys.* 91, 030501. doi:10.1103/RevModPhys.91.030501.
- Mudrich, M., LaForge, A.C., Ciavardini, A., O'Keeffe, P., Callegari, C., Coreno, M., Demidovich, A., Devetta, M., Di Fraia, M., Drabbels, M., Finetti, P., Gessner, O., Grazioli, C., Hernando, A., Neumark, D.M., Ovcharenko, Y., Piseri, P., Plekan, O., Prince, K.C., Richter, R., Ziemkiewicz, M.P., Möller, T., Eloranta, J., Pi, M., Barranco, M., Stienkemeier, F., 2020. Ultrafast relaxation of photoexcited superfluid He nanodroplets. *Nat. Commun.* 11, 112. doi:10.1038/s41467-019-13681-6.
- Mukamel, S., Abramavicius, D., Yang, L., Zhuang, W., Schweigert, I.V., Voronine, D.V., 2009. Coherent multidimensional optical probes for electron correlations and exciton dynamics: From NMR to x-rays. *Acc. Chem. Res.* 42, 553–562. doi:10.1021/ar800258z.
- Müller, A.D., Artemyev, A.N., Demekhin, P.V., 2018. Photoelectron circular dichroism in the multiphoton ionization by short laser pulses. II. Three- and four-photon ionization of fenchone and camphor. *J. Chem. Phys.* 148, 214307. doi:10.1063/1.5032295.
- Muller, H.G., 2002. Reconstruction of attosecond harmonic beating by interference of two-photon transitions. *Appl. Phys. B* 74, s17–s21. doi:10.1007/s00340-002-0894-8.
- Murphy, J.B., Pellegrini, C., 1985. Free electron lasers for the XUV spectral region. *Nucl. Instrum. Methods Phys. Res. A* 237, 159–167.

- doi:10.1016/0168-9002(85)90344-4.
- Nagasono, M., Harries, J.R., Iwayama, H., Togashi, T., Tono, K., Yabashi, M., Senba, Y., Ohashi, H., Ishikawa, T., Shigemasa, E., 2011. Observation of free-electron-laser-induced collective spontaneous emission (superfluorescence). *Phys. Rev. Lett.* 107, 193603. doi:10.1103/PhysRevLett.107.193603.
- Nagaya, K., Iablonskyi, D., Golubev, N.V., Matsunami, K., Fukuzawa, H., Motomura, K., Nishiyama, T., Sakai, T., Tachibana, T., Mondal, S., Wada, S., Prince, K.C., Callegari, C., Miron, C., Saito, N., Yabashi, M., Demekhin, P.V., Cederbaum, L.S., Kuleff, A.I., Yao, M., Ueda, K., 2016. Interatomic Coulombic decay cascades in multiply excited neon clusters. *Nat. Commun.* 7, 13477. doi:10.1038/ncomms13477.
- Nakajima, T., Nikolopoulos, L.A.A., 2002. Use of helium double ionization for autocorrelation of an xuv pulse. *Phys. Rev. A* 66, 041402R. doi:10.1103/PhysRevA.66.041402.
- Nayak, A., Orfanos, I., Makos, I., Dumergue, M., Kühn, S., Skantzakakis, E., Bodi, B., Varju, K., Kalpouzos, C., Banks, H.I.B., Emmanouilidou, A., Charalambidis, D., Tzallas, P., 2018. Multiple ionization of argon via multi-XUV-photon absorption induced by 20-GW high-order harmonic laser pulses. *Phys. Rev. A* 98, 023426. doi:10.1103/physreva.98.023426.
- Nest, M., 2009. The multi-configuration electron-nuclear dynamics method. *Chem. Phys. Lett.* 472, 171–174. doi:10.1016/j.cpllett.2009.03.013.
- Nikolopoulos, G.M., Lambropoulos, P., 2015. Resonantly enhanced multiphoton ionization under XUV FEL radiation: a case study of the role of harmonics. *J. Phys. B: At. Mol. Opt. Phys.* 48, 244006. doi:10.1088/0953-4075/48/24/244006.
- Nikolopoulos, L.A.A., 2013. Time-dependent theory of angular correlations in sequential double ionization. *Phys. Rev. Lett.* 111, 093001. doi:10.1103/PhysRevLett.111.093001.
- Nikolopoulos, L.A.A., Kelly, T.J., Costello, J.T., 2011. Theory of ac Stark splitting in core-resonant Auger decay in strong x-ray fields. *Phys. Rev. A* 84, 063419. doi:10.1103/PhysRevA.84.063419.
- Nikolopoulos, L.A.A., Parker, J.S., Taylor, K.T., 2008. Combined R-matrix eigenstate basis set and finite-difference propagation method for the time-dependent Schrödinger equation: The one-electron case. *Phys. Rev. A* 78, 063420. doi:10.1103/PhysRevA.78.063420.
- Nishiyama, T., Kumagai, Y., Niozu, A., Fukuzawa, H., Motomura, K., Bucher, M., Ito, Y., Takanashi, T., Asa, K., Sato, Y., You, D., Li, Y., Ono, T., Kukk, E., Miron, C., Neagu, L., Callegari, C., Di Fraia, M., Rossi, G., Galli, D.E., Pincelli, T., Colombo, A., Kameshima, T., Joti, Y., Hatsui, T., Owada, S., Katayama, T., Togashi, T., Tono, K., Yabashi, M., Matsuda, K., Bostedt, C., Nagaya, K., Ueda, K., 2019. Ultrafast structural dynamics of nanoparticles in intense laser fields. *Phys. Rev. Lett.* 123, 123201. doi:10.1103/PhysRevLett.123.123201.
- nuClock, 2015. The project nuClock. URL: [www.nuclock.eu](http://www.nuclock.eu). Accessed May 26, 2020.
- Ó Broin, C., Nikolopoulos, L.A.A., 2015. R-matrix-incorporating-time method for  $H_2^+$  in short and intense laser fields. *Phys. Rev. A* 92, 063428. doi:10.1103/PhysRevA.92.063428.
- Ó Broin, C., Nikolopoulos, L.A.A., 2017. R-matrix-incorporating-time theory of one-electron atomic and molecular systems in intense laser fields. *J. Phys. B* 50, 033001. doi:10.1088/1361-6455/aa51a5.
- Oberli, S., González-Vázquez, J., Rodríguez-Perelló, E., Sodupe, M., Martín, F., Picón, A., 2019. Site-selective-induced isomerization of formamide. *Phys. Chem. Chem. Phys.* 21, 25626–25634. doi:10.1039/c9cp04441h.
- Ohmori, K., Katsuki, H., Chiba, H., Honda, M., Hagihara, Y., Fujiwara, K., Sato, Y., Ueda, K., 2006. Real-time observation of phase-controlled molecular wave-packet interference. *Phys. Rev. Lett.* 96, 093002. doi:10.1103/PhysRevLett.96.093002.
- O’Keeffe, P., Feyer, V., Bolognesi, P., Coreno, M., Callegari, C., Cautero, G., Moise, A., Prince, K.C., Richter, R., Sergio, R., Alagia, M., de Simone, M., Kivimäki, A., Devetta, M., Mazza, T., Piseri, P., Lyamayev, V., Katzy, R., Stienkemeier, F., Ovcharenko, Y., Möller, T., Avaldi, L., 2012. A velocity map imaging apparatus for gas phase studies at FERMI@Elettra. *Nucl. Instrum. Methods Phys. Res. B* 284, 69–73. doi:10.1016/j.nimb.2011.07.020.
- O’Keeffe, P., Mihelič, A., Bolognesi, P., Žitnik, M., Moise, A., Richter, R., Avaldi, L., 2013. Near-threshold photoelectron angular distributions from two-photon resonant photoionization of He. *New J. Phys.* 15, 013023. doi:10.1088/1367-2630/15/1/013023.
- Omiste, J.J., Madsen, L.B., 2019. Effects of core space and excitation levels on ground-state correlation and photoionization dynamics of Be and Ne. *J. Chem. Phys.* 150, 084305. doi:10.1063/1.5082940.
- Orimo, Y., Sato, T., Ishikawa, K.L., 2019. Application of the time-dependent surface flux method to the time-dependent multiconfiguration self-consistent-field method. *Phys. Rev. A* 100, 013419. doi:10.1103/PhysRevA.100.013419.
- Orimo, Y., Sato, T., Scrinzi, A., Ishikawa, K.L., 2018. Implementation of the infinite-range exterior complex scaling to the time-dependent complete-active-space self-consistent-field method. *Phys. Rev. A* 97, 023423. doi:10.1103/PhysRevA.97.023423.
- Ott, C., Kaldun, A., Argenti, L., Raith, P., Meyer, K., Laux, M., Zhang, Y., Blättermann, A., Hagstotz, S., Ding, T., Heck, R., Madroñero, J., Martín, F., Pfeifer, T., 2014. Reconstruction and control of a time-dependent two-electron wave packet. *Nature* 516, 374–378. doi:10.1038/nature14026.
- Ott, C., Kaldun, A., Raith, P., Meyer, K., Laux, M., Evers, J., Keitel, C.H., Greene, C.H., Pfeifer, T., 2013. Lorentz meets Fano in spectral line shapes: A universal phase and its laser control. *Science* 340, 716–720. doi:10.1126/science.1234407.
- Ovcharenko, Y., LaForge, A., Langbehn, B., Plekan, O., Cucini, R., Finetti, P., O’Keeffe, P., Iablonskyi, D., Nishiyama, T., Ueda, K., Piseri, P., DiFraia, M., Richter, R., Coreno, M., Callegari, C., Prince, K.C., Stienkemeier, F., Moeller, T., Mudrich, M., 2020. Autoionization dynamics of He nanodroplets resonantly excited by intense XUV laser pulses. *New J. Phys.* doi:10.1088/1367-2630/ab9554. accepted manuscript.
- Ovcharenko, Y., Lyamayev, V., Katzy, R., Devetta, M., LaForge, A., O’Keeffe, P., Plekan, O., Finetti, P., Di Fraia, M., Mudrich, M., Krikunova, M., Piseri, P., Coreno, M., Brauer, N.B., Mazza, T., Stranges, S., Grazioli, C., Richter, R., Prince, K.C., Drabbels, M., Callegari, C., Stienkemeier, F., Möller, T., 2014. Novel collective autoionization process observed in electron spectra of He clusters. *Phys. Rev. Lett.* 112, 073401. doi:10.1103/PhysRevLett.112.073401.
- Owada, S., Togawa, K., Inagaki, T., Hara, T., Tanaka, T., Joti, Y., Koyama, T., Nakajima, K., Ohashi, H., Senba, Y., Togashi, T., Tono, K., Yamaga, M., Yumoto, H., Yabashi, M., Tanaka, H., Ishikawa, T., 2018. A soft x-ray free-electron laser beamline at SACLA: the light source, photon beamline and experimental station. *J. Synchrotron Radiat.* 25, 282–288. doi:10.1107/s1600577517015685.
- Palacios, A., Bachau, H., Martín, F., 2006. Enhancement and control of  $H_2$  dissociative ionization by femtosecond VUV laser pulses. *Phys. Rev. Lett.* 96, 143001. doi:10.1103/PhysRevLett.96.143001.
- Palacios, A., Martín, F., 2020. The quantum chemistry of attosecond molecular science. *WIREs Comput. Mol. Sci.* 10, e1430. doi:10.1002/

- wcms.1430.
- Palacios, A., Sanz-Vicario, J.L., Martín, F., 2015. Theoretical methods for attosecond electron and nuclear dynamics: Applications to the H<sub>2</sub> molecule. *J. Phys. B* 48, 242001. doi:10.1088/0953-4075/48/24/242001.
- Parker, J.S., Moore, L.R., Meharg, K.J., Dundas, D., Taylor, K.T., 2001. Double-electron above threshold ionization of helium. *J. Phys. B* 34, L69–L78. doi:10.1088/0953-4075/34/3/103.
- Pathak, H., Sato, T., Ishikawa, K.L., 2020a. Time-dependent optimized coupled-cluster method for multielectron dynamics. II. A coupled electron-pair approximation. *J. Chem. Phys.* 152, 124115. doi:10.1063/1.5143747.
- Pathak, S., Ibele, L.M., Boll, R., Callegari, C., Demidovich, A., Erk, B., Feifel, R., Forbes, R., Di Fraia, M., Giannesi, L., Hansen, C.S., Holland, D.M.P., Ingle, R.A., Mason, R., Plekan, O., Prince, K.C., Rouzée, A., Squibb, R.J., Tross, J., Ashfold, M.N.R., Curchod, B.F.E., Rolles, D., 2020b. Tracking the ultraviolet photochemistry of thiophenone during and beyond the initial ultrafast ring opening. *Nat. Chem.* in press. arXiv:1912.00531.
- Paul, P.M., Toma, E.S., Breger, P., Mullot, G., Augé, F., Balcou, P., Muller, H.G., Agostini, P., 2001. Observation of a train of attosecond pulses from high harmonic generation. *Science* 292, 1689–1692. doi:10.1126/science.1059413.
- Pazourek, R., Nagele, S., Burgdörfer, J., 2015. Attosecond chronoscopy of photoemission. *Rev. Mod. Phys.* 87, 765–802. doi:10.1103/RevModPhys.87.765.
- Penco, G., Allaria, E., De Ninno, G., Ferrari, E., Giannesi, L., 2015. Experimental demonstration of enhanced self-amplified spontaneous emission by an optical klystron. *Phys. Rev. Lett.* 114, 013901. doi:10.1103/PhysRevLett.114.013901.
- Phillips, R., 1960. The Ubitron, a high-power traveling-wave tube based on a periodic beam interaction in unloaded waveguide. *IRE Trans. Electron Devices* 7, 231–241. doi:10.1109/t-ed.1960.14687.
- Phillips, R.M., 1988. History of the ubitron. *Nuclear Instrum. Methods Phys. Research A* 272, 1–9. doi:10.1016/0168-9002(88)90185-4.
- Picard, Y.J., Manschwetus, B., Gèlèoc, M., Böttcher, M., Casagrande, E.M.S., Lin, N., Ruchon, T., Carrè, B., Hergott, J.F., Lepetit, F., Taïeb, R., Maquet, A., Huetz, A., 2004. Attosecond evolution of energy- and angle-resolved photoemission spectra in two-color (XUV + IR) ionization of rare gases. *Phys. Rev. A* 89, 031401(R). doi:10.1103/PhysRevA.89.031401.
- Pinzola, M.S., Abdel-Naby, S.A., Colgan, J.P., 2019. Triple autoionization of atomic ions. *J. Phys. B* 52, 095201. doi:10.1088/1361-6455/aafa37.
- Plésiat, E., Declève, P., Martín, F., 2012. Vibrationally resolved photoelectron angular distributions from randomly oriented and fixed-in-space N<sub>2</sub> and CO molecules. *J. Phys. B: At. Mol. Opt. Phys.* 45, 194008. doi:10.1088/0953-4075/45/19/194008.
- Prat, E., Dijkstal, P., Ferrari, E., Reiche, S., 2020. Demonstration of large bandwidth hard X-ray free-electron laser pulses at SwissFEL. *Phys. Rev. Lett.* 124, 074801. doi:10.1103/PhysRevLett.124.074801.
- Prat, E., Reiche, S., 2018. Compact coherence enhancement by subharmonic self-seeding in X-ray free-electron laser facilities. *J. Synchrotron Radiat.* 25, 329–335. doi:10.1107/s1600577518000395.
- Prat, E., Reiche, S., 2019. A simple and compact scheme to enhance the brightness of self-amplified spontaneous emission free-electron-lasers. *J. Synchrotron Radiat.* 26, 1085–1091. doi:10.1107/s1600577519005435.
- Prince, K.C., Allaria, E., Callegari, C., Cucini, R., De Ninno, G., Di Mitri, S., Diviacco, B., Ferrari, E., Finetti, P., Gauthier, D., Giannesi, L., Mahne, N., Penco, G., Plekan, O., Raimondi, L., Rebernik, P., Roussel, E., Svetina, C., Trovò, M., Zangrando, M., Negro, M., Carpeggiani, P., Reduzzi, M., Sansone, G., Grum-Grzhimailo, A.N., Gryzlova, E.V., Strakhova, S.I., Bartschat, K., Douguet, N., Venzke, J., Iablonskyi, D., Kumagai, Y., Takanashi, T., Ueda, K., Fischer, A., Coreno, M., Stienkemeier, F., Ovcharenko, Y., Mazza, T., Meyer, M., 2016. Coherent control with a short-wavelength free-electron laser. *Nat. Photonics* 10, 176–179. doi:10.1038/nphoton.2016.13.
- Quééré, F., Mairesse, Y., Itatani, J., 2005. Temporal characterization of attosecond XUV fields. *J. Mod. Opt.* 52, 339–360. doi:10.1080/09500340412331307942.
- Ranitovic, P., Tong, X.M., Hogle, C.W., Zhou, X., Liu, Y., Toshima, N., Murnane, M.M., Kapteyn, H.C., 2011. Laser-enabled Auger decay in rare-gas atoms. *Phys. Rev. Lett.* 106, 053002. doi:10.1103/PhysRevLett.106.053002.
- Ratner, D., Abela, R., Amann, J., Behrens, C., Bohler, D., Bouchard, G., Bostedt, C., Boyes, M., Chow, K., Cocco, D., Decker, F.J., Ding, Y., Eckman, C., Emma, P., Fairley, D., Feng, Y., Field, C., Flechsig, U., Gassner, G., Hastings, J., Heimann, P., Huang, Z., Kelez, N., Krzywinski, J., Loos, H., Lutman, A., Marinelli, A., Marcus, G., Maxwell, T., Montanez, P., Moeller, S., Morton, D., Nuhn, H.D., Rodes, N., Schlotter, W., Serkez, S., Stevens, T., Turner, J., Walz, D., Welch, J., Wu, J., 2015. Experimental demonstration of a soft X-ray self-seeded free-electron laser. *Phys. Rev. Lett.* 114, 054801. doi:10.1103/PhysRevLett.114.054801.
- Raubenheimer, T., 2018. The LCLS-II-HE, a high energy upgrade of the LCLS-II, in: *Proc. 60th ICFA Advanced Beam Dynamics Workshop (FLS'18)*, Shanghai, China, 5-9 March 2018, JACoW Publishing, Geneva, Switzerland. pp. 6–11. doi:10.18429/JACoW-FLS2018-MOP1WA02.
- Rebernik Ribič, P., Abrami, A., Badano, L., Bossi, M., Braun, H.H., Bruchon, N., Capotondi, F., Castronovo, D., Cautero, M., Cinquegrana, P., Coreno, M., Couprie, M.E., Cudin, I., Danailov, M.B., De Ninno, G., Demidovich, A., Di Mitri, S., Diviacco, B., Fawley, W.M., Feng, C., Ferianis, M., Ferrari, E., Foglia, L., Frassetto, F., Gaio, G., Garzella, D., Ghaith, A., Giacuzzo, F., Giannesi, L., Grattoni, V., Grulja, S., Hemsing, E., Iazzourene, F., Kurdi, G., Lonza, M., Mahne, N., Malvestuto, M., Manfreda, M., Masciovecchio, C., Miotti, P., Mirian, N.S., Nikolov, I.P., Penco, G.M., Penn, G., Poletto, L., Pop, M., Prat, E., Principi, E., Raimondi, L., Reiche, S., Roussel, E., Sauro, R., Scafuri, C., Sigalotti, P., Spampinati, S., Spezzani, C., Sturari, L., Svandrlík, M., Tanikawa, T., Trovò, M., Veronese, M., Vivoda, D., Xiang, D., Zaccaria, M., Zangrando, D., Zangrando, M., Allaria, E.M., 2019. Coherent soft X-ray pulses from an echo-enabled harmonic generation free-electron laser. *Nat. Photonics* 13, 555–561. doi:10.1038/s41566-019-0427-1.
- Reiss, H.R., 1980. Effect of an intense electromagnetic field on a weakly bound system. *Phys. Rev. A* 22, 1786–1813. doi:10.1103/PhysRevA.22.1786.
- Rice, S.A., 1992. New ideas for guiding the evolution of a quantum system. *Science* 258, 412. doi:10.1126/science.258.5081.412.
- Richardson, V., Costello, J.T., Cubaynes, D., Düsterer, S., Feldhaus, J., van der Hart, H.W., Juranić, P., Li, W.B., Meyer, M., Richter, M., Sorokin, A.A., Tiedke, K., 2010. Two-photon inner-shell ionization in the extreme ultraviolet. *Phys. Rev. Lett.* 105, 013001. doi:10.1103/PhysRevLett.105.013001.
- Roberson, C.W., Sprangle, P., 1989a. A Review of Free Electron Lasers. Naval Research Laboratory (U.S.). Also published as Roberson and Sprangle (1989b).



- Roberson, C.W., Sprangle, P., 1989b. A review of free-electron lasers. *Phys. Fluids B: Plasma Phys.* 1, 3–42. doi:10.1063/1.859102.
- Rohringer, N., Ryan, D., London, R.A., Purvis, M., Albert, F., Dunn, J., Bozek, J.D., Bostedt, C., Graf, A., Hill, R., Hau-Riege, S.P., Rocca, J.J., 2012. Atomic inner-shell X-ray laser at 1.46 nanometres pumped by an X-ray free-electron laser. *Nature* 481, 488–491. doi:10.1038/nature10721.
- Rohringer, N., Santra, R., 2012. Strongly driven resonant Auger effect treated by an open-quantum-system approach. *Phys. Rev. A* 86, 043434. doi:10.1103/PhysRevA.86.043434.
- Roussel, E., Ferrari, E., Allaria, E., Penco, G., Di Mitri, S., Veronese, M., Danailov, M., Gauthier, D., Giannessi, L., 2015. Multicolor high-gain free-electron laser driven by seeded microbunching instability. *Phys. Rev. Lett.* 115, 214801. doi:10.1103/PhysRevLett.115.214801.
- Rouxel, J.R., Kowalewski, M., Mukamel, S., 2017. Photoinduced molecular chirality probed by ultrafast resonant X-ray spectroscopy. *Struct. Dyn.* 4, 044006. doi:10.1063/1.4974260.
- Rouzée, A., Johnsson, P., Gryzlova, E.V., Fukuzawa, H., Yamada, A., Siu, W., Huismans, Y., Louis, E., Bijkerk, F., Holland, D.M.P., Grum-Grzhimailo, A.N., Kabachnik, N.M., Vrakking, M.J.J., Ueda, K., 2011. Angle-resolved photoelectron spectroscopy of sequential three-photon triple ionization of neon at 90.5 eV photon energy. *Phys. Rev. A* 83, 031401. doi:10.1103/PhysRevA.83.031401.
- Rouzée, A., Johnsson, P., Rading, L., Hundertmark, A., Siu, W., Huismans, Y., Düsterer, S., Redlin, H., Tavella, F., Stojanovic, N., Al-Shemmary, A., Lépine, F., Holland, D.M.P., Schlatholter, T., Hoekstra, R., Fukuzawa, H., Ueda, K., Vrakking, M.J.J., 2013. Towards imaging of ultrafast molecular dynamics using FELs. *J. Phys. B* 46, 164029. doi:10.1088/0953-4075/46/16/164029.
- Rudawski, P., Heyl, C.M., Brizuela, F., Schwenke, J., Persson, A., Mansten, E., Rakowski, R., Rading, L., Campi, F., Kim, B., Johnsson, P., L'Huillier, A., 2013. A high-flux high-order harmonic source. *Rev. Sci. Instrum.* 84, 073103. doi:10.1063/1.4812266.
- Rudek, B., Son, S.K., Foucar, L., Epp, S.W., Erk, B., Hartmann, R., Adolph, M., Andritschke, R., Aquila, A., Berrah, N., Bostedt, C., Bozek, J., Coppola, N., Filsinger, F., Gorke, H., Gorkhover, T., Graafsma, H., Gumprecht, L., Hartmann, A., Hauser, G., Herrmann, S., Hirsemann, H., Holl, P., Hömke, A., Journal, L., Kaiser, C., Kimmel, N., Krasniqi, F., Kühnel, K.U., Matysek, M., Messerschmidt, M., Miesner, D., Möller, T., Moshhammer, R., Nagaya, K., Nilsson, B., Potdevin, G., Pietschner, D., Reich, C., Rupp, D., Schaller, G., Schlichting, I., Schmidt, C., Schopper, F., Schorb, S., Schröter, C.D., Schulz, J., Simon, M., Soltau, H., Strüder, L., Ueda, K., Weidenspointner, G., Santra, R., Ullrich, J., Rudenko, A., Rolles, D., 2012. Ultra-efficient ionization of heavy atoms by intense X-ray free-electron laser pulses. *Nat. Photonics* 6, 858–865. doi:10.1038/nphoton.2012.261.
- Rudek, B., Toyota, K., Foucar, L., Erk, B., Boll, R., Bomme, C., Correa, J., Carron, S., Boutet, S., Williams, G.J., Ferguson, K.R., Alonso-Mori, R., Koglin, J.E., Gorkhover, T., Bucher, M., Lehmann, C.S., Krässig, B., Southworth, S.H., Young, L., Bostedt, C., Ueda, K., Marchenko, T., Simon, M., Jurek, Z., Santra, R., Rudenko, A., Son, S.K., Rolles, D., 2018. Relativistic and resonant effects in the ionization of heavy atoms by ultra-intense hard X-rays. *Nat. Commun.* 9, 4200. doi:10.1038/s41467-018-06745-6.
- Rudenko, A., Foucar, L., Kurka, M., Ergler, T., Kühnel, K.U., Jiang, Y.H., Voitkiv, A., Najjari, B., Kheifets, A., Lüdemann, S., Havermeier, T., Smolarski, M., Schössler, S., Cole, K., Schöffler, M., Dörner, R., Düsterer, S., Li, W., Keitel, B., Treusch, R., Gensch, M., Schröter, C.D., Moshhammer, R., Ullrich, J., 2008. Recoil-ion momentum distributions for two-photon double ionization of He and Ne by 44 eV free-electron laser radiation. *Phys. Rev. Lett.* 101, 073003. doi:10.1103/PhysRevLett.101.073003.
- Saldin, E., Schneidmiller, E., Yurkov, M., 2008. Coherence properties of the radiation from X-ray free electron laser. *Opt. Commun.* 281, 1179–1188. doi:10.1016/j.optcom.2007.10.044.
- Salén, P., van der Meulen, P., Schmidt, H.T., Thomas, R.D., Larsson, M., Feifel, R., Piancastelli, M.N., Fang, L., Murphy, B., Osipov, T., Berrah, N., Kukk, E., Ueda, K., Bozek, J.D., Bostedt, C., Wada, S., Richter, R., Feyer, V., Prince, K.C., 2012. Experimental verification of the chemical sensitivity of two-site double core-hole states formed by an X-ray free-electron laser. *Phys. Rev. Lett.* 108, 153003. doi:10.1103/PhysRevLett.108.153003.
- Santra, R., Kryzhevoi, N.V., Cederbaum, L.S., 2009. X-ray two-photon photoelectron spectroscopy: A theoretical study of inner-shell spectra of the organic para-aminophenol molecule. *Phys. Rev. Lett.* 103, 013002. doi:10.1103/PhysRevLett.103.013002.
- Sasaki, S., 1994. Analyses for a planar variably-polarizing undulator. *Nucl. Instrum. Methods Phys. Res. A* 347, 83–86. doi:10.1016/0168-9002(94)91859-7.
- Sassoli de Bianchi, M., 2012. Time-delay of classical and quantum scattering processes: a conceptual overview and a general definition. *Open Phys.* 10, 282–319. doi:10.2478/s11534-011-0105-5.
- Sato, T., Ishikawa, K.L., 2013. Time-dependent complete-active-space self-consistent-field method for multielectron dynamics in intense laser fields. *Phys. Rev. A* 88, 023402. doi:10.1103/PhysRevA.88.023402.
- Sato, T., Ishikawa, K.L., 2015. Time-dependent multiconfiguration self-consistent-field method based on the occupation-restricted multiple-active-space model for multielectron dynamics in intense laser fields. *Phys. Rev. A* 91, 023417. doi:10.1103/PhysRevA.91.023417.
- Sato, T., Ishikawa, K.L., Březinová, I., Lackner, F., Nagele, S., Burgdörfer, J., 2016. Time-dependent complete-active-space self-consistent-field method for atoms: Application to high-order harmonic generation. *Phys. Rev. A* 94, 023405. doi:10.1103/PhysRevA.94.023405.
- Sato, T., Orimo, Y., Teramura, T., Tugs, O., Ishikawa, K.L., 2018a. Time-dependent complete-active-space self-consistent-field method for ultrafast intense laser science, in: Yamanouchi, K., Martin, P., Sentis, M., Ruxin, L., Normand, D. (Eds.), *Progress in Ultrafast Intense Laser Science XIV*. Springer International Publishing, volume 118 of *Springer Series in Chemical Physics*, pp. 143–171. doi:10.1007/978-3-030-03786-4\_8.
- Sato, T., Pathak, H., Orimo, Y., Ishikawa, K.L., 2018b. Communication: Time-dependent optimized coupled-cluster method for multielectron dynamics. *J. Chem. Phys.* 148, 051101. doi:10.1063/1.5020633.
- Sato, T., Teramura, T., Ishikawa, K.L., 2018c. Gauge-invariant formulation of time-dependent configuration interaction singles method. *Appl. Sci.* 8, 433. doi:10.3390/app8030433.
- Schawlow, A.L., Townes, C.H., 1958. Infrared and optical masers. *Phys. Rev.* 112, 1940–1949. doi:10.1103/PhysRev.112.1940.
- Schins, J.M., Breger, P., Agostini, P., Constantinescu, R.C., Müller, H.G., Grillon, G., Antonetti, A., Mysyrowicz, A., 1994. Observation of laser-assisted Auger decay in argon. *Phys. Rev. Lett.* 73, 2180–2183. doi:10.1103/PhysRevLett.73.2180.
- Schmiegelow, C.T., Schulz, J., Kaufmann, H., Ruster, T., Poschinger, U.G., Schmidt-Kaler, F., 2016. Transfer of optical orbital angular momentum to a bound electron. *Nature Communications* 7, 12998. doi:10.1038/ncomms12998.
- Schnorr, K., Senftleben, A., Kurka, M., Rudenko, A., Foucar, L., Schmid, G., Broska, A., Pfeifer, T., Meyer, K., Anielski, D., Boll, R., Rolles, D., Kübel, M., Kling, M.F., Jiang, Y.H., Mondal, S., Tachibana, T., Ueda, K., Marchenko, T., Simon, M., Brenner, G., Treusch, R., Scheit, S.,

- Averbukh, V., Ullrich, J., Schröter, C.D., Moshhammer, R., 2013. Time-resolved measurement of interatomic coulombic decay in Ne<sub>2</sub>. *Phys. Rev. Lett.* 111, 093402. doi:10.1103/PhysRevLett.111.093402.
- Schoenlein, R., Elsaesser, T., Holldack, K., Huang, Z., Kapteyn, H., Murnane, M., Woerner, M., 2019. Recent advances in ultrafast X-ray sources. *Phil. Trans. R. Soc. A* 377, 20180384. doi:10.1098/rsta.2018.0384.
- Schultze, M., Fieß, M., Karpowicz, N., Gagnon, J., Korbman, M., Hofstetter, M., Neppl, S., Cavalieri, A.L., Komninos, Y., Mercouris, T., Nicolaides, C.A., Pazourek, R., Nagele, S., Feist, J., Burgdörfer, J., Azzeer, A.M., Ernstorfer, R., Kienberger, R., Kleineberg, U., Goulielmakis, E., Krausz, F., Yakovlev, V.S., 2010. Delay in photoemission. *Science* 328, 1658–1662. doi:10.1126/science.1189401.
- Schütte, B., Arbeiter, M., Fennel, T., Jabbari, G., Kuleff, A., Vrakking, M., Rouzée, A., 2015. Observation of correlated electronic decay in expanding clusters triggered by near-infrared fields. *Nat. Commun.* 6, 8596. doi:10.1038/ncomms9596.
- Seddon, E.A., Clarke, J.A., Dunning, D.J., Masciovecchio, C., Milne, C.J., Parmigiani, F., Rugg, D., Spence, J.C.H., Thompson, N.R., Ueda, K., Vinko, S.M., Wark, J.S., Wurth, W., 2017. Short-wavelength free-electron laser sources and science: a review. *Rep. Prog. Phys.* 80, 115901. doi:10.1088/1361-6633/aa7cca.
- Semenov, S.K., Cherepkov, N.A., Fecher, G.H., Schönhense, G., 2000. Generalization of the atomic random-phase-approximation method for diatomic molecules: N<sub>2</sub> photoionization cross-section calculations. *Phys. Rev. A* 61, 032704. doi:10.1103/PhysRevA.61.032704.
- Seres, E., Seres, J., Spielmann, C., 2006. X-ray absorption spectroscopy in the keV range with laser generated high harmonic radiation. *Appl. Phys. Lett.* 89, 181919. doi:10.1063/1.2364126.
- Serkez, S., Decking, W., Froehlich, L., Gerasimova, N., Grünert, J., Guetg, M., Huttula, M., Karabekyan, S., Koch, A., Kocharyan, V., Kot, Y., Kuk, E., Laksman, J., Lytaev, P., Maltezopoulos, T., Mazza, T., Meyer, M., Saldin, E., Schneidmiller, E., Scholz, M., Tomin, S., Vannoni, M., Wohlenberg, T., Yurkov, M., Zagorodnov, I., Geloni, G., 2020. Opportunities for two-color experiments in the soft X-ray regime at the european XFEL. *Appl. Sci.* 10, 2728. doi:10.3390/app10082728.
- Serkez, S., Geloni, G., Tomin, S., Feng, G., Gryzlova, E.V., Grum-Grzhimailo, A.N., Meyer, M., 2018. Overview of options for generating high-brightness attosecond x-ray pulses at free-electron lasers and applications at the European XFEL. *J. Opt.* 20, 024005. doi:10.1088/2040-8986/aa9f4f.
- Shintake, T., Tanaka, H., Hara, T., Tanaka, T., Togawa, K., Yabashi, M., Otake, Y., Asano, Y., Bizen, T., Fukui, T., Goto, S., Higashiya, A., Hirono, T., Hosoda, N., Inagaki, T., Inoue, S., Ishii, M., Kim, Y., Kimura, H., Kitamura, M., Kobayashi, T., Maesaka, H., Masuda, T., Matsui, S., Matsushita, T., Maréchal, X., Nagasono, M., Ohashi, H., Ohata, T., Ohshima, T., Onoe, K., Shirasawa, K., Takagi, T., Takahashi, S., Takeuchi, M., Tamasaku, K., Tanaka, R., Tanaka, Y., Tanikawa, T., Togashi, T., Wu, S., Yamashita, A., Yanagida, K., Zhang, C., Kitamura, H., Ishikawa, T., 2008. A compact free-electron laser for generating coherent radiation in the extreme ultraviolet region. *Nat. Photonics* 2, 555–559. doi:10.1038/nphoton.2008.134.
- Siegbahn, K., 1971. ESCA applied to free molecules. North-Holland Publishing Company, Amsterdam.
- Smith, F.T., 1960. Lifetime matrix in collision theory. *Phys. Rev.* 118, 349–356. doi:10.1103/PhysRev.118.349.
- Smyth, E.S., Parker, J.S., Taylor, K., 1998. Numerical integration of the time-dependent Schrödinger equation for laser-driven helium. *Comput. Phys. Commun.* 114, 1–14. doi:10.1016/S0010-4655(98)00083-6.
- Sommerfeld, A., 1916a. Zur Quantentheorie der Spektrallinien. *Ann. Phys.* 356, 1–94. doi:10.1002/andp.19163561702.
- Sommerfeld, A., 1916b. Zur Quantentheorie der Spektrallinien. *Ann. Phys.* 356, 125–167. doi:10.1002/andp.19163561802.
- Son, S.K., Santra, R., 2011. Impact of hollow-atom formation on coherent x-ray scattering at high intensity. *Phys. Rev. A* 83, 033402. doi:10.1103/PhysRevA.83.033402.
- Son, S.K., Santra, R., 2012. Monte Carlo calculation of ion, electron, and photon spectra of xenon atoms in x-ray free-electron laser pulses. *Phys. Rev. A* 85, 063415. doi:10.1103/PhysRevA.85.063415.
- Sorensen, S.L., Åberg, T., Tulkki, J., Rachlew-Källne, E., Sundström, G., Kirm, M., 1994. Argon 3s autoionization resonances. *Phys. Rev. A* 50, 1218–1230. doi:10.1103/PhysRevA.50.1218.
- Sorokin, A.A., Wellhöfer, M., Bobashev, S.V., Tiedtke, K., Richter, M., 2007. X-ray-laser interaction with matter and the role of multiphoton ionization: Free-electron-laser studies on neon and helium. *Phys. Rev. A* 75, 051402. doi:10.1103/PhysRevA.75.051402.
- Squibb, R.J., Sapunar, M., Ponzi, A., Richter, R., Kivimäki, A., Plekan, O., Finetti, P., Sisourat, N., Zhaunerchyk, V., Marchenko, T., Journal, L., Guillemin, R., Cucini, R., Coreno, M., Grazioli, C., Di Fraia, M., Callegari, C., Prince, K.C., Declava, P., Simon, M., Eland, J.H.D., Došlić, N., Feifel, R., Piancastelli, M.N., 2018. Acetylacetone photodynamics at a seeded free-electron laser. *Nat. Commun.* 9, 63. doi:10.1038/s41467-017-02478-0.
- Starke, K., 2000. Magnetic Dichroism in Core-Level Photoemission. volume 159 of *Springer Tracts in Modern Physics*. Springer, Berlin Heidelberg. doi:10.1007/bfb0109607.
- Stener, M., Toffoli, D., Fronzoni, G., Declava, P., 2007. Recent advances in molecular photoionization by density functional theory based approaches. *Theor. Chem. Acc.* 117, 943–956. doi:10.1007/s00214-006-0212-3.
- Stratmann, R.E., Lucchese, R.R., 1995. A graphical unitary group approach to study multiplet specific multichannel electron correlation effects in the photoionization of O<sub>2</sub>. *J. Chem. Phys.* 102, 8493–8505. doi:10.1063/1.468841.
- Strickland, D., 2019. Nobel lecture: Generating high-intensity ultrashort optical pulses. *Rev. Mod. Phys.* 91, 030502. doi:10.1103/RevModPhys.91.030502.
- Suckewer, S., Jaeglé, P., 2009. X-ray laser: past, present, and future. *Laser Phys. Lett.* 6, 411–436. doi:10.1002/lapl.200910023.
- Suckewer, S., Skinner, C.H., Milchberg, H., Keane, C., Voorhees, D., 1985. Amplification of stimulated soft x-ray emission in a confined plasma column. *Phys. Rev. Lett.* 55, 1753–1756. doi:10.1103/physrevlett.55.1753.
- Sun, Y.P., Rinkevicius, Z., Wang, C.K., Carniato, S., Simon, M., Täieb, R., Gel'mukhanov, F., 2010. Two-photon-induced x-ray emission in neon atoms. *Phys. Rev. A* 82, 043430. doi:10.1103/PhysRevA.82.043430.
- Suzuki, T., 2006. Femtosecond time-resolved photoelectron imaging. *Annu. Rev. Phys. Chem.* 57, 555–592. doi:10.1146/annurev.physchem.57.032905.104601.
- Takahashi, E., Nabekawa, Y., Midorikawa, K., 2002. Generation of 10-μJ coherent extreme-ultraviolet light by use of high-order harmonics. *Opt. Lett.* 27, 1920. doi:10.1364/ol.27.001920.
- Takahashi, O., Tashiro, M., Ehara, M., Yamasaki, K., Ueda, K., 2011. Theoretical molecular double-core-hole spectroscopy of nucleobases. *J.*

- Phys. Chem. A 115, 12070–12082. doi:10.1021/jp205923m.
- Takanashi, T., Golubev, N.V., Callegari, C., Fukuzawa, H., Motomura, K., Iablonskyi, D., Kumagai, Y., Mondal, S., Tachibana, T., Nagaya, K., Nishiyama, T., Matsunami, K., Johnsson, P., Piseri, P., Sansone, G., Dubrouil, A., Reduzzi, M., Carpegiani, P., Vozzi, C., Devetta, M., Negro, M., Faccialà, D., Calegari, F., Trabattoni, A., Castrovilli, M.C., Ovcharenko, Y., Mudrich, M., Stienkemeier, F., Coreno, M., Alagia, M., Schütte, B., Berrah, N., Plekan, O., Finetti, P., Spezzani, C., Ferrari, E., Allaria, E., Penco, G., Serpico, C., De Ninno, G., Diviacco, B., Di Mitri, S., Giannessi, L., Jabbari, G., Prince, K.C., Cederbaum, L.S., Demekhin, P.V., Kuleff, A.I., Ueda, K., 2017. Time-resolved measurement of interatomic coulombic decay induced by two-photon double excitation of Ne<sub>2</sub>. *Phys. Rev. Lett.* 118, 033202. doi:10.1103/PhysRevLett.118.033202.
- Tan, H.S., 2008. Theory and phase-cycling scheme selection principles of collinear phase coherent multi-dimensional optical spectroscopy. *J. Chem. Phys.* 129, 124501. doi:10.1063/1.2978381.
- Tanaka, S., Mukamel, S., 2002. X-ray four-wave mixing in molecules. *J. Chem. Phys.* 116, 1877–1891. doi:10.1063/1.1429950.
- Tannor, D.J., 2007. *Introduction to Quantum Mechanics. A Time-Dependent Perspective.* University science Books, Sausalito, California.
- Tashiro, M., Ehara, M., Fukuzawa, H., Ueda, K., Buth, C., Kryzhevoi, N.V., Cederbaum, L.S., 2010a. Molecular double core hole electron spectroscopy for chemical analysis. *J. Chem. Phys.* 132, 184302. doi:10.1063/1.3408251.
- Tashiro, M., Ehara, M., Ueda, K., 2010b. Double core-hole electron spectroscopy for open-shell molecules: Theoretical perspective. *Chem. Phys. Lett.* 496, 217–222. doi:10.1016/j.cpl.2010.07.046.
- Teichmann, S.M., Silva, F., Cousin, S.L., Hemmer, M., Biegert, J., 2016. 0.5-keV Soft X-ray attosecond continua. *Nat. Commun.* 7, 11493. doi:10.1038/ncomms11493.
- Tilley, M., Karamatskou, A., Santra, R., 2015. Wave-packet propagation based calculation of above-threshold ionization in the x-ray regime. *J. Phys. B* 48, 124001. doi:10.1088/0953-4075/48/12/124001.
- Toffoli, D., Stener, M., Fronzoni, G., Decleva, P., 2002. Convergence of the multicenter B-spline DFT approach for the continuum. *Chem. Phys.* 276, 25–43. doi:10.1016/S0301-0104(01)00549-3.
- Tong, X.M., Ranitovic, P., Hogle, C.W., Murnane, M.M., Kapteyn, H.C., Toshima, N., 2011. Theory and experiment on laser-enabled inner-valence Auger decay of rare-gas atoms. *Phys. Rev. A* 84, 013405. doi:10.1103/PhysRevA.84.013405.
- Tschentscher, T., Bressler, C., Grünert, J., Madsen, A., Mancuso, A., Meyer, M., Scherz, A., Sinn, H., Zastra, U., 2017. Photon beam transport and scientific instruments at the European XFEL. *Applied Sciences* 7, 592. doi:10.3390/app7060592.
- Ullrich, J., Rudenko, A., Moshhammer, R., 2012. Free-electron lasers: New avenues in molecular physics and photochemistry. *Annu. Rev. Phys. Chem.* 63, 635–660. doi:10.1146/annurev-physchem-032511-143720.
- Usenko, S., Przystawik, A., Jakob, M.A., Lazzarino, L.L., Brenner, G., Toleikis, S., Haunhorst, C., Kip, D., Laarmann, T., 2017. Attosecond interferometry with self-amplified spontaneous emission of a free-electron laser. *Nature Communications* 8, 15626. doi:10.1038/ncomms15626.
- Vrakking, M.J.J., Lepine, F. (Eds.), 2019. *Attosecond Molecular Dynamics. Theoretical and Computational Chemistry Series, The Royal Society of Chemistry.* doi:10.1039/9781788012669.
- Wang, H., Chini, M., Chen, S., Zhang, C.H., He, F., Cheng, Y., Wu, Y., Thumm, U., Chang, Z., 2010. Attosecond time-resolved autoionization of argon. *Phys. Rev. Lett.* 105, 143002. doi:10.1103/PhysRevLett.105.143002.
- Wang, Y., Granados, E., Pedaci, F., Alessi, D., Luther, B., Berrill, M., Rocca, J.J., 2008. Phase-coherent, injection-seeded, table-top soft-X-ray lasers at 18.9 nm and 13.9 nm. *Nat. Photonics* 2, 94–98. doi:10.1038/nphoton.2007.280.
- Wang, Y., Guo, T., Li, J., Zhao, J., Yin, Y., Ren, X., Li, J., Wu, Y., Weidman, M., Chang, Z., Jager, M.F., Kaplan, C.J., Geneaux, R., Ott, C., Neumark, D.M., Leone, S.R., 2018. Enhanced high-order harmonic generation driven by a wavefront corrected high-energy laser. *J. Phys. B* 51, 134005. doi:10.1088/1361-6455/aac59e.
- Wang, Z.M., Elliott, D.S., 2001. Determination of the phase difference between even and odd continuum wave functions in atoms through quantum interference measurements. *Phys. Rev. Lett.* 87, 173001. doi:10.1103/PhysRevLett.87.173001.
- Wigner, E.P., 1955. Lower limit for the energy derivative of the scattering phase shift. *Phys. Rev.* 98, 145. doi:10.1103/PhysRev.98.145.
- Wituschek, A., Bruder, L., Allaria, E., Bangert, U., Binz, M., Callegari, C., Cerullo, G., Cinquegrana, P., Gianessi, L., Danailov, M., Demidovich, A., Di Fraia, M., Drabbels, M., Feifel, R., Laarmann, T., Michiels, R., Mirian, N.S., Mudrich, M., Nikolov, I., O’Shea, F.H., Penco, G., Piseri, P., Plekan, O., Prince, K.C., Przystawik, A., Ribič, P.R., Sansone, G., Sigalotti, P., Spampinati, S., Spezzani, C., Squibb, R.J., Stranges, S., Uhl, D., Stienkemeier, F., 2020. Tracking attosecond electronic coherences using phase-manipulated extreme ultraviolet pulses. *Nat. Commun.* 11, 883. doi:10.1038/s41467-020-14721-2.
- Wolf, T., Holzmeier, F., Wagner, I., Berrah, N., Bostedt, C., Bozek, J., Bucksbaum, P., Coffee, R., Cryan, J., Farrell, J., Feifel, R., Martinez, T., McFarland, B., Mücke, M., Nandi, S., Tarantelli, F., Fischer, I., Gühr, M., 2017a. Observing femtosecond fragmentation using ultrafast X-ray-induced Auger spectra. *Appl. Sci.* 7, 681. doi:10.3390/app7070681.
- Wolf, T.J.A., Myhre, R.H., Cryan, J.P., Coriani, S., Squibb, R.J., Battistoni, A., Berrah, N., Bostedt, C., Bucksbaum, P., Coslovich, G., Feifel, R., Gaffney, K.J., Grilj, J., Martinez, T.J., Miyabe, S., Moeller, S.P., Mücke, M., Natan, A., Obaid, R., Osipov, T., Plekan, O., Wang, S., Koch, H., Gühr, M., 2017b. Probing ultrafast  $\pi\pi^*/n\pi^*$  internal conversion in organic chromophores via K-edge resonant absorption. *Nat. Commun.* 8, 29. doi:10.1038/s41467-017-00069-7.
- Wolkow, D.V., 1935. Über eine Klasse von Lösungen der Diracschen Gleichung. *Z. Phys* 94, 250–260. doi:10.1007/BF01331022.
- Wragg, J., Parker, J.S., van der Hart, H.W., 2015. Double ionization in R-matrix theory using a two-electron outer region. *Phys. Rev. A* 92, 022504. doi:10.1103/PhysRevA.92.022504.
- Yabashi, M., Tanaka, H., Tanaka, T., Tomizawa, H., Togashi, T., Nagasono, M., Ishikawa, T., Harries, J.R., Hikosaka, Y., Hishikawa, A., Nagaya, K., Saito, N., Shigemasa, E., Yamanouchi, K., Ueda, K., 2013. Compact XFEL and AMO sciences: SACLA and SCSS. *J. Phys. B* 46, 164001. doi:10.1088/0953-4075/46/16/164001.
- Yamazaki, R., Elliott, D.S., 2007. Observation of the phase lag in the asymmetric photoelectron angular distributions of atomic barium. *Phys. Rev. Lett.* 98, 053001. doi:10.1103/PhysRevLett.98.053001.
- Yan, J., Mueller, J.M., Ahmed, M.W., Hao, H., Huang, S., Li, J., Litvinenko, V.N., Liu, P., Mikhailov, S.F., Popov, V.G., Sikora, M.H., Vinokurov, N.A., Wu, Y.K., 2019. Precision control of gamma-ray polarization using a crossed helical undulator free-electron laser. *Nat. Photonics* 13, 629–635. doi:10.1038/s41566-019-0467-6.

- Yang, X., Mirian, N., Giannessi, L., 2020. Postsaturation dynamics and superluminal propagation of a superradiant spike in a free-electron laser amplifier. *Phys. Rev. Accel. Beams* 23, 010703. doi:10.1103/PhysRevAccelBeams.23.010703.
- Ye, L., Rouxel, J.R., Asban, S., Rösner, B., Mukamel, S., 2019. Probing molecular chirality by orbital-angular-momentum-carrying x-ray pulses. *J. Chem. Theory Comput.* 15, 4180–4186. doi:10.1021/acs.jctc.9b00346.
- Yin, Y.Y., Chen, C., Elliott, D.S., Smith, A.V., 1992. Asymmetric photoelectron angular distributions from interfering photoionization processes. *Phys. Rev. Lett.* 69, 2353–2356. doi:10.1103/PhysRevLett.69.2353.
- Yoneda, H., Inubushi, Y., Nagamine, K., Michine, Y., Ohashi, H., Yumoto, H., Yamauchi, K., Mimura, H., Kitamura, H., Katayama, T., Ishikawa, T., Yabashi, M., 2015. Atomic inner-shell laser at 1.5 ångström wavelength pumped by an X-ray free-electron laser. *Nature* 524, 446–449. doi:10.1038/nature14894.
- Yong, Y., Qinming, L., Jiayue, Y., Guanglei, W., Lei, S., Hongli, D., Kai, T., Zhenxing, T., Zhigang, H., Zhichao, C., Yuhuan, T., Dongxu, D., Guorong, W., Weiqing, Z., Xueming, Y., Chao, F., Si, C., Zhen, W., Duan, G., Jie, C., Xiaoqing, L., Taihe, L., Lie, F., Wenyang, Z., Shaopeng, Z., Junqiang, Z., Lin, L., Chengcheng, X., Hao, L., Huan, Z., Guanghua, C., Haijun, Z., Jianguo, D., Maomao, H., Wei, Z., Longwei, L., Fubin, Y., Guanghong, W., Shengwang, X., Yiyong, H.X., Sen, S., Fei, G., Zhiqiang, J., Xiaoxuan, Z., Yongfang, L., Yonghua, W., Zhihao, C., Ruiping, W., Dazhang, H., Meng, Z., Haixiao, D., Bin, L., Guoqiang, L., Luyang, Y., Yingbing, Y., Shanchuan, Y., Xiaobin, X., Qiaogen, Z., Bo, L., Qiang, G., Ming, G., Guoping, F., Yongbin, L., Lixin, Y., Dong, W., Zhentang, Z., 2019. Dalian extreme ultraviolet coherent light source. *Chinese J. Lasers* 46, 0100005. doi:10.3788/cj1201946.0100005. in Chinese.
- You, D., Fukuzawa, H., Luo, Y., Saito, S., Berholts, M., Gaumnitz, T., Huttula, M., Johnsson, P., Kishimoto, N., Myllynen, H., Nemer, A., Niozu, A., Patanen, M., Pelimanni, E., Takanashi, T., Wada, S., Yokono, N., Owada, S., Tono, K., Yabashi, M., Nagaya, K., Kuk, E., Ueda, K., 2020a. Multi-particle momentum correlations extracted using covariance methods on multiple-ionization of diiodomethane molecules by soft-X-ray free-electron laser pulses. *Phys. Chem. Chem. Phys.* 22, 2648–2659. doi:10.1039/c9cp03638e.
- You, D., Ueda, K., Gryzlova, E.V., Grum-Grzhimailo, A.N., Popova, M.M., Staroselskaya, E.I., Tugs, O., Orimo, Y., Sato, T., Ishikawa, K.L., Carpegiani, P.A., Csizmadia, T., Füle, M., Sansone, G., Maroju, P.K., D’Elia, A., Mazza, T., Meyer, M., Callegari, C., Di Fraia, M., Plekan, O., Richter, R., Giannessi, L., Allaria, E., De Ninno, G., Trovò, M., Badano, L., Diviacco, B., Gauthier, D., Mirian, N., Penco, G., Rebernik Ribič, P., Spampinati, S., Spezzani, C., Gaio, G., Prince, K.C., 2020b. A new method for measuring angle-resolved phases in photoemission. *Phys. Rev. X*, in press.
- You, D., Ueda, K., Ruberti, M., Ishikawa, K.L., Carpegiani, P.A., Csizmadia, T., Oldal, L.G., NG, H., Sansone, G., Maroju, P.K., Kooser, K., Callegari, C., Di Fraia, M., Plekan, O., Giannessi, L., Allaria, E., De Ninno, G., Trovò, M., Badano, L., Diviacco, B., Gauthier, D., Mirian, N., Penco, G., Ribič, P.R., Spampinati, S., Spezzani, C., Di Mitri, S., Gaio, G., Prince, K.C., 2019. A detailed investigation of single-photon laser enabled Auger decay in neon. *New J. Phys.* 21, 113036. doi:10.1088/1367-2630/ab520d.
- Young, L., Kanter, E.P., Krässig, B., Li, Y., March, A.M., Pratt, S.T., Santra, R., Southworth, S.H., Rohringer, N., DiMauro, L.F., Doumy, G., Roedig, C.A., Berrah, N., Fang, L., Hoener, M., Bucksbaum, P.H., Cryan, J.P., Ghimire, S., Glowacki, J.M., Reis, D.A., Bozek, J.D., Bostedt, C., Messerschmidt, M., 2010. Femtosecond electronic response of atoms to ultra-intense X-rays. *Nature* 466, 56–61. doi:10.1038/nature09177.
- Yu, L.H., 1984. Optical klystron harmonic generator with electron microbunches induced and frozen by lasers as an intense coherent soft X-ray source. *Phys. Rev. Lett.* 53, 254–257. doi:10.1103/PhysRevLett.53.254.
- Yu, L.H., 1991. Generation of intense uv radiation by subharmonically seeded single-pass free-electron lasers. *Phys. Rev. A* 44, 5178–5193. doi:10.1103/PhysRevA.44.5178.
- Yu, L.H., Babzien, M., Ben-Zvi, I., Dimauro, L.F., Doyuran, A., Graves, W., Johnson, E., Krinsky, S., Malone, R., Pogorelsky, I., Skaritka, J., Rakowsky, G., Solomon, L., X. J., W.A.N.G., Woodle, M., Yakimenko, V., Biedron, S.G., Galayda, J.N., Gluskin, E., Jagger, J., Sajaev, V., Vasserman, I., 2000. High-gain harmonic-generation free-electron laser. *Science* 289, 932–934. doi:10.1126/science.289.5481.932.
- Yu, L.H., DiMauro, L., Doyuran, A., Graves, W.S., Johnson, E.D., Heese, R., Krinsky, S., Loos, H., Murphy, J.B., Rakowsky, G., Rose, J., Shaftan, T., Sheehy, B., Skaritka, J., Wang, X.J., Wu, Z., 2003. First ultraviolet high-gain harmonic-generation free-electron laser. *Phys. Rev. Lett.* 91, 074801. doi:10.1103/PhysRevLett.91.074801.
- Yuan, K.J., Bandrauk, A.D., 2019. Probing attosecond electron coherence in molecular charge migration by ultrafast X-ray photoelectron imaging. *Appl. Sci.* 9, 1941. doi:doi:10.3390/app9091941.
- Zandee, L., Bernstein, R.B., 1979. Resonance-enhanced multiphoton ionization and fragmentation of molecular beams: NO, I<sub>2</sub>, benzene, and butadiene. *J. Chem. Phys.* 71, 1359–1371. doi:10.1063/1.438436.
- Zanghellini, J., Kitzler, M., Fabian, C., Brabec, T., Scrinzi, A., 2003. An MCTDHF approach to multielectron dynamics in laser fields. *Laser Phys.* 13, 1064–1068.
- Zatsarinny, O., 2006. BSR: B-spline atomic R-matrix codes. *Comput. Phys. Commun.* 174, 273–356. doi:10.1016/j.cpc.2005.10.006.
- Zatsarinny, O., Bartschat, K., 2013. The B-spline R-matrix method for atomic processes: application to atomic structure, electron collisions and photoionization. *J. Phys. B* 46, 112001. doi:10.1088/0953-4075/46/11/112001.
- Zewail, A.H., 2000. Femtochemistry: Atomic-scale dynamics of the chemical bond using ultrafast lasers (Nobel Lecture). *Angew. Chem. Int. Ed.* 39, 2586–2631. doi:10.1002/1521-3773(20000804)39:15<2586::aid-anie2586>3.0.co;2-o.
- Zhang, L., Zheng, Y., Li, G., Jia, Z., Li, Y., Xu, Y., Leng, Y., Zeng, Z., Li, R., Xu, Z., 2018. Bright high-order harmonic generation around 30 nm using hundred-terawatt-level laser system for seeding full coherent XFEL. *Applied Sciences* 8, 1446. doi:10.3390/app8091446.
- Zhang, S.B., Kimberg, V., Rohringer, N., 2016. Nonlinear resonant auger spectroscopy in CO using an x-ray pump-control scheme. *Phys. Rev. A* 94, 063413. doi:10.1103/PhysRevA.94.063413.
- Zhao, Z., Wang, D., Gu, Q., Yin, L., Fang, G., Gu, M., Leng, Y., Zhou, Q., Liu, B., Tang, C., Huang, W., Liu, Z., Jiang, H., 2017a. SXFEL: A soft X-ray free electron laser in China. *Synchrotron Radiat. News* 30, 29–33. doi:10.1080/08940886.2017.1386997.
- Zhao, Z., Wang, D., Gu, Q., Yin, L., Gu, M., Leng, Y., Liu, B., 2017b. Status of the SXFEL facility. *Applied Sciences* 7, 607. doi:10.3390/app7060607.
- Zhao, Z., Wang, D., Yin, L., Gu, Q., Fang, G., Gu, M., Leng, Y., Zhou, Q., Liu, B., Tang, C., Huang, W., Liu, Z., Jiang, H., Weng, Z., 2019. Shanghai soft X-ray free-electron laser facility. *Chinese J. Lasers* 46, 0100004. doi:10.3788/cj1201946.0100004. in chinese.
- Žitnik, M., Mihelič, A., Bučar, K., Kavčič, M., Rubensson, J.E., Svanquist, M., Söderström, J., Feifel, R., Sâthe, C., Ovcharenko, Y., Lyamayev, V., Mazza, T., Meyer, M., Simon, M., Journel, L., Lüning, J., Plekan, O., Coreno, M., Devetta, M., Di Fraia, M., Finetti, P., Richter, R., Grazioli,

C., Prince, K.C., Callegari, C., 2014. High resolution multiphoton spectroscopy by a tunable free-electron-laser light. *Phys. Rev. Lett.* 113, 193201. doi:10.1103/PhysRevLett.113.193201.

Zwanzig, R., 1964. On the identity of three generalized master equations. *Physica* 30, 1109–1123. doi:10.1016/0031-8914(64)90102-8.